The Dissertation Committee for Bertha Shontae Kirkland Certifies that this is the approved version of the following dissertation:

Gas Transport Properties of Poly(n-alkyl acrylate) Blends and Modeling of Modified Atmosphere Storage Using Selective and Non-selective Membranes

Committee:

Donald R. Paul, Supervisor

Benny D. Freeman

Isaac C. Sanchez

Venkat Ganesan

Arumugam Manthiram

Gas Transport Properties of Poly(n-alkyl acrylate) Blends and Modeling of Modified Atmosphere Storage Using Selective and Non-selective Membranes

by

Bertha Shontae Kirkland, B.S.; M.S.E.

Dissertation

Presented to the Faculty of the Graduate School of
The University of Texas at Austin
in Partial Fulfillment
of the Requirements
for the Degree of

Doctor of Philosophy

The University of Texas at Austin
December 2007

To my family

Acknowledgements

I would like to express my sincere gratitude to Dr. Paul for his unwavering support and patience. His ideas and guidance throughout this experience are invaluable. I would like to thank my committee members, Dr. Freeman, Dr. Sanchez, Dr. Ganesan, and Dr. Manthiram for their time and support. I would also like to thank Mark Phillips, Jim Smitherman, Eddie Ibarra, and Kevin Haynes for their eagerness to help with repairing, building and ordering equipment that made these tasks painless and enjoyable.

I am appreciative for the opportunity to collaborate with fellow group members and visiting scientist, especially Kelly O'leary and Shuichi Takahashi. I would like to thank the graduate students of Dr. Lloyd for the use of their equipment and unlimited access to their laboratory.

I am deeply grateful to my family for their support. I am especially grateful to my mother for her faith and dedication to provide a solid foundation for me. I am forever indebted to my fiancé for many long trips over the last few years to visit and nurture my being.

This research was supported by the National Science Foundation and the Separations Research Program at the University of Texas at Austin. Support was also provided by GEM through MS and Ph.D fellowships.

Bertha Kirkland

December 2007

Gas Transport Properties of Poly(n-alkyl acrylate) Blends and Modeling of Modified Atmosphere Storage Using Selective and Non-selective Membranes

Publication No._____________

Bertha Shontae Kirkland, Ph.D.
The University of Texas at Austin, 2007

Supervisor: Donald R. Paul

The gas transport properties of side-chain crystalline poly(*n*-alkyl acrylate) and poly(*m*-alkyl acrylate) blends are determined as a function of temperature for varying side-chain lengths, *n* and *m*, and blend compositions. The side chains of poly(*n*-alkyl acrylate)s crystallize independently of the main chain for $n \geq 10$ which leads to an extraordinary increase in the permeability at the melting temperature of the crystallites. The compatibility of these polymers are examined and macroscopic homogeneity is observed for a small range of *n* and *m* when the difference $|n - m|$ is between 2 – 4 methylene units. Thermal analysis shows that the blend components crystallize independently of one another; at the same time, the crystallization of each component is hindered by the presence the other component. The permeation responses of these blends show two distinct permeation jumps as the crystallites from each component melt at their respective melting temperatures. Blends with continuous permeation responses are found to have higher effective activation energies than observed for common polymers.

Thermal analysis proved to be a useful tool to help predict the permeation response for poly(alkyl acrylates); thus the thermal behavior of poly(*n*-alkyl acrylate) blended with n-aliphatic materials and random copolymers of poly(*n*-alkyl acrylates) are briefly examined.

A bulk modified atmospheric storage design is proposed where produce is stored in a rigid chamber that is equipped with both selective and non-selective membrane modules that help regulate the oxygen entering and the carbon dioxide leaving the produce compartment. The design enables control of the atmosphere inside the chamber by modulating gas flow, i.e. the gas flow rate and composition, through the non-selective membrane by delivering fresh air upstream of the non-selective membrane. The model shows that the choice of materials for the selective and non-selective membranes dictate the range of concentrations achievable; however, the air flow rate allows the control between these ranges. The method to design a practical chamber from this model is also described.

Table of Contents

List of Tables

List of Figures

Chapter 1: Introduction

INTRODUCTION

Semi-crystalline polymers with *n*-alkyl pendant side chains have been extensively studied over several decades due to their unique crystallizing properties[1-8]. In contrast main-chain crystalline polymers such as polyethylene, the side chains crystallize independently of the polymer main backbone when the length of the *n*-alkyl group is sufficiently long[2, 9]. In particular poly(alkyl acrylate)s and poly(alkyl methacrylate)s, have garnered much interest as pour point depressants in lubricating oils by co-crystallization or adsorption mechanisms[10], thus their physical, thermal, and structural properties have been extensively studied[1, 2, 4, 11, 12]. More recent fundamental transport studies on poly(*n*-alkyl acrylate)s show that the permeability to small molecule penetrants can change dramatically as the melting temperature of the side-chain crystals is traversed[13]. The side chains have a strong propensity to crystallize as the side-chain length increases; hence, side-chain crystallinity can be used as a design parameter controlled by the side chain length.

The concept of thermally tunable properties have made poly(*n*-alkyl acrylate)s attractive for many applications in very diverse industries[14-16]; here, we are interested in their use as membrane devices for modified atmospheric packaging of fresh produce. Modified atmospheric (MA) technology utilizes polymeric membranes to regulate the O_2 that enters and the CO_2 that leaves a package which encloses fruits or vegetables to prolong freshness. It has been an arduous task to design membranes with appropriate gas transmission rates and gas selectivities to safely package continually respiring produce when the storage temperature varies since produce respiration rates vary more strongly with temperature than do permeation rates of most common polymers[17]. Optimal oxygen and carbon dioxide concentrations (low O_2 and elevated CO_2 levels) help reduce respiration rates, i.e., extending produce shelf-life. Side-chain crystalline polymers offer a pathway to create membranes that are more thermally responsive for MA packaging or storage methods by capitalizing on the dramatic increase in permeability as the melting point of the crystallites is traversed.

Determination of a suitable polymer to either package the produce or use as a membrane device on the package requires that both the permeation and respiration rates are available. Often the packaging or membrane label alone is insufficient to maintain a defined atmosphere inside the package; therefore, techniques using non-selective transport mediums such as perforations (pores or tubes) or porous membranes have been used to reach the desired concentration ranges and equilibrate the pressure inside the package.

DISSERTATION ORGANIZATION

The goal of this research is to examine how to tailor semi-crystalline polymers for specific permeation responses that are more thermally responsive than common polymers by blending poly(*n*-alkyl acrylate)s. This work is divided into two parts, the examination of gas permeation properties of poly(*n*-alkyl acrylate)s blends and the design or modeling of MA packages or bulk containers. Chapter 2 contains background information for both parts. The physical and structural properties of poly(*n*-alkyl acrylate) are explained in Chapter 2. The theory that describes gas transport through semi-crystalline polymers is also discussed using the two-phase transport model introduced by Michaels et al. that assumes the crystallites are impenetrable to gas permeation. Chapter 2 also describes the approach to using poly(*n*-alkyl acrylate)s of various side-chain lengths to obtain more thermally responsive materials. The motivation and background of MA packaging or storage methods are also discussed. Chapter 3 describes the thermal and permeation behavior of homopolymer blends of poly(*n*-alkyl acrylate)s and poly(*m*-alkyl arylate)s of side-chain lengths *n* and *m* with varying composition. This chapter also examines the compatibility of the polymers over a wide range of *n* and *m* and explores the effects of crystallization conditions on the permeation response of the blends.

Thermal analysis has proved to be a useful tool to predict the permeation behavior of poly(alkyl acrylate)s. Chapter 4 is a brief study on the thermal behavior of poly(*n*-alkyl acrylate) and *n*-aliphatic blends. This chapter also examines the thermal properties of homopolymer and copolymer poly(*n*-alkyl acrylate) blends.

The second part of this work, Chapters 5 and 6, looks at modeling the MA of packages and bulk containers. Chapter 5 is a comprehensive review of how to design a MA package. This Chapter explains the way in which respiration rates are determined and the expressions, enzyme kinetics based, that best represent the respiration process of produce phenomenologically. The Paul-Clark MA package model is used to design a package with a high-flux membrane label while examining the effects of temperature on the gas concentration inside the package. A mathematical model is developed to attain a MA of a bulk container using both selective and non-selective membrane modules in Chapter 6. The choice of selective and non-selective polymers on the MA concentration is examined; equations are developed to aid in practical design.

Chapter 7 is a brief summary of the conclusions from both the thermally responsive blends and the MA modeling work and recommendations for future work. Appendix A contains additional permeation measures for penetrants that were not explicitly shown in Chapter 3.

REFERENCES

1. Rehberg CE and Fisher CH. Journal of the American Chemical Society 1944;66:1203-1207.
2. Greenberg SA and Alfrey T. Journal of the American Chemical Society 1954;76:6280-6285.
3. Kaufman HS, Sacher A, Alfrey T, and Fankuchen I. Journal of the American Chemical Society 1948;70:3147.
4. Wiley RH and Brauer GM. Journal of Polymer Science 1948;3:455-461.
5. Overberger CG, Frazier C, Mandelman J, and Smith HF. Journal of the American Chemical Society 1953;75:3326-3330.
6. Pittman AG and Ludwig BA. Journal of Polymer Science, Polymer Chemistry Edition 1969;7(11):3053-3066.
7. Yokota K and Hirabayashi T. Polymer Journal (Tokyo, Japan) 1986;18(2):177-180.
8. Hirabayashi T and Yokota K. Polymer Journal (Tokyo, Japan) 1987;19(9):1115-1119.
9. Plate NA, Shibaev VP, Petrukhin BS, and Kargin VA. Journal of Polymer Science, Polymer Symposia 1968;No. 23(Pt. 1):37-44.
10. Jordan EF, Jr., Smith S, Jr., Parker WE, Artymyshyn B, and Wrigley AN. Journal of Applied Polymer Science 1978;22(6):1509-1528.
11. Shibayev VA. Vysokomolekulyarnye Soedineniya, Seriya A 1968;10(1):216-226.
12. Artyukhov AI, Borisova TI, Birshtein LL, Dmitrochenko DA, and Shevelev VA. Vysokomolekulyarnye Soedineniya, Seriya A 1975;17(11):2552-2557.
13. Mogri Z. Gas transport properties of side-chain crystalline polymers. Chemical Engineering. Austin: University of Texas at Austin, 2001. pp. 289.
14. Clarke R. Temperature switchable pressure sensitive adhesives. Adhesives Age, vol. 36, 1993. pp. 39.
15. Temperature compensating films for produce. Prepared Foods, vol. v161: Business News Publishing Co., 1992. pp. 95(91).

16. Refojo MR. Polymers and devices in ophthalmology. Biomedical Engineering Conference, 1995., Proceedings of the 1995 Fourteenth Southern, 1995. pp. 143-147.
17. Exama A, Arul J, Lencki RW, Lee LZ, and Toupin C. Journal of Food Science 1993;58(6):1365-1370.
18. R.T. Parry and Editor. Principles and Applications of Modified Atmosphere Packaging of Food, 1st ed. London: Blackie Academic and Professional (Am Imprint of Chapman & Hall), 1993.
19. O'Leary KA and Paul DR. Polymer 2006;47(4):1226-1244.
20. O'Leary KA and Paul DR. Polymer 2006;47(4):1245-1258.
21. Paul DR and Clarke R. Journal of Membrane Science 2002;208(1-2):269-283.

Chapter 2: Background

POLY (N-ALKYL ACRYLATE) S

The use of poly(*n*-alkyl acrylate)s is prevalent across industries owing to their ability to crystallize. Side-chain crystallinity found in polymers such as poly(*n*-alkyl acrylate)s and poly(*n*-alkyl methacrylate)s has a profound effect on physical, thermal and transport properties. However, not all poly(*n*-alkyl acrylate)s crystallize. In fact, side chain crystallization requires that a critical side-chain length is reached to maintain stable nucleation and growth. This critical side-chain length varies among homologous series and is often determined by main chain flexibility and other substituents present in the alkyl side chain. For poly(*n* alkyl acrylate)s, this critical side-chain length is approximately 9-10 carbon atoms beyond the ester connection extending from the main chain as shown in Figure 2.1.

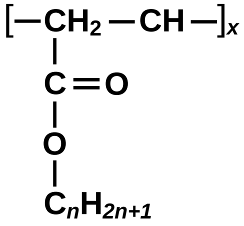

$$[-CH_2-CH-]_x,\quad -C(=O)-O-C_nH_{2n+1}$$

Figure 2.1: Poly (*n*-alkyl acrylate) repeat unit

These polymers remain completely amorphous below this critical side-chain length as no crystallization occurs. Jordan[1] observed a linear increase of the heat of fusion with an increase in side-chain length, n. This relationship along with the fact that the incremental enthalpy increase compared well with enthalpy changes for methylene units of hexagonally packed alkanes provided much evidence that above ten carbon atoms only the side-chains crystallize, independently of the polymer main chain. It is thought that the 9-10 carbon atoms of the alkyl side chain closest to the backbone remain in an amorphous phase while the remaining alkyl side chain crystallize into a hexagonal packing arrangement. When n is sufficiently long, these polymers are referred as comb-like polymers due to the ordered arrangement of the side-chains perpendicular to the backbone. Other comb-like polymers crystallize into a similar arrangement; however, the extent of crystallization depends on the flexibility of the backbone and the mobility of the side chain that is influenced by substituents groups. Yokota et al. copolymerized butadiene and long alkyl methacrylates to widen the distance between side chains increasing main chain flexibility[2]. Like conventional comb-like polymers that have side chains every two main chain carbon atoms, these widely spaced comb-like polymers with side chains every seven main chain carbon atoms were also found to crystallize and to a greater extent. Crystallographic studies on side-chain crystallization of poly(acrylamide)s proved that adding an amide group did not prevent crystallization[3]. When a second amide group was added, crystallization was not affected as long as the addition was made to the normal amorphous phase and the remaining alkyl chain was of adequate length for crystallization.

Upon crystallization, side-chain crystalline polymers form a structure that resembles a layered configuration with alternating amorphous and crystalline phases. Interestingly, there are varying degrees of order in both the molten and crystalline states. In the molten state the side chains exist with some short range order where the side chains are in a random confirmation emerging from the backbone in all directions[4, 5]. In the crystalline state, the side chains take on a trans-conformation perpendicular to the main chain. The side chains crystallize into hexagonal packing characterized by a single adsorption band at 720 cm^{-1}. The presence of bands in the 720 cm^{-1} region was correlated with the CH_2 rocking mode of crystalline long alkyl chain compounds where a single band indicated hexagonal packing and a doublet associated with orthorhombic sub-cell due to the interaction between nearby chains[6]. This was further supported by X-ray studies; poly(*n*-alkyl acrylate)s have a characteristic interplanar d-spacing of 4.2 Å[4, 7-9]. From this interplanar distance, the average diameter of a side chain crystalline methylene unit is determined to be 4.85 Å. The symmetrical nature of the alkyl side sides and rotation about the long alkyl axis leads to efficient hexagonal packing in *n*-alkyl acrylate polymers. A typical layout of the hexagonally packing of the side chains is shown in Figure 2.2

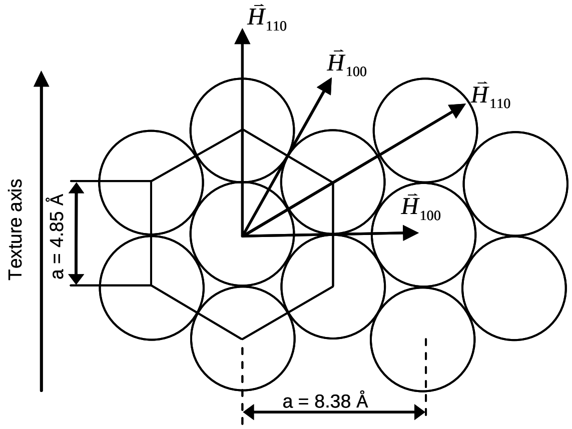

Figure 2.2: A schematic of hexagonal packing of side chains adapted from ref[9].

It is generally accepted that the flexible main chains allow the side chains to organize into a one-layer or two-layer arrangement forming a layered lamellar structure similar to that illustrated in Figure 2.3. This layered arrangement results in a long period d-spacing observed by small angle x-ray scattering. In the one-layered structure, the main chains of two adjacent molecules aligned end to end such that this d-spacing is defined by twice the length of the side chains with a small gap space between them. Shibayev et al. found that the long period of poly(hexadecyl acrylate) compared well with twice the long period of the side-chain analogue margaric acid[9]. However, the two-layer structure has a d-spacing similar to the length of approximately one side-chain length as a result of interdigitating side chains. Although both structures have been observed in crystalline poly(*n*-alkyl acrylate)s, the single layered arrangement is the more dominate which is attributed to more uniform packing. Crystallization conditions can influence the formation of single or double layer packing and the population of each.

Poly(*n*-alkyl methacrylate)s crystallize into the double layer arrangement commonly ascribed to the more restrictive main chain due to the bulky methyl unit. The packing of poly(*n*-alkyl methacrylate)s crystalline side chains is also less efficient due to the incorporation of chain ends within the two-layer packing. The higher melting points and crystallinity, i.e. to more uniform packing, of poly(*n*-alkyl acrylate)s than poly(*n*-alkyl methacrylate)s as a function of side chain length are often explained by contrasting crystallization arrangements[4, 7].

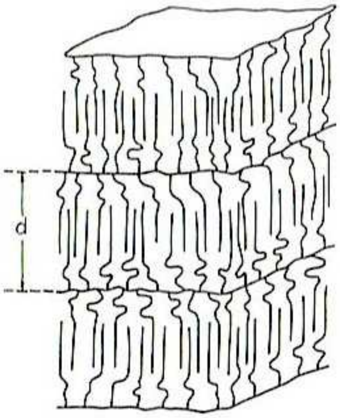

Figure 2.3: A schematic of the long d-spacing between the side chains of poly(*n*-alkyl acrylate)s in the one-layer packing arrangement.

The highly organized alternating amorphous-crystalline phase regions are not exclusively characteristic of poly(*n*-alkyl acrylates). Similar arrangements have been observed in biomaterials such as polypeptides and polysaccharides[4, 10]. The layered structure of poly(*n*-alkyl acrylate)s also resemble the smectic layers of liquid crystals. The smectic phase consists of well-defined layers of lattice ordered molecules with some degree of directional orientation. Side-chain liquid crystalline polyacrylates containing 4-methoxyphenyl 4-hexyloxybenzoate or 4-cyanophenyl 4-hexyloxybenzoate mesogenic side groups have reduced mobility in the more ordered nematic and smectic phases as evidenced by higher activation energies of gas permeation[11]. Molecular ordering whether by side-chain mesogenic groups or alkyl groups restricts the mobility of the smectic or amorphous phases, respectively which is evident from properties such gas transport behavior[11, 12].

GAS TRANSPORT IN SEMI-CRYSTALLINE RUBBERY POLYMERS

Gas transport properties directly depend on the nature of the polymer (i.e. the free volume and the segmental mobility). Small molecule gas permeation through dense or nonporous polymer films occurs by a solution-diffusion mechanism. Gas molecules are sorbed into the upper polymer surface at high pressure, diffuse through the film and then desorb downstream on the low pressure side. The gas permeability coefficient, P

$$P = D \cdot S \tag{2.1}$$

is the product of D, the gas diffusion coefficient and S, the solubility coefficient. The diffusion coefficient is a kinetic parameter that reflects the mobility of the penetrant in the polymer matrix and the solubility coefficient is a thermodynamic parameter that depends on the polymer-penetrant interactions as well as penetrant condensability. Sorption of simple gases through rubbery polymers at moderate pressures is well-described by Henry's law

$$C = S \cdot p \tag{2.2}$$

where C, the penetrant equilibrium concentration, is proportional to p, its partial pressure, and S, the solubility coefficient of the gas in the polymer. In the case of semi-crystalline poly(*n*-alkyl acrylates), gas transport is more complex than in simple amorphous polymers owing to side-chain crystallinity. Michaels et al. introduced a two-phase model that modified the solubility and diffusion coefficients to account for the presence of crystallites in semi-crystalline polyethylene[13, 14]. Experimental results suggested that the solubility in several polyethylenes of varying crystallinity is proportional to the amorphous volume fraction, α

$$S = \alpha \cdot S^* \tag{2.3}$$

where S^* is the solubility coefficient in a completely amorphous polymer sample. These results imply that the crystals are impenetrable to gas permeation. The crystals affect the diffusion coefficient in two separate ways as described by the following.

$$D = D^* / \tau\beta \tag{2.4}$$

where D^* is the penetrant diffusion coefficient in the amorphous phase, τ is a geometric impedance factor, and β is a chain immobilization factor. The geometric impedance factor accounts for the tortuous path gas molecules must take through the amorphous phase since they cannot permeate through the crystallites. The chain immobilization factor accounts for reduced mobility of the amorphous phase caused by the crystallites. Dielectric relaxation measurements show reduced mobility in semi-crystalline state of comb-like polymers due to the presence of crystallites[15]. Finally, the permeability coefficient can be expressed as follows

$$P = P^* \alpha / \tau\beta \tag{2.5}$$

where P^* is the permeability of a completely amorphous sample. The thermal history of a polymer can significantly affect crystallite size, shape, and orientation and in turn affect permeation properties.

The temperature dependence of the gas permeability coefficient is generally described by an Arrhenius relationship

$$P = P_o \exp\left(-E_p / RT\right) \tag{2.6}$$

where E_p is the activation energy and P_o a constant. The diffusion and solubility coefficients have similar Arrhenius expressions where upon substituting into Equation 1 the E_p can be expressed as

$$E_p = E_D + \Delta H_S \tag{2.7}$$

where E_D is the activation energy for diffusion, and ΔH_S is the heat of solution for dissolution of the penatrant in the polymer. If α, β and τ are all constant, then the activation energy for gas permeation in the semi-crystalline state should be the same as in the molten state; however, this is generally not the case[16], and this is usually attributed to the temperature dependence of β when the crystalline content and morphology is fixed[16]. However, in some cases, melting can occur progressively over a range of temperatures such that α and τ are changing, and this will increase the effective activation energy for permeation which can be useful for making membranes that are more thermally responsive as needed for some packaging applications.

DESIGNING THERMALLY RESPONSIVE MEMBRANES USING POLY (*N*-ALKYL ACRYLATE)S

Copolymers and homopolymers of *n*-alkyl acrylates have long been used as pour point depressants and viscosity index improvers in lubricating oils due to their unique side-chain crystallization properties[17]. More recently, poly(alkyl acrylate)s have been used to increase the viscosity of aqueous ophthalmologic gels for increased residence time on the eye[18]. Not only does poly(alkyl acrylate)s continue to be useful as viscosity index improvers in many applications, these semi-crystalline polymers also offer other property improvements such as increased permeability as phase changes occur with increases in temperature. Discontinuities in transport properties at the transition temperature are prevalent in semi-crystalline polymers; however, the increase in permeability is largest for poly(*n*-alkyl acrylate)s[19].

Mogri and Paul found that gas permeability increases, for *n*-alkyl acrylate homopolymers, as a function of side-chain length for completely amorphous polymers ($n < 10$ or $T > T_m$) due to increased free volume. The typical permeation response for homopolymers is shown in Figure 2.4. Below the melting point of poly(*n*-alkyl acrylate)s that crystallize, the permeability is greatly reduced owing to the tortuous path the gas molecules must follow within the amorphous phases since the crystallites are impenetrable and the constraints these crystallites impose on molecular motions, within the amorphous phase. There is a jump in the gas permeability by a factor of 10 to 100 upon traversing the melting point that is primarily diffusion based. A similar jump is observed for copolymers of *n*-alkyl acrylate monomers since they show a single melting point following the rules of co-crystallization or melting point depression depending on the side-chain length[5, 20].

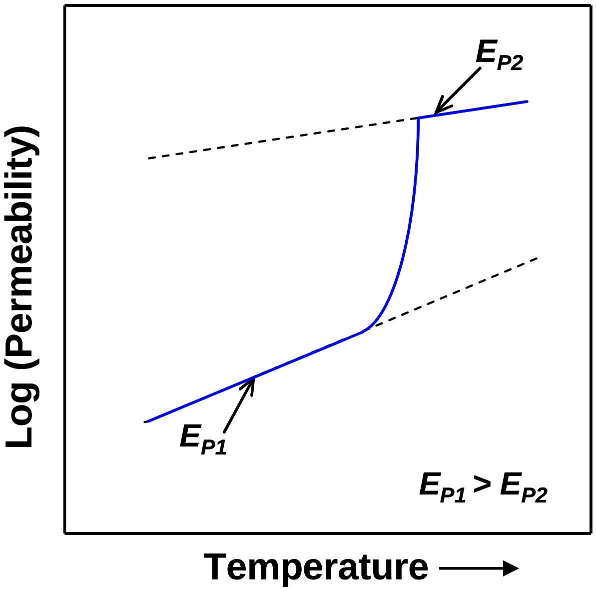

Figure 2.4: Typical semi-crystalline poly(*n*-alkyl acryalte) permeation response adapted from ref[21].

The increase in permeability that results from melting the side-chain crystals provides an interesting avenue to create membranes that are more thermally responsive than can be achieved by the usual Arrhenius response. One approach would be to create laminates composed of successive layers of poly(*n*-alkyl acrylate) of varying side chain length as suggested in Figure 2.5. Each layer, *i* has a different melting point with a corresponding permeability jump. The composite permeability coefficient can ideally be described by a series model

$$\frac{l}{P} = \sum_{i=1}^{N} \frac{l_i}{P_i} \tag{2.8}$$

where l_i is the thickness of polymer *i* and P_i is the permeability of polymer *i*. In principle, as more layers are added the more closely the successive step functions approach a monotonic function like the dotted line shown. This would be facilitated by broadening the crystallite distribution and allowing crystallites to melt over a wider range of temperatures thereby increasing the breadth of the permeability jump. An interesting alternative to the highly structured laminates is to make blends of two or more homopolymers or copolymers of *n*-alkyl acrylate monomers of varying *n*. The basic issues associated with this strategy are explored in Chapter 3.

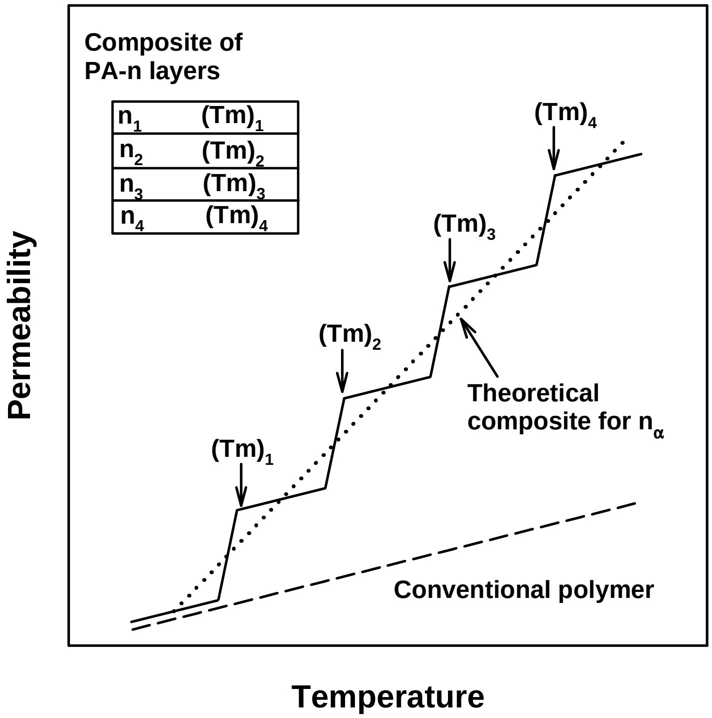

Figure 2.5: Illustrates the use of laminates with i layers of poly(*n*-alkyl acrylate)s with varying side-chain length, *n*, to increase thermal responsiveness.

MODIFIED ATMOSPHERIC PACKAGING

Over the last decade, the steady increasing demand for fresh fruits and vegetables has been fueled by consumer desire for a healthier lifestyle, as encouraged by USFDA to consume 5-9 servings of fruits and vegetables per day[22, 23]. Consumers search for the fresh produce with the best texture and appearance as possible. Organic foods are often viewed as healthier, absent the use of synthetic chemicals, antibiotics and hormones. Consequently, organic cropland has increased by 1 million acres from 1995 to 2003 and retail organic sales reached $10.4 billion in 2003 accounting for nearly 2% of all U.S.

food sales[23]. In this thriving industry, on average approximately half of fruit and vegetable production is allocated for fresh produce sales where the remainder is used for processing such as canned and juice products[24]. Fresh produce losses can be substantial depending on the produce type and the post-harvest distribution process. In a recent report, fresh fruit and vegetable losses in developed countries were estimated at an average of 12% from production to retail stores and 20% at retail, food service and consumer sites[25, 26]. There are obvious economic benefits to reducing fresh produce losses. Currently, proper low temperature management throughout the transport and storage processes is the primary method used to help extend and maintain produce freshness thereby reducing losses. Modifying the gaseous atmosphere surrounding produce, reduced O_2 and elevated CO_2 concentrations, is a supplemental method used to also help extend shelf and delay senescence by inhibiting metabolic activity of produce.

Modified atmospheric (MA) packaging and controlled atmospheric (CA) storage are two techniques used to alter the gas concentration surrounding the product. CA storage is a bulk method used during storage and transport that actively maintains a defined gas concentration by use of gas exchange membrane units. MA packaging is a passive method that utilizes the packaging film transport properties to regulate the O_2 entering and the CO_2 leaving smaller retail packages. Although both methods are applicable during the transportation and bulk storage, MA packaging is applicable and most beneficial from harvest to consumption. Modified atmospheres help inhibit the metabolic process that brings about physiological changes that commonly characterize produce quality and, in some cases, indirectly arrest pathological disorders.

Unlike other perishable products, e.g. meats, fruits and vegetables continue to undergo respiration post-harvest. Respiration is an oxidative process where complex substrates are broken down into CO_2 and H_2O with the release of heat, metabolic energy and production of other molecules during a series of metabolic steps. Generally, the aerobic respiration process can be represented by the following overall chemical equation where glucose represents the substrate

$$C_6H_{12}O_6 + 6O_2 \rightarrow 6CO_2 + 6H_2O + chemical\ energy + heat \tag{2.9}$$

Or more generally were $(CH_2O)_n$ represents a the carbohydrate molecule oxidized during the respiration process. The respiration rate reflects the rate at which catabolic changes take place and the deterioration rate of the produce, which is quantified as the rate of O_2 consumed or CO_2 generated. Often, the respiration rate is represented by the respiratory quotient, RQ, which is the ratio of CO_2 produced to the O_2 consumed. Produce are largely made up of water and carbohydrates (cellulose, starches and sugars) and low composition of lipids; thus, respiration rates inherently dependent upon the type of substrate, maturity and variety[27].

It has long been known that reduced O_2 and elevated CO_2 levels inhibit produce shelf life. For each produce type and cultivar, there is an optimal range of oxygen and carbon dioxide concentrations that help to best suppress respiration and retard the ripening process. Although these modified atmospheres help extend shelf life, when oxygen levels diminish to very low concentrations, typically below 1 – 2 % O_2, anaerobic conditions ensue that can cause undesirable changes in flavor and create favorable conditions for harmful anaerobic pathogens, e.g., Clostridium botulinum. The challenge of MA package has been to design packages with the proper permeation characteristics to match the respiration rates of produce such that anaerobic conditions are never reached.

PAUL-CLARKE MAP MODEL FOR RETAIL PACKAGE COMPRISED OF A HIGH-FLUX MEMBRANE AND PERFORATIONS

There has been much effort to create modified atmospheres using low cost alternatives such as passive methods. The MA packaging method involves balancing the gas exchange of the produce and the packaging material, thus it is important to characterize the respiratory process of produce and the transport processes of packaging materials. Predicting the viability of a polymer for packaging of a particular produce prior to implementation is an extremely useful tool. Many researchers [28-34] have developed models to predict the modified atmosphere of an individual retail package that depends on the interaction of the respiration rate of the produce and the permeation rate of the packaging material. Produce packages have utilized microporous, such as $CaCO_3$ filled polymers, and perforated films[35]. Paul and Clarke developed a model for predicting the internal composition of small retail size packages, that consists of a high-flux membrane label and perforations or holes as shown in Figure 2.6.

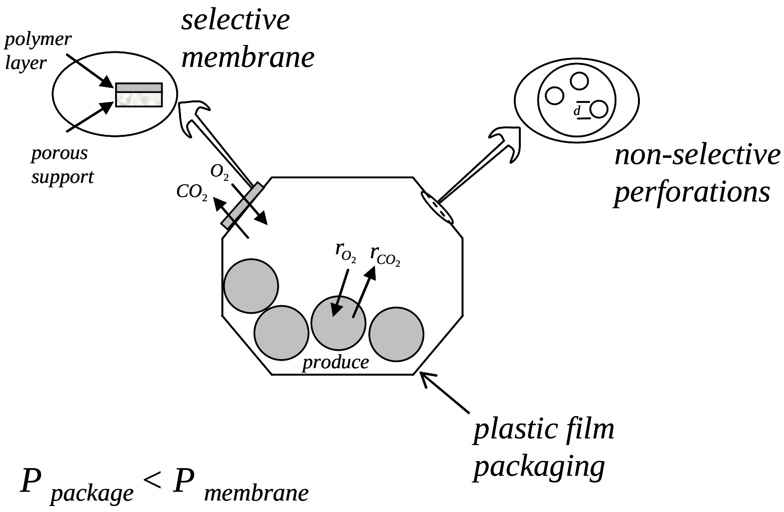

Figure 2.6: A schematic of a package design for MA packaging with a selective membrane of high flux and a non-selective membrane. Adapted from Paul and Clarke[28].

A series of balances were applied to the MA package to obtain an expression for the O_2 and CO_2 concentrations inside the package.

$$x_{CO_2} = \frac{r_{O_2} RQ}{K_{O_2}[K_{CO_2}/K_{O_2}) + \beta]p_t} = \frac{Wf(x_{O_2}, x_{CO_2})RQ}{A_m(P_{mO_2}/\ell_m)[(K_{CO_2}/K_{O_2}) + \beta]p_t} \tag{2.10}$$

The CO_2 mole fraction is a function of the membrane label properties (K_i the parallel permeation coefficient of gas i through the package film and the high-flux membrane, A_m and ℓ_m the area and thickness of the membrane, β is the ratio of a diffusive transport parameter H to the parallel permeation coefficient, K_{O_2}), produce properties (W the weight of the produce, RQ the respiratory quotient, and the respiration rates that are a function of x_{O_2}, x_{CO_2} and temperature) and the total pressure, p_t. The O_2 concentration is expressed as

$$x_{O_2} = 0.21\left[1-\left(\frac{W}{A_m}\right)\times\frac{f(x_{O_2}, x_{CO_2})RQ}{(P_{mO_2}/\ell_m)(x_{CO_2})_0[(K_{CO_2}/K_{O_2}+\beta]p_t}\right] \qquad (2.11)$$

where $(x_{CO_2})_0$ is the CO_2 concentration at zero percent oxygen. This parameter is a useful mathematical quantity that can be related to physical quantities as follows

$$(x_{O_2})_0 = 0.21\frac{1+1.266\beta+0.266(K_{N_2}/K_{O_2})}{[(K_{CO_2}/K_{O_2})+\beta]/RQ+0.266(K_{N_2}/K_{O_2}+\beta)} \qquad (2.12)$$

The concentration for a retail package with or without a high-flux membrane label and perforations can be determined from Equations 2.10 and 2.11. This is useful for evaluating possible films to create optimal concentrations for produce.

REFERENCES

1. Jordan EF, Jr., Feldeisen DW, and Wrigley AN. Journal of Polymer Science, Polymer Chemistry Edition 1971;9(7):1835-1852.
2. Yokota K, Kougo T, and Hirabayashi T. Polymer Journal (Tokyo, Japan) 1983;15(12):891-898.
3. Hsieh HWS, Post B, and Morawetz H. Journal of Polymer Science, Polymer Physics Edition 1976;14(7):1241-1255.
4. Plate NA and Shibaev VP. Comb-shaped polymers and liquid crystals. New York: Plenum Press, 1987.
5. O'Leary KA and Paul DR. Polymer 2006;47(4):1226-1244.
6. Chapman D. Journal of the Chemical Society 1957:4489-4491.
7. Greenberg SA and Alfrey T. Journal of the American Chemical Society 1954;76:6280-6285.
8. Kaufman HS, Sacher A, Alfrey T, and Fankuchen I. Journal of the American Chemical Society 1948;70:3147.
9. Shibaev VP, Petrukhin BS, Zubov YA, Plate NA, and Kargin VA. Vysokomolekulyarnye Soedineniya, Seriya A 1968;10(1):216-226.
10. Compan V, Zanuy D, Andrio A, Morillo M, Aleman C, and Munoz-Guerra S. Macromolecules 2002;35(11):4521-4530.
11. Chen DS, Hsiue GH, and Hsu CS. Makromolekulare Chemie-Macromolecular Chemistry and Physics 1992;193(6):1469-1479.
12. Mogri Z and Paul DR. Journal of Polymer Science, Part B: Polymer Physics 2001;39(10):979-984.
13. Michaels AS and Bixler HJ. Journal of Polymer Science 1961;50:413-439.
14. Michaels AS and Parker RB, Jr. Journal of Polymer Science 1959;41:53-71.
15. Alig I, Jarek M, and Hellmann GP. Macromolecules 1998;31(7):2245-2251.
16. Mogri Z and Paul DR. Polymer 2001;42(18):7765-7780.
17. Jordan EF, Jr., Smith S, Jr., Parker WE, Artymyshyn B, and Wrigley AN. Journal of Applied Polymer Science 1978;22(6):1509-1528.
18. Lobering H-G and Polzere H. Gel, especially for ophthalmology. United States: Medproject Pharma Entwicklungs and Vertriebs Gesellschaft, 1993.
19. Barrer RM and Chio HT. Journal of Polymer Science: Part C 1965(10):111-138.

20. O'Leary KA and Paul DR. Polymer 2006;47(4):1245-1258.
21. Mogri Z. Gas transport properties of side-chain crystalline polymers. Chemical Engineering. Austin: University of Texas at Austin, 2001. pp. 289.
22. Ooraikul B, M.E. Stiles, and Editors. Modified Atmosphere Packaging of Food. New York: Ellis Horwood, 1991.
23. Greene C. United States Department of Agriculture: Economic Research Service, www.ers.usda.gov. AREI Chapter 4.9: U.S. Organic Agriculture.
24. Lucier G, Pollock S, Ali M, and Perez A. Fruit and Vegetable Backgrounder. Electronic Outlook Report from the Economic Research Service, United States Department of Agriculture, www.ers.usda.gov, 2006.
25. Kader AA. HortScience 2003;38(5):1004-1008.
26. Kader AA. Increasing food availability by reducing postharvest losses of fresh produce. In: Mencarelli R and Tonutti O, editors. Proceedings of the Fifth International Postharvest Symposium, 2005. pp. 2169-2175.
27. Kader AA. Respiration of Gas Exchange of Vegetables. In: Weichmann J, editor. Postharvest physiology of vegetables. New York: Marcel Dekker, Inc., 1987. pp. 25-43.
28. Paul DR and Clarke R. Journal of Membrane Science 2002;208(1-2):269-283.
29. Edmond JP, Chau KV, and Brecht JK. Modeling respiration rates of blueberry in a perforation-generated modifeid atmosphere package. Proceedings from the Sixth International Controlled Atmosphere Research Conference. Cornell University, Ithaca, New York, 1993. pp. 134-144.
30. Sanz C, Perez AG, Olias R, and Olias JM. Food Science and Technology International 2000;6(1):33-38.
31. Talasila PC and Cameron AC. Journal of Food Science 1997;62(5):926-930.
32. Fishman S, Rodov V, Peretz J, and Ben-Yehoshua S. Journal of Food Science 1995;60(5):1078-1087.
33. Fonseca SC, Oliveira FAR, Lino IBM, Brecht JK, and Chau KV. Journal of Food Engineering 2000;43(1):9-15.
34. Makino Y, Iwasaki K-i, and Hirata T. Journal of Agricultural Engineering Research 1997;67:47-59.
35. Kano Y, Akiyama S, Kasemura T, and Kobayashi S. Polymer Journal 1995;27(4):339-346.

Chapter 3: Gas transport of poly (*n*-alkyl acrylate) and poly (*m*-alkyl acrylate) blends

INTRODUCTION

Side-chain crystalline homopolymers give rise to a dynamic change in the permeability coefficient at the melting temperature of the crystallites. The melting temperature increases with an increase in the side-chain length n, thus, the side chain length can be used as a tunable parameter to control the increase in permeability. In this chapter, the gas permeation response of poly(*n*-alkyl acrylate) and poly(*m*-alkyl acrylate) blends as a function of temperature are examined for varying side chain lengths, n and m, and blend composition in the semi-crystalline and molten states. In addition, the homogeneity of these systems is examined to understand the compatibility of the components for comparative and predictive purposes.

Thermal behavior of poly(*n*-alkyl acrylate)s is a rather good indicator of the general permeation response; therefore, detailed thermal analyses is used to understand the crystallization in the blends and parenthetically their permeation responses. It is shown that blending poly(*n*-alkyl acrylate)s of various side-chain lengths provide a practical route to more thermally responsive materials for applications such as modified atmospheric packaging.

EXPERIMENTAL

Polymerization and material characterization

Hexyl (A-6), octyl (A-8), and decyl (A-10) acrylate monomers were purchased from Scientific Polymer Products. Tetradecyl (A-14), hexadecyl (A-16), octadecyl (A-18) and behenyl (A-22) acrylate monomers were donated by Landec Corporation. All monomers were dissolved in toluene and purified over Sigma-Aldrich aluminum oxide to remove a low concentration of inhibitor, monomethyl ether hydroquinone (MEHQ).

Amorphous monomers at room temperature are mixed directly with solvent; however, A-18 and A-22 monomers were more carefully handled as they tend to crystallize and stratify. Whatman® 0.2µm filter membrane discs were used to filter out particulate impurities from the monomers; following this, the monomers were ready for polymerization. Free radical solution polymerization was performed using 35 wt% monomer in toluene at 60°C for 24 hours to achieve nearly 100% conversion of atactic polymer[1]. Solutions were charged to a 3-neck round bottom flask and purged with N_2 to remove oxygen (possible inhibitor) and subsequently charged with purified initiator, α, α′-azobis(isobutyronitrile) (AIBN)[2]. After 24 hours, the polymer product was slowly precipitated into ethanol, recovered and purified by using toluene/ethanol re-precipitation through three cycles. The polymers were characterized by gel permeation chromatography (GPC), calibrated using polystyrene standards, to determine relative molecular weights. A Perkin-Elmer DSC-7 differential scanning calorimeter, equipped with an intercooler capable of measurement from -40°C, was used to determine the melting points and heats of fusion. The DSC-7 was calibrated with certified reference materials, indium and zinc. However, the semi-crystalline materials analyzed had comparatively low melting points; therefore, 4-nitrotoluene was also used as a calibration standard. All samples were subjected to a series of heating and cooling cycles to eliminate the influence of previous thermal history, thus, to ensure identical crystallization conditions for comparative morphologies. Therefore, all thermal properties were analyzed on second heating cycles from a 1°C/min cooling rate with subsequent heating at 10°C/min to ensure a common thermal history.

Membrane formation

All homopolymer and polymer blend films were formed by solution casting techniques with the exception of PA-8, PA-10 and PA-14. The latter are all soft, tacky, amorphous polymers at room temperature; therefore, they were cast directly onto a custom composite support[3] in an enclosed oven at elevated temperatures. Samples were allowed to equilibrate forming a smooth, uniform film. Sample thickness was calculated by mass balance techniques using an estimated amorphous density of 0.985 g/cm^3. All other polymer systems were solid, brittle materials at room temperature. This brittleness stems from the side-chain crystalline character and is not owing to low sample molecular weight[4, 5]. These polymer systems were solution cast from 5-10wt% polymer in toluene onto silicon wafers and covered for slow evaporation in a fume hood. Films formed in this way were subsequently removed by using water to release them from the silicon surface and placed under vacuum at elevated temperatures for further solvent removal. Depending on the melting temperature of the polymers involved, removal from the casting surface could require using cool water and subsequent cool storage. PA-8/PA-10 blends were formed by this same method and then cast directly onto the custom composite support similar to the above mentioned amorphous samples[6]. For polymers that were solid at room temperature, the polymer thickness was measured using a micrometer before assembling the composite.

For gas permeability measurements of poly(*n*-alkyl acrylate) films, a modified sample assembly was developed in our laboratory[3] that supported their brittle nature below the melting point and liquid-like behavior above Tm. An asymmetric Whatman Anopore$^{\text{TM}}$ porous ceramic disc without the annular polypropylene support ring was used for mechanical support. The ceramic discs have 200 Å pores on the surface that extend to ~1µm below the surface and connect to 2000 Å pores. Permeability measurements above the melting point required a suitable polymer coating to prevent molten polymer from flowing into the ceramic disc pores and changing the apparent polymer thickness. Poly (2,6-dimethyl- 1,4 phenylene oxide) (PPO), from General Electric Plastics with an intrinsic viscosity of 0.46 dL/g, MW= 46,000 and a T_g~220^{o}C, was used to coat the top surface of the ceramic disc. A trichloroethylene solution containing 13wt% PPO was deposited onto the ceramic disc using 2 mL syringes spread by a scoopula which removed excess PPO solution which left a thin film that completely seals the ceramic pores.

Gas permeation measurements

Permeability experiments were conducted using constant volume permeation cells, at an upstream pressure of 2 atm[7], immersed in a water-bath equipped with a temperature controlled Haake circulator. Permeability measurements were made with a range of gases, He, H_2, O_2, N_2, CH_4 and CO_2, from Matheson Tri-gas with a minimum 99.9% purity. However, for brevity, we report here only the permeation results of O_2 as a typical example with an occasional comparison to N_2 and CO_2 as these gases are of interest for MAP. The permeation results for other gases may be found in Appendix A. Prior to testing the *n*-alkyl acrylate polymers, the quality of the support assembly was determined by comparing gas permeation selectivities with literature values for PPO to ensure that the pores were completely sealed. Upon adequate support selection, the permeance of the thin, glassy PPO layer was characterized to account for physical aging. After quantifying the physical aging response, the poly (*n*-alkyl acrylate) film was placed on top of the assembly for permeability determination. The measured composite permeation resistance was corrected for the contribution of the PPO layer, which was always less than 5% of the total except for CH_4 where it sometimes was as high as 15%, to obtain just the contribution of the poly (*n*-alkyl acrylate) film.

As mentioned previously, thermal history can have a discernable effect on phase morphology and subsequently on permeation properties. Therefore, a Linkman hot-stage, model HFS91, and a programmable controller, model TMS91, system was used to establish a known polymer thermal history. Samples were heated to approximately $10^{o}C$ above the polymer melting point and held for sufficient time to completely remove any residual crystallinity and then cooled mostly at a rate of $1.0^{o}C/min$ except for a few variable rate experiments.

RESULTS AND DISCUSSION

Poly (*n*-alkyl acrylate) blend compatibility

A fundamental issue is whether blends of a poly(*n*-alkyl acrylate) and a poly(*m*-alkyl acrylate) are miscible in the molten state, and if so, do they co-crystallize on cooling. Clearly, both issues may be influenced by the values of m and n; the closer m and n are to each other, the more likely the two polymers are to be miscible and exhibit co-crystallization. At a practical level, the question is over what ranges of m and n can useful membranes be cast by the procedures used here. To explore this, 50/50 weight blends were prepared by solution casting films of all combinations of poly(*n*-alkyl acrylate) homopolymers with side-chain lengths, m and n, from 6 to 22. Each binary homopolymer blend was visually inspected for homogeneity. Figure 3.1 shows a matrix of the results of this simple assessment where the coordinates represent the homopolymer components of a binary blend by the lengths of their side chains, n and m. The solid line represents the limiting case of blends with the same side-chain length which, of course, are homogenous. Viable homogeneous blends are represented by the filled circles. These blends were optically clear in the melt and macroscopically homogenous after crystallization. PA-8 and PA-10, the only feasible amorphous blend, was clear at room temperature and for the temperature range of interest. Semi-crystalline blends were transparent above the melting point and by nature opaque at room temperature with varying degrees of clarity depending on m and n. Inhomogeneous blends are indicated by open circles. Although all inhomogeneous blends appeared optically clear in the amorphous and melt states, upon cooling or crystallization two phases were easily distinguishable. Heterogeneous blends containing two amorphous components resulted in a transparent mixture with two separate phases noticeable only by slight density differences. Inhomogeneous systems with one amorphous and one semi-crystalline component and with two semi-crystalline component mixtures resulted in varying heterogeneous morphologies influenced by the blend components (n and m) and composition. For the most part, the components of inhomogeneous blends exhibited macroscopic segregation.

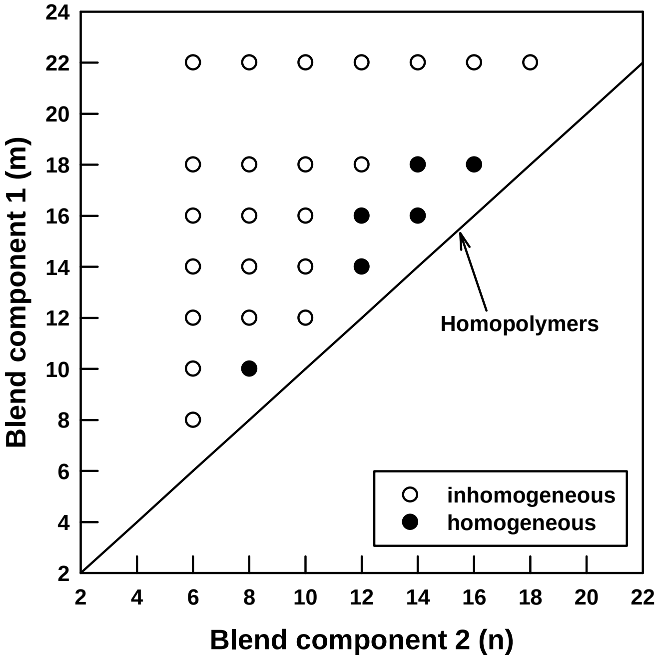

Figure 3.1: Map of film homogeneity for 50/50 weight poly(*m*-alkyl acrylate) and poly(*n*-alkyl acrylate) blends with side-chain lengths, m and n; the filled circles represent homogeneous mixtures while the open circles represent grossly heterogeneous mixtures.

Thermal analyses conducted on samples from various regions within a given polymer-polymer mixture resulted in widely varying thermal properties indicating gross phase segregation using this film preparation technique. In general, homogeneity was observed when the difference in side-chain length (n - m) between components was small, $|n - m| \leq$ 2-4 methylene units, and when the components possessed similar crystallization characteristics. Surprisingly, neither PA-10 nor PA-22 resulted in any homogenous semi-crystalline blends regardless of the choice of the other component.

It would be useful to know over what range of *m* and *n* these blends are miscible in the melt state; however such a determination is a very challenging experimental problem. Blend miscibility is often assessed by determining glass transition temperature

(T_g) behavior. However, the glass transitions of poly(*n*-alkyl acrylates) occur at very low temperatures and are difficult to measure with any accuracy and reliability owing to the side-chain crystallinity. It was well beyond the scope of this work to pursue the issue of miscibility further.

Thermal characterization

Thermal characterization has proved to be a useful tool for predicting the permeation response of *n*-alkyl acrylate polymers as a function of temperature[8-10]. Table 3.1 summarizes the melting temperature, heat of fusion, crystallinity and molecular weight of the semi-crystalline ($n \geq 10$) n-alkyl acrylate homopolymers, with thermal histories, used in this study. The melting point and the heat of fusion, ΔH_f, or crystallinity, x_c, increase as the side-chain length increases[8].

Table 3.1: Thermal and physical properties of semi-crystalline polymers studied in this work.

Polymer	T_m (°C)	ΔH_f (cal/g)	x_c	M_w
PA-14	22.4	16.6	0.32	307,000
PA-16	36.2	19.5	0.37	204,000
PA-18	50.2	22.9	0.44	175,000

Figure 3.2 shows DSC thermograms for blends of PA-14 and PA-18 which are typical of all the blends of semi-crystalline poly (*n*-alkyl acrylate) and poly(*m*-alkyl acrylate) blends examined. For the pure components, the peak width decreases as side-chain length increases suggesting a narrowing of the crystallite distribution[11]. The blends show two endothermic peaks implying independent crystallization of the respective components (i.e., no co-crystallization). The magnitude of the component peaks became larger as the content of that component in the blend increases as expected. The melting point for each component, taken as the apex of the peak, shifts to a slightly lower temperature upon dilution by the other polymer, as shown in Figure 3.3, suggesting some alteration of the crystal formation due to blending; however, the effect is very small

with the maximum shift in Tm being of the order of 2°C. Extracting heats of fusion for each component from the thermograms requires some assumptions about how to construct the baseline and interpret of some subtle features of the DSC traces. A small but distinguished third peak can be seen between the peaks of the two blend components; this intermediate peak could be a result of co-crystallization or simply overlap from the individual melting transitions. This peak is visible at various scanning rates suggesting that it is not an artifact.

A straight [12] baseline construction was used in the two methods of interpretation described next. In the first method, a nearly horizontal, straight baseline was drawn from the initial point of deviation to the point where the signal returned to the baseline, enclosing the entire area under the PA-14, PA-18 and the intermediate peaks as illustrated in Figure 3.4. The area defined in this way is considered to be the total heat of fusion for the blend, ΔH_{blend}. In the second method, separate baselines are constructed for each major peak. The area under the first peak is designated as the heat of fusion for the low melting component or ΔH_1. Similarly, the area under the second peak is designated as the heat of fusion for the higher melting component or ΔH_2. The sum of the individual heats of fusion for each component, $\Delta H_{sum} = \Delta H_1 + \Delta H_2$, could also be interpreted as the total heat of fusion for the blend components.

Figures 3.5 – 3.7 show the heat of fusion values calculated by each of these methods, ΔH_{blend} represented by filled circles and ΔH_{sum} by open circles. If the individual components in the blend crystallize without any interference from the other blend component, then one would expect heats of fusion for the individual components or the total heat of fusion for the blend as a function of blend composition to form straight lines connecting the end points at the two composition extremes represented as dashed lines in Figures 3.5 – 3.7. The values calculated by the baseline construction methods described above always fall below these additivity relations. The values of ΔH_{blend} come closer to this ideal than the attempts to separate the melting processes of the two components. In general, it seems clear for these blends that one component has some effect on the crystallization and, hence, melting behavior of the other. Owing to the difficulties associated with knowing the correct baseline construction, it is not possible to be more precise about these effects. Certainly if any degree of co-crystallization occurs, it is very slight indeed.

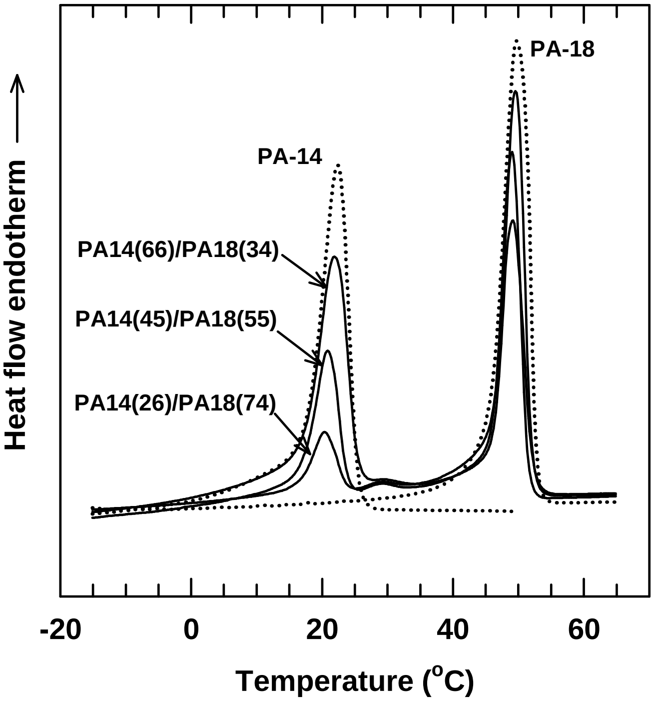

Figure 3.2: DSC scans for PA-14/PA-18 blends of various compositions

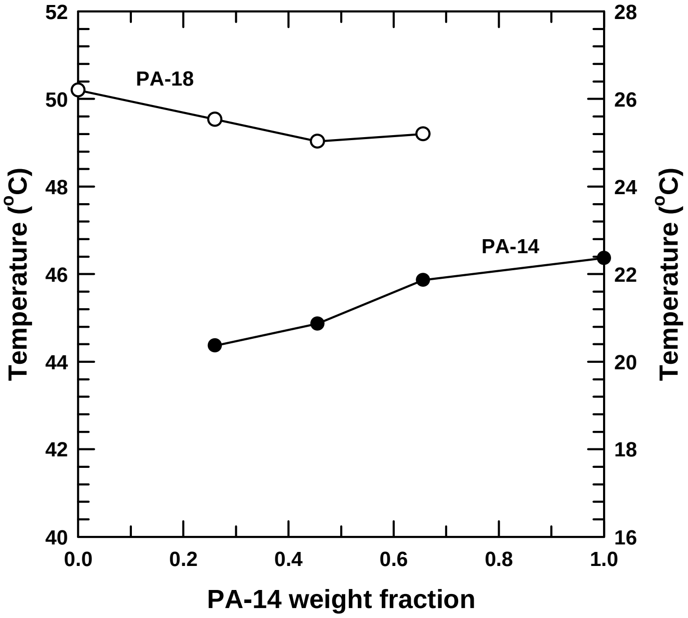

Figure 3.3: Melting temperatures of the components in PA-14/ PA-18 blends as a function of blend composition.

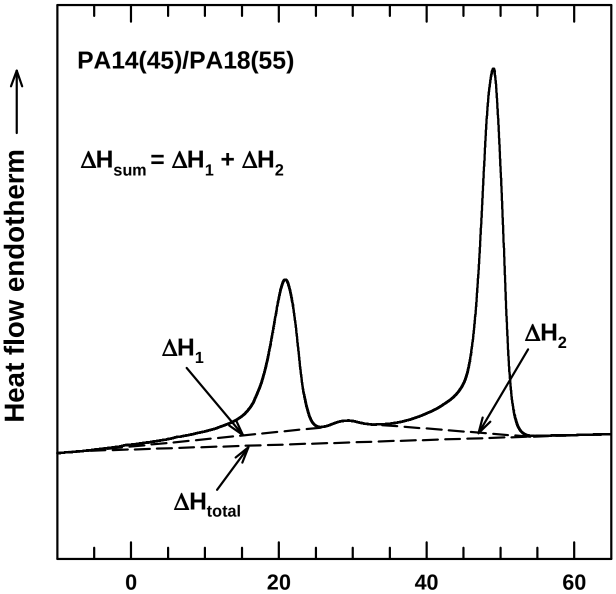

Figure 3.4: Illustration of baseline construction methods used to compute heats of fusion from blend thermograms.

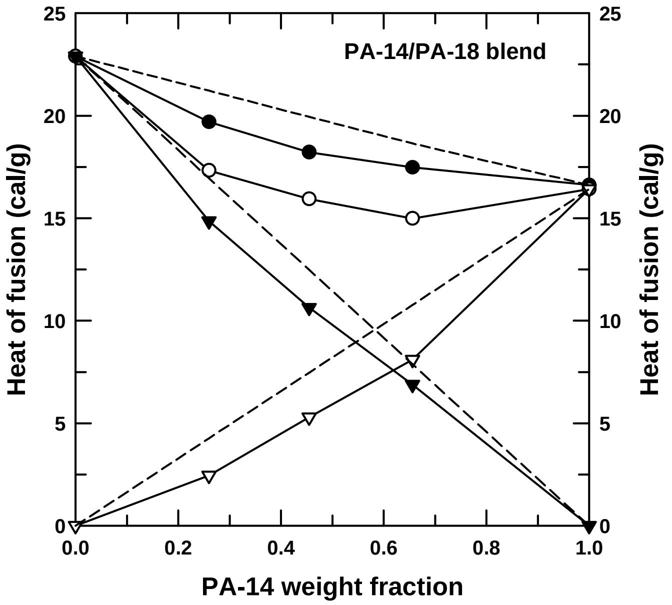

Figure 3.5: Heats of fusion as a function of composition for PA-14/ PA-18 blends.

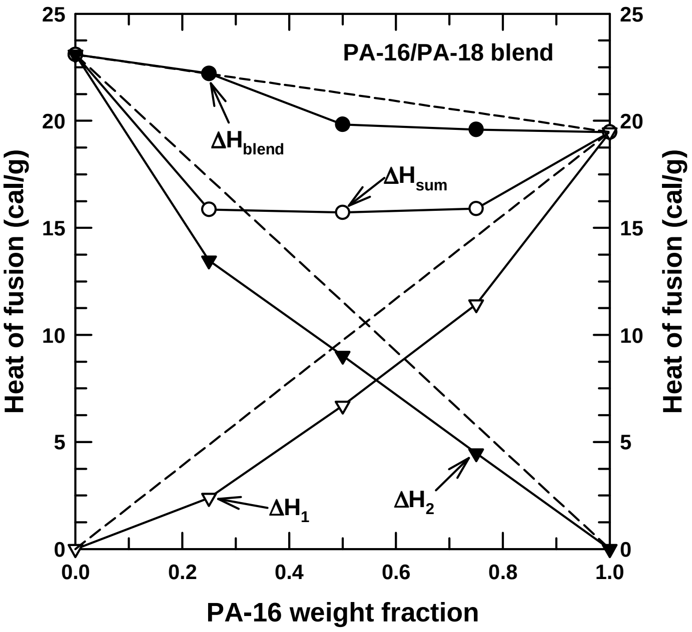

Figure 3.6: Heats of fusion as a function of composition for PA-16/PA-18 blends.

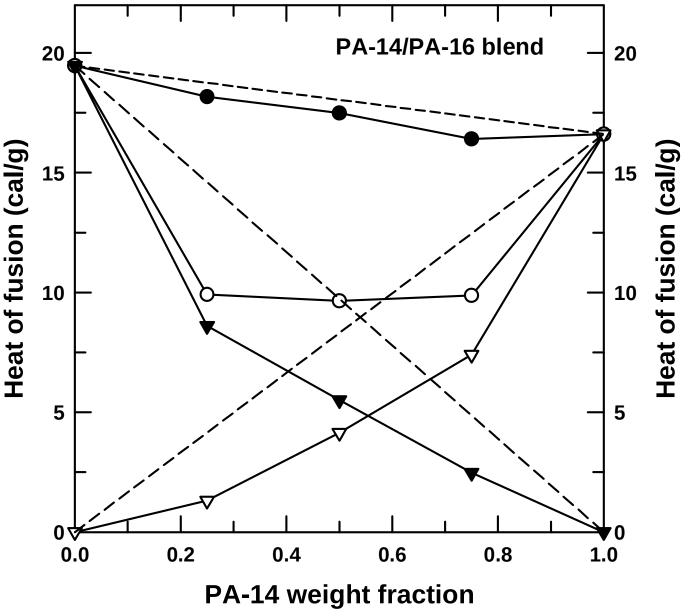

Figure 3.7: Heats of fusion as a function of composition for PA-14/PA-16 blends.

Permeation behavior

Poly(tetradecyl acrylate) and poly(octadecyl acrylate) blends

Figures 3.8 – 3.12 show the permeation behavior of PA-14 and PA-18 blends with their corresponding DSC thermograms. As mentioned in the previous section, polymer films were cooled at a fixed rate of 1.0^{o}C/min to provide similar thermal histories since permeability depends on the resulting crystalline morphology which is controlled by the thermal history. A subsequent section briefly addresses the effect of cooling rate on the permeability of poly(*n*-alkyl acrylate) blends. Permeability switch behavior of the homopolymers shown in Figures 3.8 and 3.12 are similar to what has been reported previously[8]. The permeability varies linearly with temperature above and below the melting temperature of the side-chain crystallites with differing slopes (i.e., activation energies for permeation). As the melting point is traversed, there is a dramatic increase in permeability. As the side-chain length decreases, the breadth of the permeation switch increases as a result of a broader crystallite distribution. As shown in Figures 3.9 – 3.11, PA-14 and PA-18 blends exhibit two distinct permeation jumps that occur at the melting point of each independently crystallized component, thus spreading the overall permeation jump over a wider temperature range. There is an intermediate state between the melting points of the pure polymers where the permeability again increases linearly, on these coordinates, with temperature.

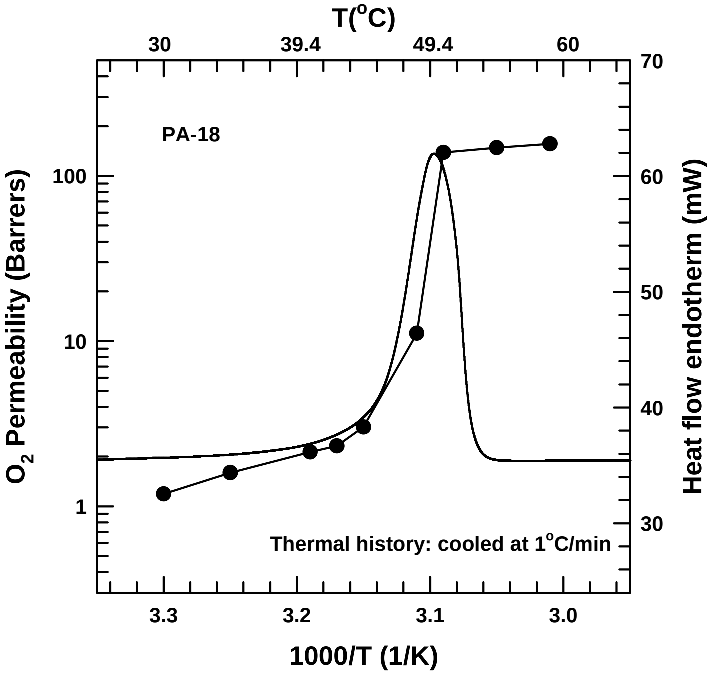

Figure 3.8: O_2 permeability and DSC thermogram for PA-18 homopolymer.

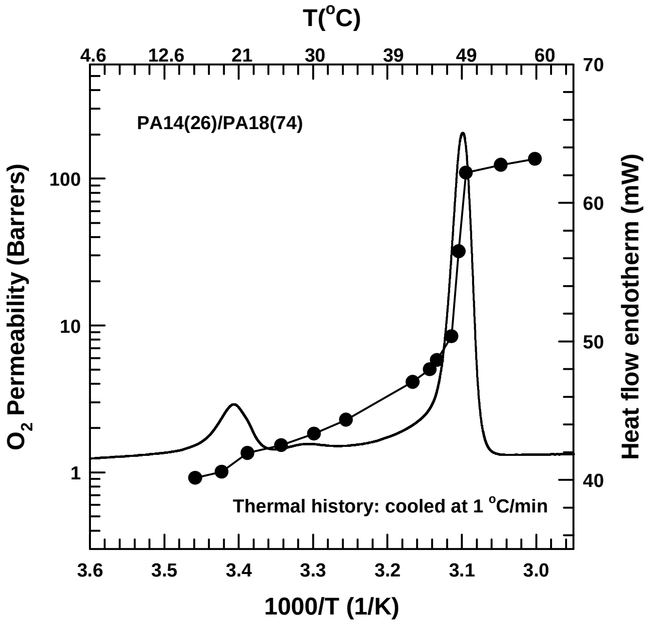

Figure 3.9: O_2 permeability and DSC thermogram for PA14(26wt%)/PA18(74wt%) blend.

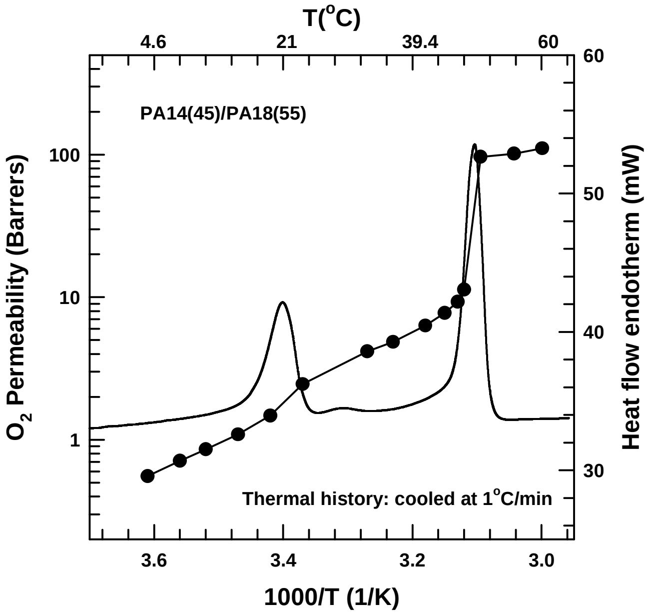

Figure 3.10: O_2 permeability and DSC thermogram for PA14(45wt%)/PA18(55wt%) blend.

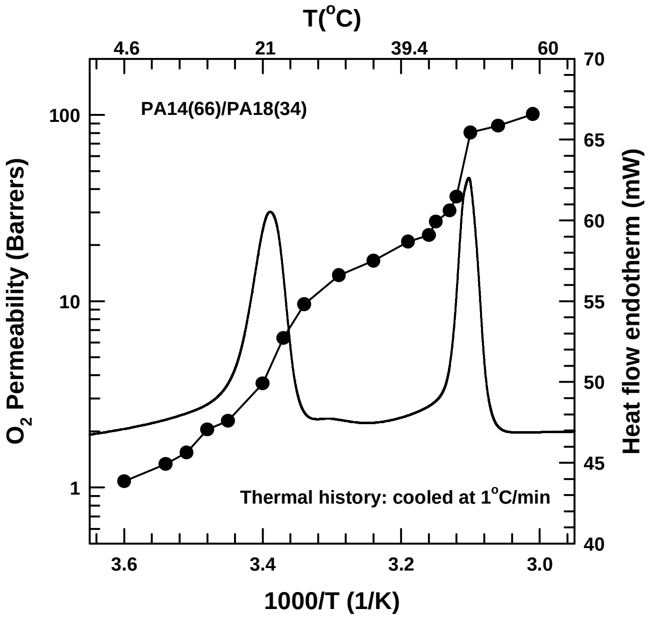

Figure 3.11: O_2 permeability and DSC thermogram for PA14(66wt%)/PA18(34wt%) blend.

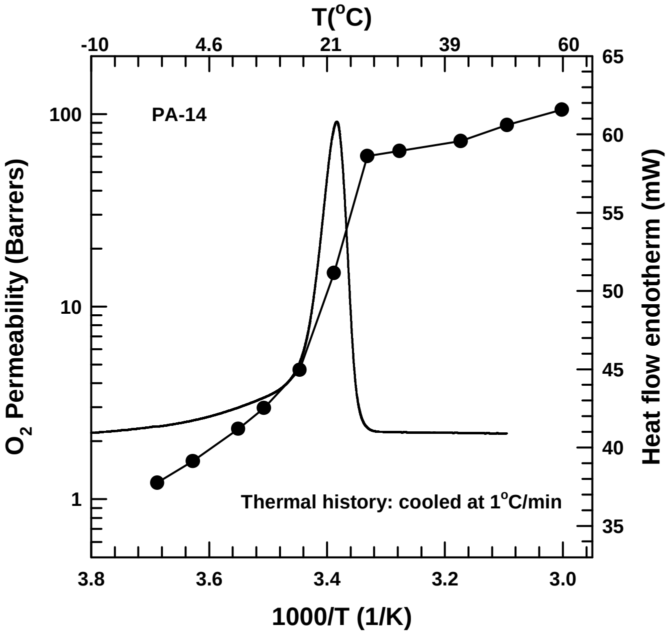

Figure 3.12: O_2 permeability and DSC thermogram for PA-14 homopolymer.

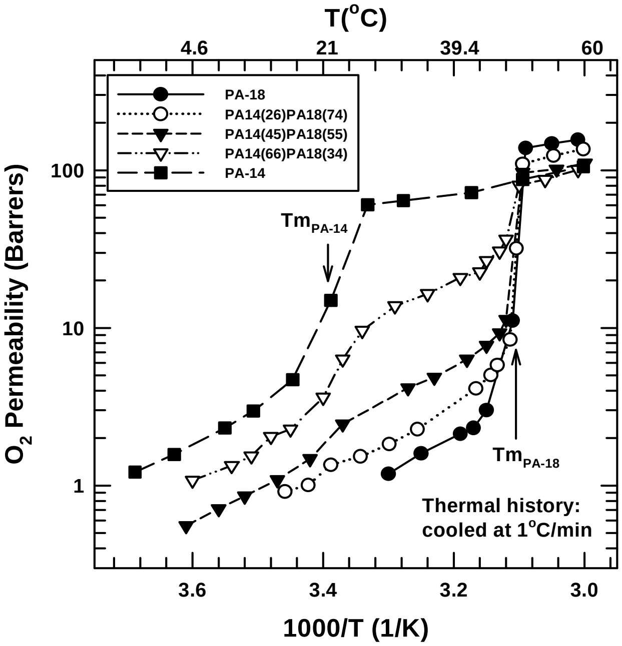

Figure 3.13: Comparison of O_2 permeabilities for various PA-14/PA-18 blends as a function of temperature.

The slight shift of melting points on blending was not observable for the permeation jumps; this is more clearly seen in Figure 3.13 where permeation responses for PA-14/PA-18 blends in the full compositional range are shown in one plot. It is also evident that the magnitude of the permeation jump for each polymer component increases as the amount of the respective component increases in the blend. At high concentrations of the shorter side-chain length chain component, it is apparent that the permeation switch is effectively reduced due to hindered crystallization resulting from the presence of the other polymer; this is supported by the lower than additive crystallinity or heats of fusion shown in Figure 3.5. Although only O_2 gas permeability is shown here, other gases showed analogous responses (see Appendix A), but with some quantitative differences; the magnitude of the permeation jump has been shown to be dependent on penetrant size[13]. There is a commensurate increase in the magnitude of permeation jump as the quantity of the respective component increases, and this response is not strictly linear. By quantifying the magnitude of the permeation switch, we can see this more explicitly.

A convenient method to quantify the homopolymer permeation switch was previously established[14]. The existence of two types of crystallites required modification of this method in order to quantify the two permeation jumps observed for crystalline *n*-alkyl acrylate polymer blends; this modified method is illustrated in Figure 3.14. The permeation jump is conveniently represented as the ratio of the penetrant permeability coefficient in the molten state to that in the semi-crystalline state at temperature, T. The magnitude of the jump can vary significantly depending on the temperature chosen due to the difference in activation energies for permeation above and below the melting temperature[8]. In evaluating the blends, we have chosen to use a temperature, T, midway between the melting points of the two pure polymers; in the case shown, T is 35°C. Below the melting temperatures of both components, the solid state permeability is determined by extrapolation to the mid-point temperature and is designated as P_T^- where the superscript minus sign denotes the solid state. It is important to obtain a representative baseline for meaningful extrapolation of permeability values by starting well below the melting point of the low-temperature component. In some cases, the more brittle nature of the higher melting components in the blend prevented permeation measurements at low temperatures necessary for good baseline determination. Above the melting point of the low melting component but below the melting point of the other component, there exists an intermediate state where the only crystallites are from the higher melting component. The permeability coefficient in this intermediate state is designated as P_T^m where the superscript letter "m" denotes the intermediate state. Above the melting point of the high-temperature melting component, the molten state permeability coefficient is designated as P_T^+. For the case considered, the ratios of these parameters are used to measure the magnitude of the permeation jumps for the low-temperature component PA-14, P_{35}^{m}/P_{35}^{-}, the high-temperature melting component PA-18, P_{35}^{+}/P_{35}^{m} and the overall permeability jump for the blend, P_{35}^{+}/P_{35}^{-}.

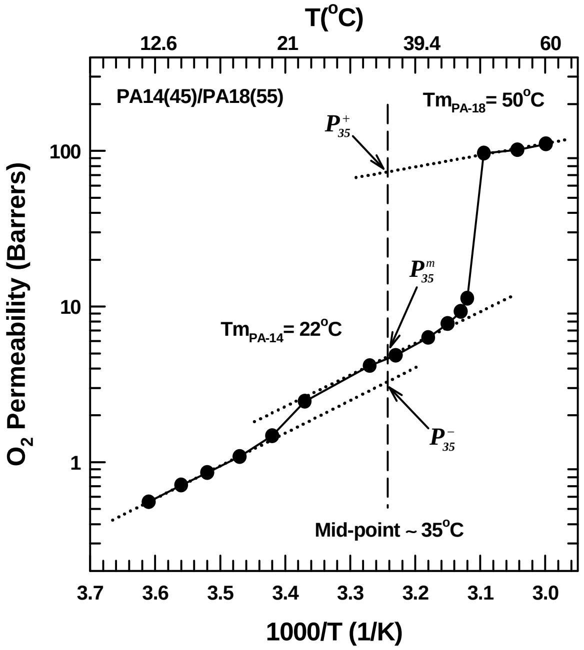

Figure 3.14: Illustration of the procedure used to calculate the magnitude of the permeation jumps for an arbitrary reference temperature of 35°C. The permeability in the semi-crystalline state, P_{35}^{-}, in the intermediate state, P_{35}^{m}, and in the molten state, P_{35}^{+}, were evaluated at or extrapolated to 35°C.

Figures 3.15 – 3.17 show each of these ratios for the PA-14 and PA-18 blends as a function of blend composition. As evident from the graphs, the permeation switch magnitude is somewhat dependent on gas penetrant size, increasing the permeation switch magnitudes increase from O_2, CO_2 to N_2. Among the gas permeation jumps examined here, nitrogen generally has the largest permeation switch. For comparative purposes, an ideal permeation switch for nitrogen was computed assuming the quantity of a given pure component added to the blend crystallized without any influence from the other component.

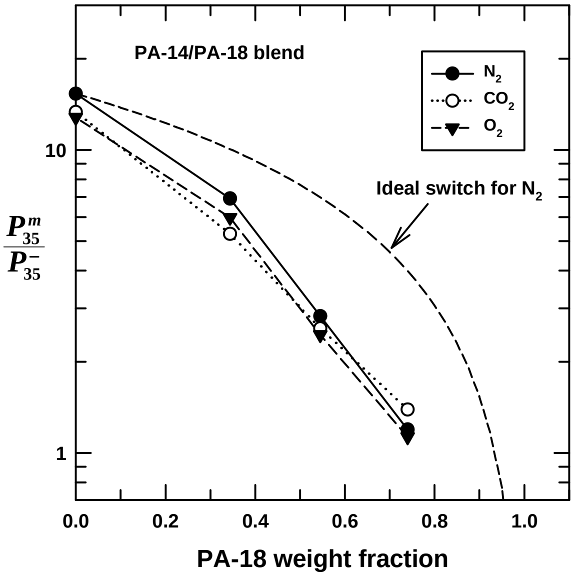

Figure 3.15: The magnitude of O_2, N_2, and CO_2 permeation jumps for PA-14/PA-18 blends as a function of composition for the PA-14 blend component.

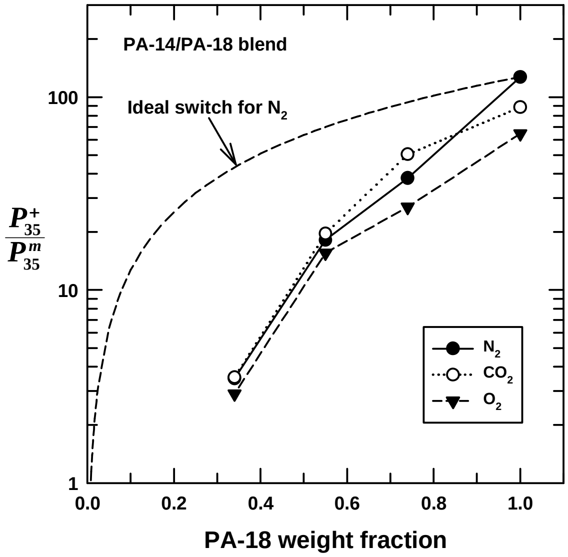

Figure 3.16: The magnitude of O_2, N_2, and CO_2 permeation jumps for PA-14/PA-18 blends as a function of composition for the PA-18 blend component.

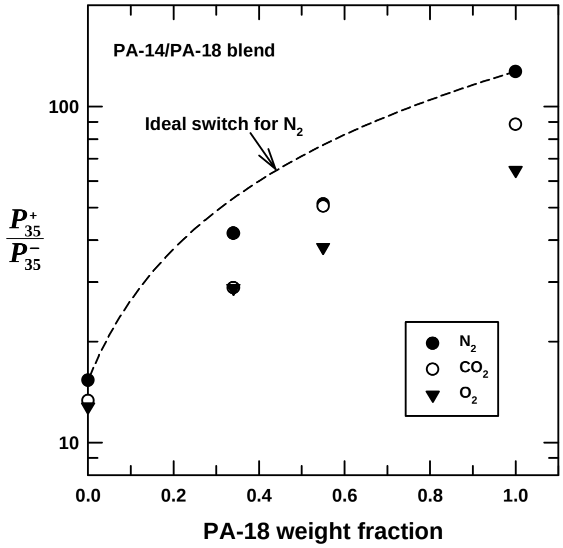

Figure 3.17: The magnitude of O_2, N_2, and CO_2 permeation jumps for PA-14/PA-18 blends as a function of composition for the overall blend. Note: The baseline for the PA14(26wt%)/PA18(74wt%) blend was assumed to be well established when computing the magnitude of the overall permeation jump.

This ideal N_2 permeation jump for the PA-14 component in the blend is assumed to be represented by the following expression

$$\left(\frac{P_{35}^{m}}{P_{35}^{-}}\right)_{PA-14} = w_{PA-14}\left(\frac{P_{35}^{m}}{P_{35}^{-}}\right)_{PA-14}^{o} \tag{3.1}$$

That is, the N_2 jump ratio for PA-14 in the blend is directly proportional to the weight fraction of PA-14 in the blend, $w_{\text{PA-14}}$, times the permeation jump for pure PA-14. The ideal permeation jump for PA-18 is represented by a similar expression. The ideal permeation switch magnitude for each blend component is represented by the dashed lines in Figures 3.15 and 3.16. These lines are not a linear function of blend composition because of the semi-logarithmic coordinates used here. Both permeation jumps for the individual components in the blend lie below this dashed curve for all penetrants indicating the permeation switch is suppressed somewhat by blending. An ideal overall N_2 permeability jump for the blend can be more generally expressed as an additive function

$$\left(\frac{P_T^+}{P_T^-}\right)_{blend} = w_i\left(\frac{P_T^m}{P_T^-}\right)_i^o + w_j\left(\frac{P_T^+}{P_T^m}\right)_j^o \tag{3.2}$$

where w represents the weight fraction of the each component, i is the low-temperature melting component and j being the high-temperature melting component, and the ratios are the respective pure component permeation jumps. The value of this ideal overall N_2 permeation switch for the blend is shown as the dashed curve in Figure 3.17. The measured blend permeation jump is lower than this additivity curve suggesting again that the permeation jumps are somewhat suppressed in the blend.

The permeation switches for the PA-14/PA-18 blends are always lower than the ideal cases, which is similar to the heat of fusion values which lie below the additivity lines indicating the components do not crystallize as though the other component was not present. The lowered permeation switch effect may reflect smaller, less perfect crystals being formed in the blend.

Poly(hexadecyl acrylate) and poly(octadecyl acrylate) blends

Representative permeation responses for PA-16/PA-18 blends and the pure components are shown in Figures 3.18 – 3.22. Similar to PA-14 and PA-18 blends, thermograms show that there are also two endothermic peaks for the blends indicating there is no significant co-crystallization between the components. The size of each peak appears to increase proportionately to the amount of polymer added. Although the T_m's are closer, i.e., 36 and 50°C, than for the PA-14/PA-18 blends components, the peaks are still resolvable without significant overlap. Generally, two separate permeation switches are observed for PA-16/PA-18 blends with the exception of the PA16(25)/PA18(75) blend. The absence of a permeation jump for the PA-16 component suggests that the melting of small crystals observable by DSC did not cause ample morphological changes to cause a permeation jump or there was insufficient low temperature data to adequately define the small permeation jump.

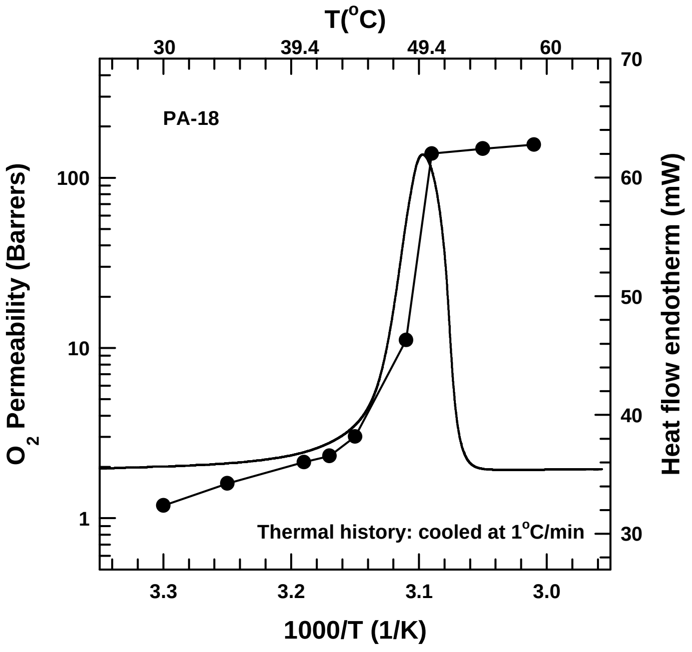

Figure 3.18: O_2 permeability and DSC thermogram for PA-18 homopolymer.

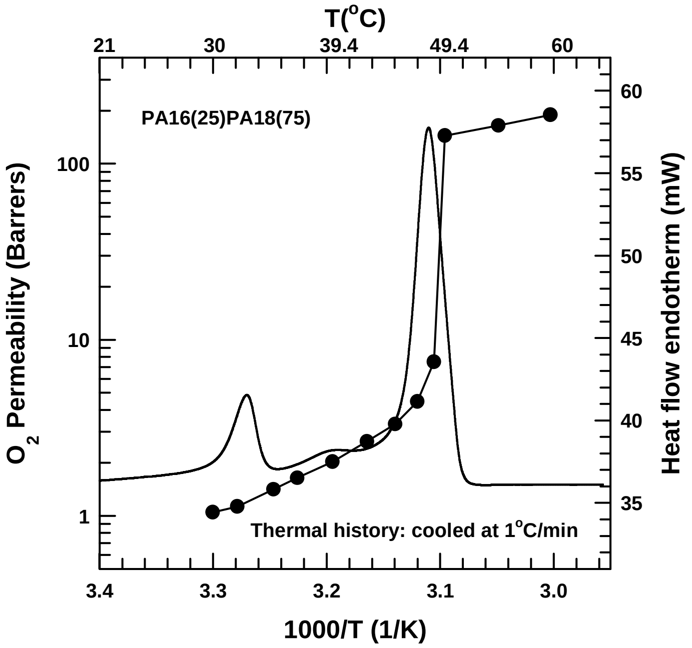

Figure 3.19: O_2 permeability and DSC thermogram for PA16(25wt%)/PA18(75wt%) blend.

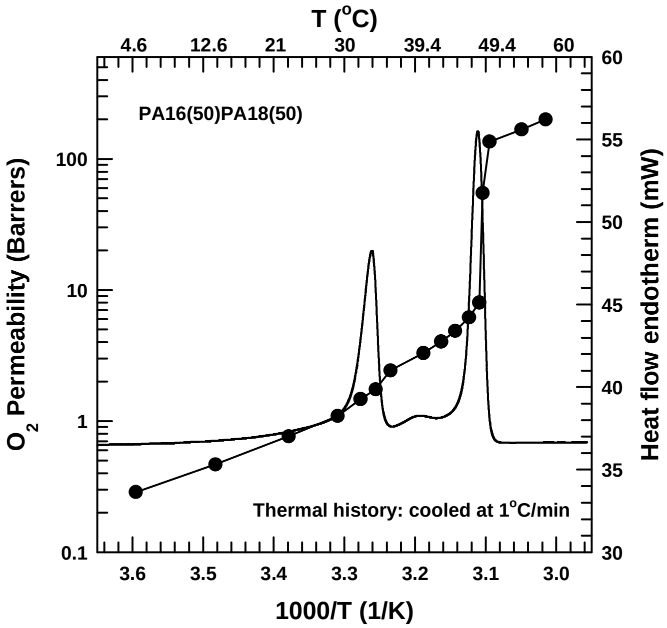

Figure 3.20: O_2 permeability and DSC thermogram for PA16(50wt%)/PA18(50wt%) blend.

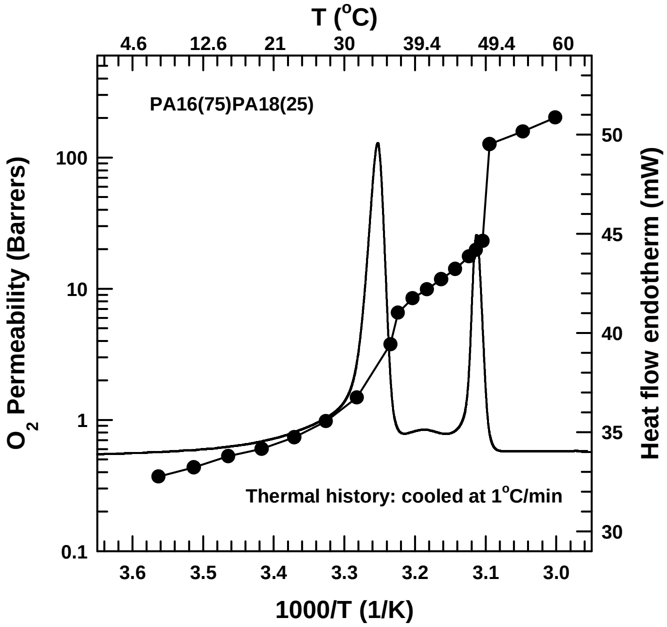

Figure 3.21: O_2 permeability and DSC thermogram for PA16(75wt%)/PA18(25wt%) blend.

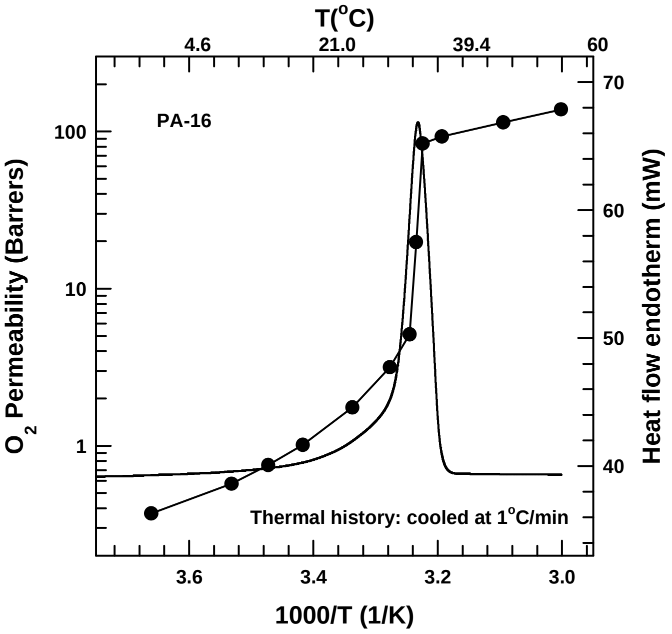

Figure 3.22: O_2 permeability and DSC thermogram for PA-16 homopolymer.

Comparing the response of the PA16(25)/PA18(75) blend to that of PA14(26)/PA18(74) in Figures 3.19 and 3.9 would suggest that the former is true; a minute permeability change is observed at the melting temperature of the shorter side-chain component. Figure 3.23 shows that the permeation switch for each blend occurs very close to the melting temperature of the pure components. The difference between the solid-state permeability of these pure components is small, and as a result, the PA-16 and PA-18 blends show negligible changes in the absolute permeability upon blending and its value is closer to that of the longer side-chain length component, PA-18. The heats of fusion for the blend by both methods show very little change upon blending which support this observation. In the melt, the permeability for this blend system is between that of both components.

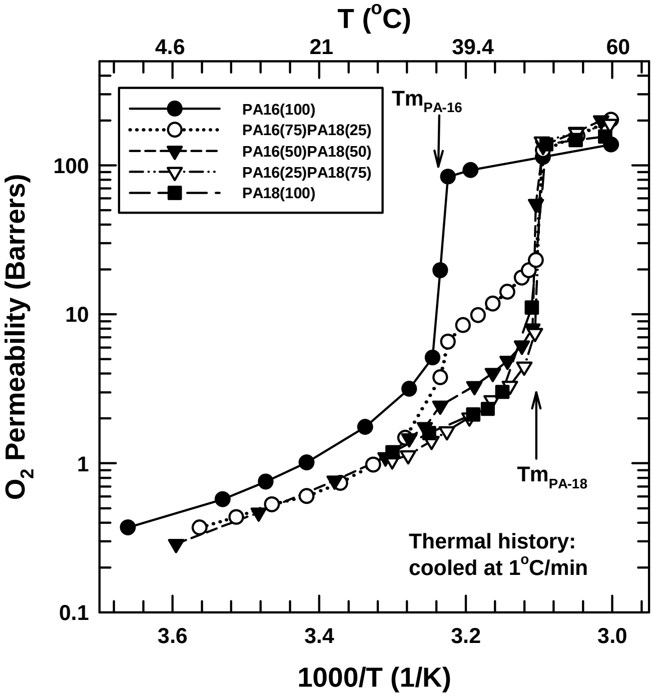

Figure 3.23: Comparison of O_2 permeability for various PA-16/ PA-18 blends as a function of temperature.

Figures 3.24 – 3.26 shows the oxygen permeation switch values at 43°C as a function of PA-16/PA-18 blend composition. The permeability jumps for PA-16 in the blends is lower than the ideal N_2 permeation jump computed for each blend composition. The PA-18 component permeation jump was lower than the ideal curve except for O_2 and N_2 for the 50/50 weight blend which is in agreement with what is expected based on the PA-18 content in the blend. The overall permeation switch for the blend is higher than the ideal dashed curve, but consistent with the solid and molten state trends. The magnitude of the overall permeation switch for PA16(25)/PA18(75) was calculated assuming the data provides an adequate permeation baseline for extrapolation. The maximum seen for the overall blend permeation jump at 50/50 weight blend is consistent with trends seen among the homologous series of *n*-alkyl acrylate polymers as shown in Figures 3.27 and 3.28. As the side chain length increases so does the crystallinity and the molten state free volume both of which increase the jump magnitude. Blending PA-16 and PA-18 leads to an increase in the thermal switch beyond that achievable by the pure homopolymers apparently due to changes in the crystal morphology. Further understanding of the crystalline morphology may help to optimize the magnitude of the thermal switch effect.

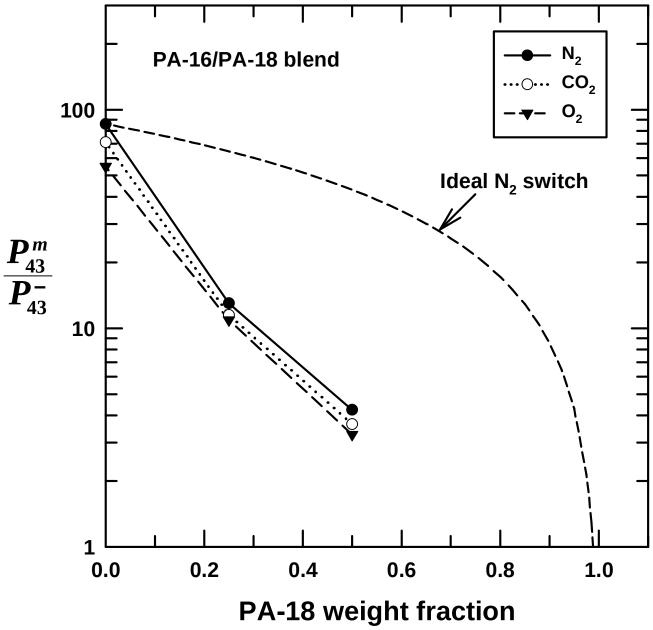

Figure 3.24: The magnitude of O_2, N_2, and CO_2 permeation jumps for PA-16/PA-18 blends as a function of composition for the PA-16 component.

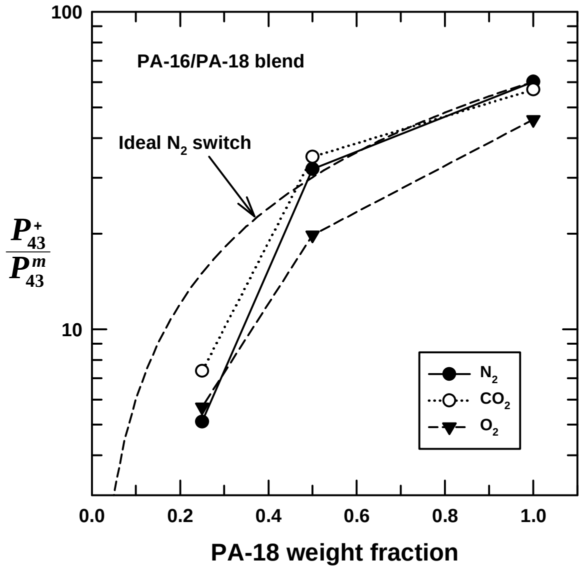

Figure 3.25: The magnitude of O_2, N_2, and CO_2 permeation jumps for PA-16/PA-18 blends as a function of composition for the PA-18 component.

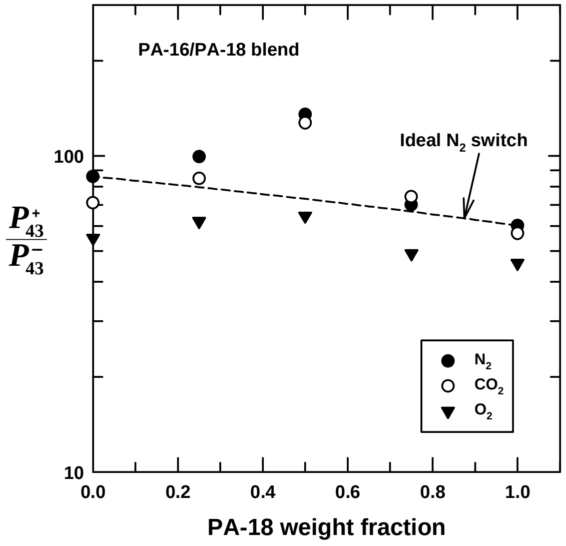

Figure 3.26: The magnitude of O_2, N_2, and CO_2 permeation jumps for PA-16/PA-18 blends as a function of composition for the overall blend. Note: The baseline for the PA16(25wt%)PA18(75wt%) blend was assumed to be well established when computing the magnitude of the overall permeation jump.

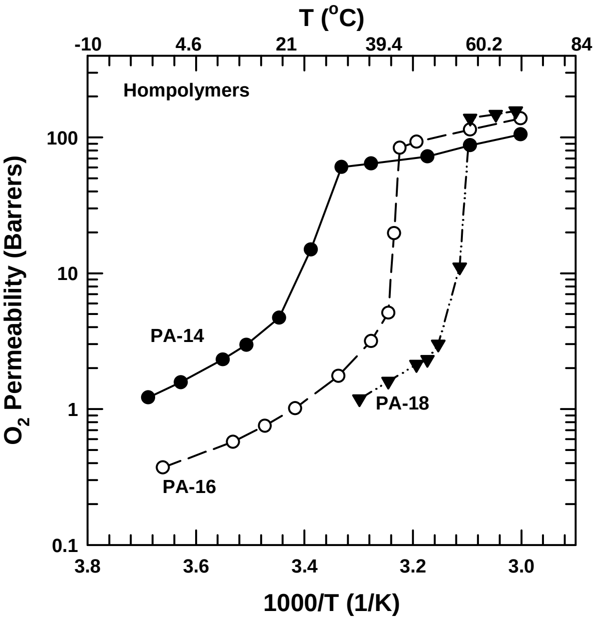

Figure 3.27: O_2 permeability of PA-14, PA-16, and PA-18 homopolymers as a function of temperature.

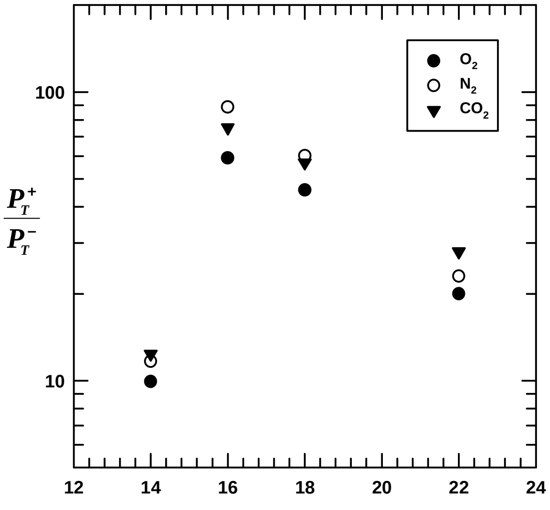

Figure 3.28: The magnitude of the O_2, N_2, and CO_2 permeation jumps for various homopolymers as a function of side-chain length where PA-22 from reference[8].

Poly(tetradecyl acrylate) and poly(hexadecyl acrylate) blends

Figures 3.29 – 3.32 show the permeation responses for PA-14/PA-16 blends. There are two distinct endothermic peaks that are closely situated resulting in more overlap than the blend systems discussed earlier. Unlike previous cases, the O_2 permeation responses for the PA-14/PA-16 blends do not show a distinct permeation jump for the lower melting PA-14 component regardless of the blend composition, but rather a higher slope in this temperature range, presumably due to progressive melting, than might be expected by a simple Arrhenius response for a material of fixed morphology. A more familiar permeation jump occurs at the T_m of the higher melting component.

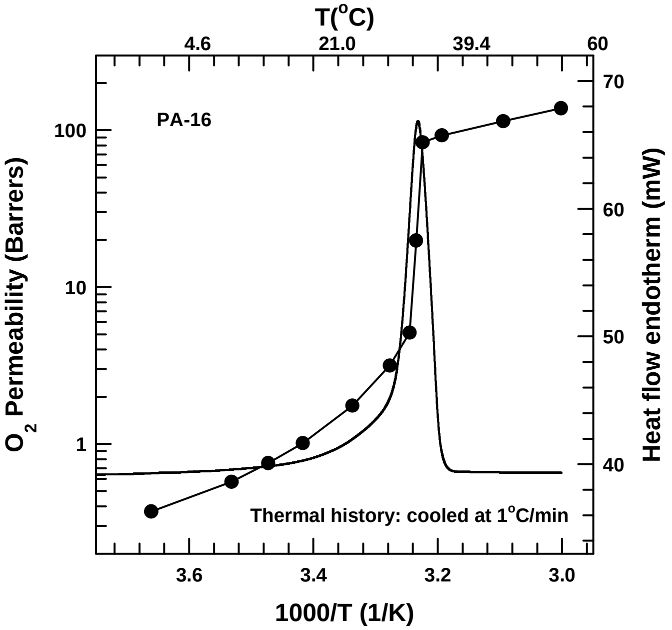

Figure 3.29: O_2 permeability and DSC thermogram for PA-16 homopolymer.

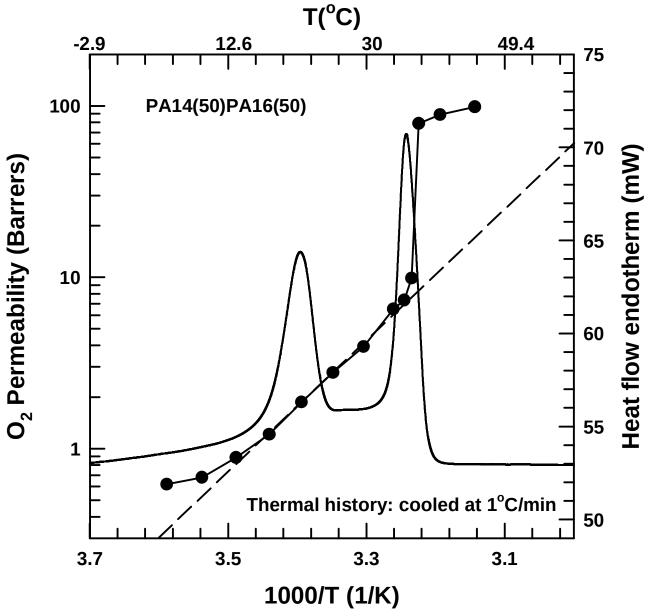

Figure 3.30: O_2 permeability and DSC thermogram for PA14(50wt%)/PA16(50wt%) blend.

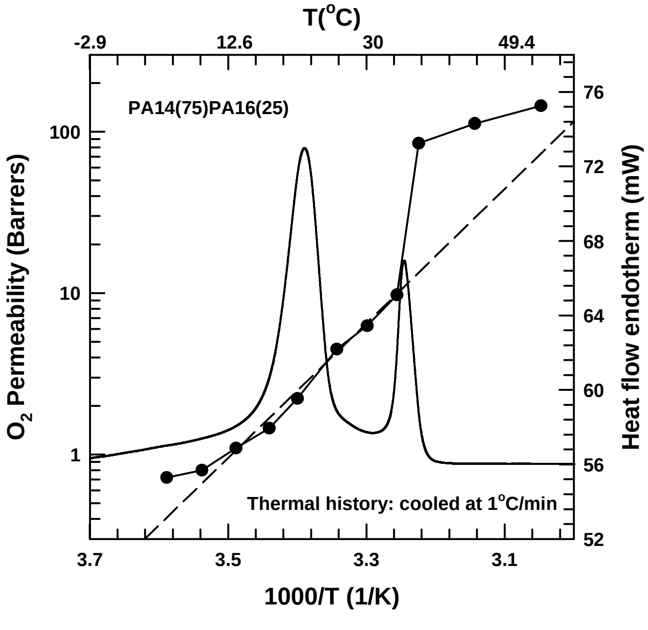

Figure 3.31: O_2 permeability and DSC thermogram for PA14(75wt%)/PA16(25wt%) blend.

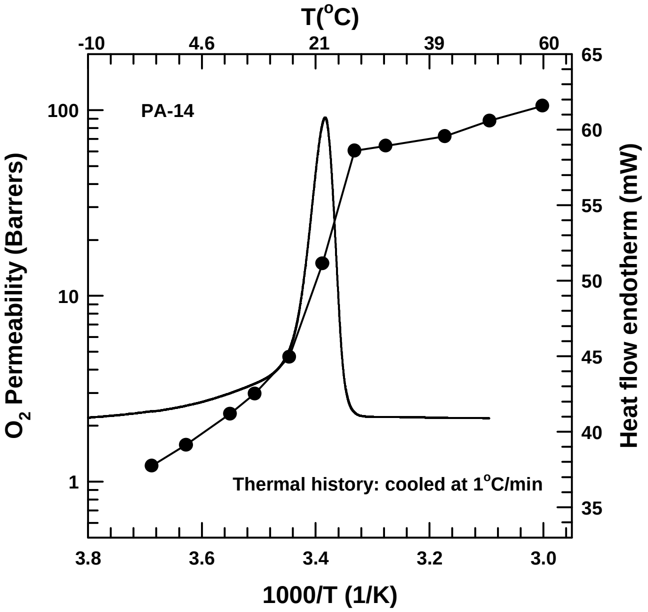

Figure 3.32: O_2 permeability and DSC thermogram for PA-14 homopolymer.

In Figure 3.30 the dashed line in the lower melting region defines an effective activation energy for O_2 permeation over the temperature range shown; the temperature range chosen for construction of such a line affects the value of the activation energy obtained. Similar lines were constructed for a few other blends and the effective activation energies obtained are shown in Table 3.2. Activation energies for permeation in homopolymers with n = 14, 16, and 18 obtained well below their T_m i.e., no progressive melting, are shown for comparison. When the side-chain lengths of the blend components are similar, the effective activation energies are considerably higher than for the homopolymers reflecting the nature of interaction of the two melting processes.

Table 3.2: Comparison of activation energy for gas permeation, E_P (kcal/mol), of homopolymers and effective activation energies of blends.

Polymer	E_{p,O_2}	E_{p,CO_2}	Temperature range (^{o}C)
PA-14	8.5	7.6	2 – 12
PA-16	9.4	8.3	2 – 20
PA-18	11.0	10.3	30 – 40
PA14(45)/PA18(55)	12.0	11.3	5 – 45
PA16(50)/PA18(50)	13.6	12.5	5 – 45
PA14(50)/PA16(50)	15.2	14.7	5 – 35
PA14(75)/PA16(25)	16.5	16.6	5 – 35

The PA-14/PA-16 blends have the largest slopes or effective activation energies of the blends considered; significantly, this enhanced thermal response is in the temperature range of greatest interest, 0 to 30^{o}C, for produce distribution. The effect of temperature on the respiration rate of produce can also be represented by an Arrhenius relation; the activation energies for respiration of selected produce are shown in Table 3.3. The effective activation energies for the PA-14/PA-16 blends are more similar to that of some of the produce than the homopolymers listed in Table 3.2 or other potential membrane materials. Thus, the PA-14/PA-16 blends are promising candidates for more thermally responsive membranes for matching rates with produce over a range of temperatures.

Table 3.3: Comparison of activation energy for respiration, E_R (kcal/mol), of selected produce[20-23].

Produce	E_{R,O_2}	E_{R,CO_2}
Blueberry	35.2	39.0
Broccoli	15.0	15.8
Banana	11.3	9.8
Raspberry	10.7	13.3

As seen by the combined data for O_2 in Figure 3.33, the value of the permeability coefficients of PA-14/PA-16 blends in the solid and molten states appear to be similar to the longer side chain length component with differing activation energies. Since there is no well-defined intermediate state in these blends, the magnitude of the permeation jumps for the individual components could not be evaluated. Figure 3.34 shows the overall permeation jump for the blend evaluated at 30°C as a function of blend composition where there is a more or less additive relationship observed, except for N_2 and CO_2 which are slightly higher than additivity.

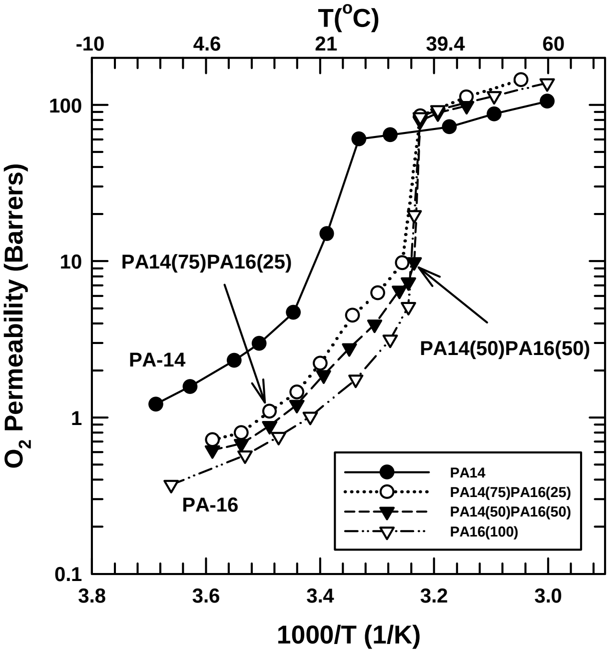

Figure 3.33: O_2 permeability for PA-14/PA-16 blends as a function of temperature.

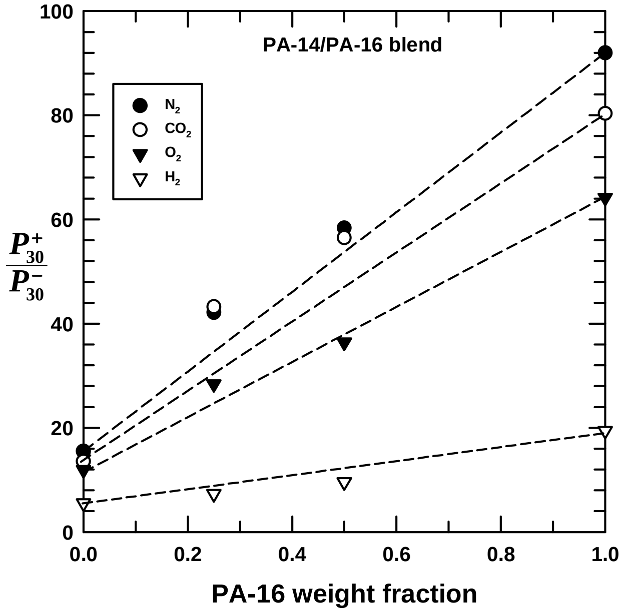

Figure 3.34: The magnitude of N_2, CO_2, O_2, and H_2 permeation jumps for PA-14/PA-16 blends as a function of composition.

Ternary blends

Based on the above, a multi-component blend might be a simple route to emulate the response suggested in Figure 2.4 for a multi-component laminate. To explore this possibility, the permeation response of a ternary blend of equal parts by weight of PA-14, PA-16, and PA-18 is shown in Figure 3.35. The DSC scan shows resolvable melting points for the individual components; however, there are no distinct permeation jumps at the melting temperatures of the shorter side-chain length components. There is a single permeation jump close to the melting point of the longer side-chain component, PA-18. The magnitude of the permeation switch at 35^{o}C for the PA-18 component in the ternary blend was determined by assuming the intermediate state baseline starts just below the transition range of PA-18. Table 3.4 lists these values along with the ideal values for the magnitude of the permeation jump for a blend containing 33 wt% of PA-18 using an expression like Equation 3.1.

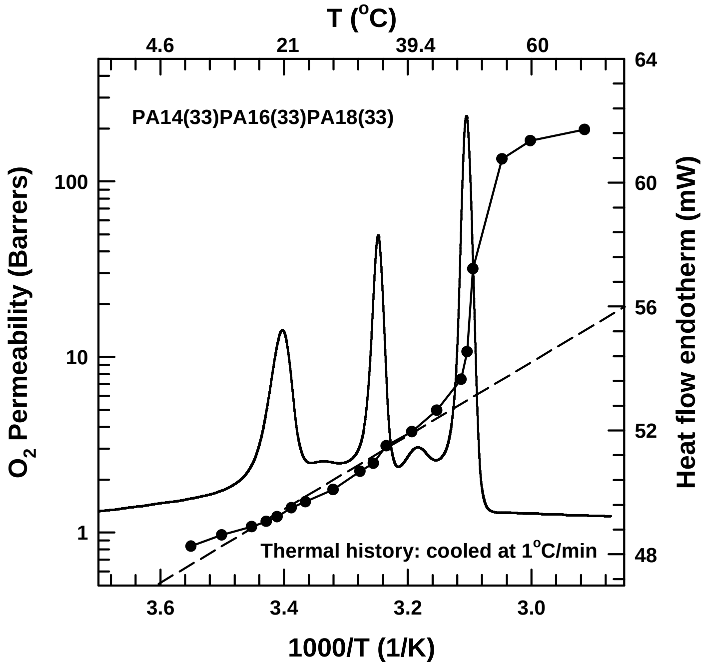

Figure 3.35: O_2 permeability and DSC thermogram for a ternary blend containing equal parts weight of PA-14, PA-16, and PA-18 as a function of temperature.

Table 3.4: Magnitude of the permeation jump for the PA-18 component, $\left(P_{35}^{+}/P_{35}^{m}\right)$, in the ternary blend and the ideal calculated for 33 wt% PA-18

Gas	Ternary $\left(P_{35}^{+}/P_{35}^{m}\right)_{PA-18}$	Ideal $w_{PA-18}\left(P_{35}^{+}/P_{35}^{m}\right)_{PA-18}^{o}$
O_2	18.3	21.5
N_2	36.7	42.3
CO_2	56.0	29.5

The magnitudes of the permeation jump for O_2 and N_2 are very similar to the ideal value; however, the magnitude of the switch for CO_2 is significantly higher than this ideal. Over the temperature region of 14 to 44°C, the permeation response to temperature is nearly linear on the Arrhenius coordinates with an effective activation energy for O_2 and CO_2 permeation of 10.0 and 8.3 kcal/mol, respectively. Despite these values comparing well with that of homopolymers, listed in Table 3.2, the existence of closely melting components broadens the temperature range over which a more continuous permeation response is observed. The permeation response of the shorter side-chain length components in the ternary blend is somewhat hindered by the presence of the other component, similar to the PA-14/PA-18 and PA-16/PA-18 binary blends with lower concentrations of these components. To achieve greater temperature responsiveness for the ternary blend in the region of the lower melting components (i.e., temperatures reached during produce distribution) higher concentrations of these components than ideality would suggest are necessary. These results suggest that blends of several side-chain crystalline polymers might be a useful avenue for tailoring the temperature response of gas permeation.

Effect of blend composition on gas permeation

The literature[15-19] suggests that the permeability of gases in random copolymers and miscible blends should follow a simple relationship of the form

$$\ln P = \phi_1 \ln P_1 + \phi_2 \ln P_2 \tag{10}$$

in certain limiting cases. Here P_i and ϕ_i refer to the permeability and volume fraction of *i* in the homogeneous blend or copolymers. Deviations from this additive relationship have been documented: negative deviations in strongly interacting systems, positive deviations when P_1 and P_2 are very different, and S-shaped curves indicate at phase inversion in immiscible blend systems.

Figures 3.36 – 3.38 shows the O_2 permeation-composition plots for blends at various temperatures. Below the melting point of the shorter side-chain component and at a temperature in the intermediate state, the permeability for the blends lie well below or along the additive line. Crystallinity complicates this analysis; therefore, examining this relationship at or above the melting point for the blend components is more informative. Above the melting point of both components, the permeability for the PA-14/PA-18 blends and PA-16/PA-18 blends shows more or less additivity of the pure component permeability coefficients. The PA-14/PA-16 blends have permeability values that are closer to that of the longer side-chain length component and, therefore, show a positive deviation from the additive line.

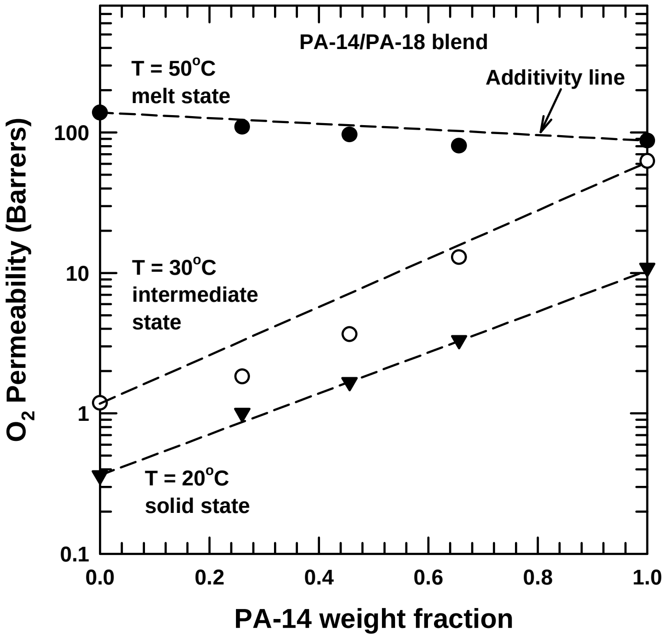

Figure 3.36: O_2 Permeability for PA-14/PA-18 blend as a function of composition in various states, solid state ($T < T_{m1} < T_{m2}$), intermediate state ($T_{m2} > T > T_{m1}$), and melt state ($T \geq T_{m2} > T_{m1}$).

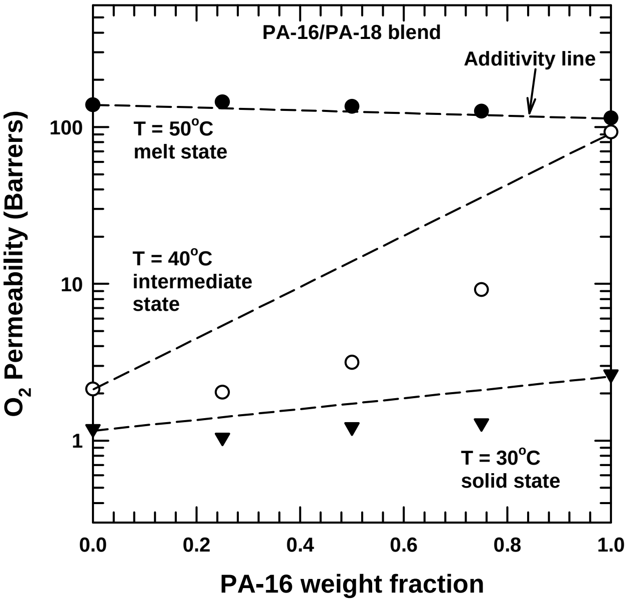

Figure 3.37: O_2 Permeability for PA-16/PA-18 blend as a function of composition in various states, solid state ($T < T_{m1} < T_{m2}$), intermediate state ($T_{m2} > T > T_{m1}$), and melt state ($T \geq T_{m2} > T_{m1}$).

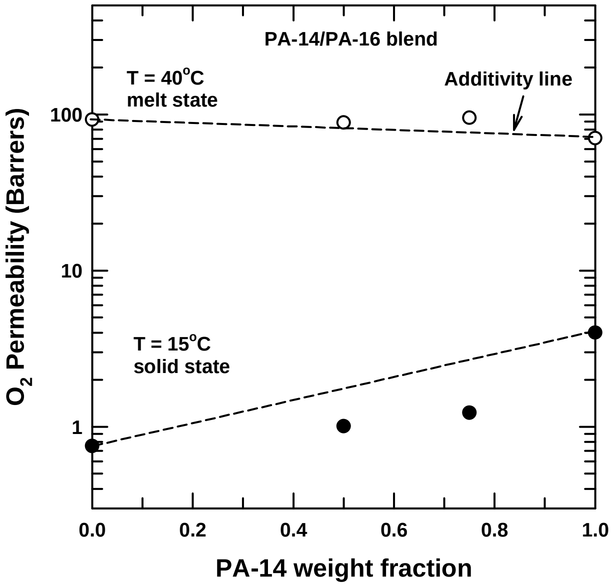

Figure 3.38: O_2 Permeability for PA-14/PA-16 blend as a function of composition in various states, solid state ($T < T_{m1} < T_{m2}$), intermediate state ($T_{m2} > T > T_{m1}$), and melt state ($T \geq T_{m2} > T_{m1}$).

Effects of thermal history on semi-crystalline blends

Changes in crystalline morphology due to differences in thermal history have a significant effect on permeation, thermal and structural properties of poly(*n*-alkyl acrylate) homopolymers[1, 13]. For homopolymers, Mogri and Paul found that slow cooled films lead to a higher permeability in spite of having a higher crystallinity. It is clear that simple crystallinity considerations are insufficient to fully explain this phenomenon and that a better understanding of crystallite size, shape, and orientation is necessary. As might be expected, the same trends are observed for blends. Figures 3.39 – 3.42 show the permeation response for a homopolymer, PA-18, and a blend, PA16(50)/PA18(50), with the corresponding DSC thermograms for film samples formed by cooling rates of 0.1^{o}C/min and 1.0^{o}C/min from the melt state. As expected the melting points and crystallinity (i.e., heat of fusion) are higher for the slower cooled samples as more stable crystals are formed. The more rapidly cooled films for PA-18 and PA16(50)/PA18(50) blend samples have lower permeabilities. As the temperature increases to the intermediate state, the difference between the permeability coefficients of the two cooling rates narrows. The activation energy of permeation for the slow cooled samples is lower than that of the 1.0^{o}C/min cooled samples. Table 3.5 summarizes the E_p values for each of the samples with the two thermal histories; E_p is always lower for the slower cooled samples of the homopolymer and the blend. For the blend in the intermediate state, there is a smaller difference between E_p for the two cooling rates suggesting the barrier to permeation has been reduced by the melting of PA-16 crystallites.

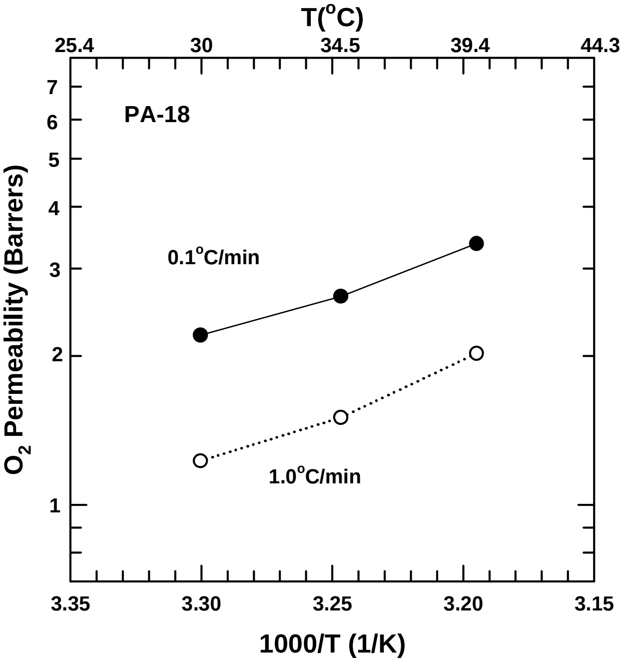

Figure 3.39: Effects of thermal history on O_2 permeability of PA-18 homopolymer as a function of temperature at two cooling rates, 0.1 and 1.0^{o}C/min.

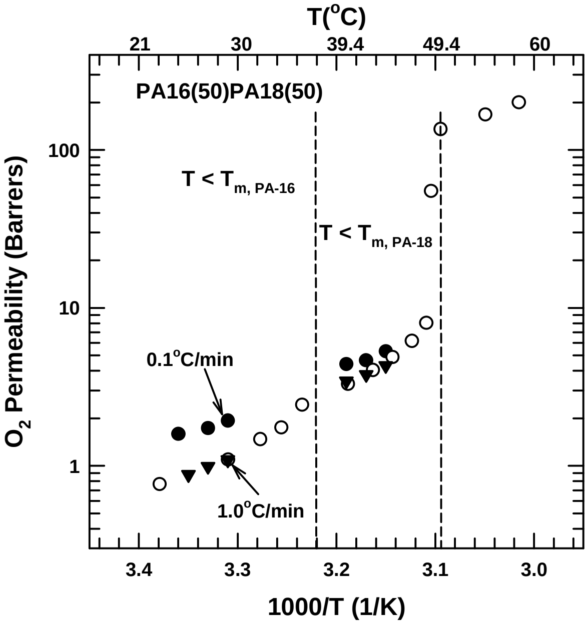

Figure 3.40: Effects of thermal history on O_2 permeability of PA16(50wt%)/PA18(50wt%) blend as a function of temperature at two cooling rates, 0.1 and 1.0^{o}C/min.

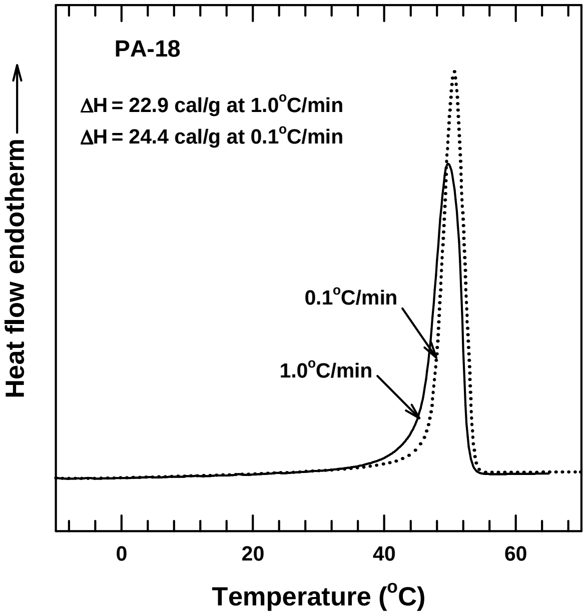

Figure 3.41: DSC thermogram of PA-18 homopolymer at two cooling rates, 0.1 and 1.0°C/min.

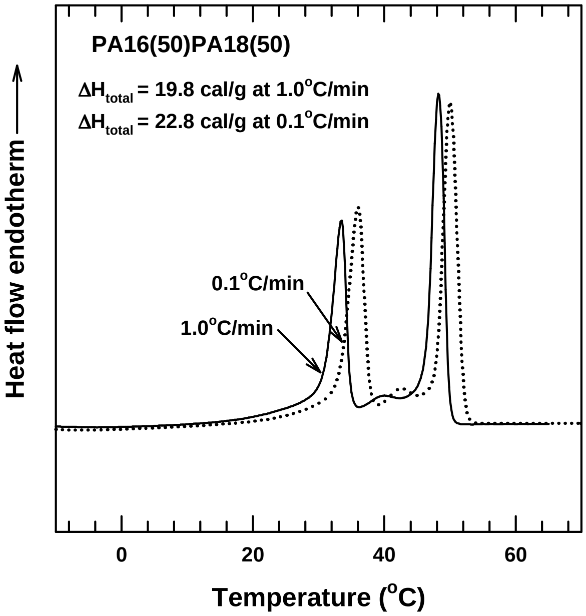

Figure 3.42: DSC thermogram of PA16(50wt%)/PA18(50wt%) blend at two cooling rates, 0.1 and 1.0°C/min.

Table 3.5: Effects of thermal history on the activation energies, E_p (kcal/mol), of O_2, N_2, and CO_2 permeation for PA-18 and PA16(50wt%)/PA18(50wt%) samples.

Polymer	Sample state	Cooling rate (°C/min)	E_{p,O_2}	E_{p,N_2}	E_{p,CO_2}
PA-18	solid	0.1	8.0	9.5	7.0
		1.0	9.4	9.3	9.1
PA16(50)/PA18(50)	solid	0.1	8.8	10.7	8.0
		1.0	9.7	16.0	12.8
PA16(50)/PA18(50)	intermediate	0.1	9.2	10.7	10.1
		1.0	11.1	13.3	12.3

CONCLUSIONS

The permeation response of semi-crystalline poly(*n*-alkyl acrylate) and poly(*m*-alkyl acrylate) blends as a function of temperature is significantly influenced by the side-chain lengths, *n* and *m*, of the blend components and blend composition. The components of each system crystallize independently of one another without any significant co-crystallization; however, the heats of fusion determined by various methods suggest that the presence of one component hinders crystallization of the other component. Changes in morphology by blending significantly influence the gas permeability as the melting temperature is traversed. PA-14/PA-18 and PA-16/PA-18 blends show two distinct permeation jumps at the melting point of each component. The permeation response of the PA-14/PA-16 and ternary blends did not show a jump at the melting point of PA-14 but showed a stronger temperature response, presumably due to progressive melting, than expected by simple Arrhenius considerations for such polymers where the crystalline morphology is fixed. This stronger temperature response occurs over the range of temperatures of interest for modified atmosphere packaging. This suggests that multi-component poly(*n*-alkyl acrylate) blends may be a route to obtain the necessary thermal responsiveness of gas permeation in membranes used in the packaging of respiring produce.

REFERENCES

1. Shibaev VP, Petrukhin BS, Zubov YA, Plate NA, and Kargin VA. Vysokomolekulyarnye Soedineniya, Seriya A 1968;10(1):216-226.
2. Armarego WLF and Chai CLL. Purification of Laboratory Chemicals, 5th ed. Amsterdam: Butterworth-Heinemann, 2003.
3. Mogri Z and Paul DR. Journal of Membrane Science 2000;175(2):253-265.
4. Rehberg CE and Fisher CH. Journal of the American Chemical Society 1944;66:1203-1207.
5. Mogri Z. Gas transport properties of side-chain crystalline polymers. Chemical Engineering. Austin: University of Texas at Austin, 2001. pp. 289 pp.
6. Kirkland BS. Chemical Engineering. Austin: University of Texas at Austin, 2007.
7. Koros WJ. Sorption and transport of gases in glassy polymers. Chemical Engineering. Austin, Texas: University of Texas at Austin, 1977. pp. 253.
8. Mogri Z and Paul DR. Polymer 2001;42(18):7765-7780.
9. O'Leary KA and Paul DR. Polymer 2006;47(4):1226-1244.
10. O'Leary KA and Paul DR. Polymer 2006;47(4):1245-1258.
11. Flory PJ. Journal of Chemical Physics 1949;17:223-240.
12. Hemminger WF and Sarge SM. Journal of Thermal Analysis 1991;37(7):1455-1477.
13. Mogri Z and Paul DR. Polymer 2000;42(6):2531-2542.
14. Mogri Z and Paul DR. Journal of Polymer Science, Part B: Polymer Physics 2001;39(10):979-984.
15. Shur YJ and Ranby B. Journal of Applied Polymer Science 1975;19(5):1337-1346.
16. Shur YJ and Ranby B. Journal of Applied Polymer Science 1976;20(11):3105-3119.
17. Shur YJ and Ranby B. Journal of Applied Polymer Science 1976;20(11):3121-3131.
18. Shur YJ and Ranby B. Journal of Macromolecular Science, Physics 1977;B14(4):565-572.

19. Ranby BG. Journal of Polymer Science, Polymer Symposia 1975;51(Int. Symp. Macromol. Honor Professor Herman F. Mark):89-104.
20. Song Y, Kim HK, and Yam KL. Journal of American Society of Horticultural Science 1992;117(6):925-929.
21. Hagger PE, Lee DS, and Yam KL. Journal of Food Process Engineering 1992;15:143-157.
22. Maneerat C, Tongta A, Kanlayanarat S, and Wongs-Aree C. A Transient Model to Predict O_2 and CO_2 Concentrations in Modified-atmosphere Packaging of Banana at Various Temperatures. CA '97 proceedings : Seventh International Controlled Atmosphere Research Conference : July 13-18, 1997, University of California, Davis., vol. 5, 1997. pp. 191-197.
23. Joles DW, Arthur C. Cameron, Ahmad Shirazi, Peter D. Petracek, and Randolph M Beaudry. Journal of the American Society for Horticultural Science 1994;119(3):540-545.

Chapter 4: Thermal behavior of poly (*n*-alkyl acrylate) blends with *n*-aliphatic materials and random copolymers poly(*n*-alkyl acrylate –co– *m*-alkyl acrylate)

INTRODUCTION

Thermal analysis is a useful tool for predicting the trend of gas permeability as a function of temperature for poly (*n*-alkyl acrylate)s. Poly (*n*-alkyl acrylate) homopolymers exhibit a single endothermic peak due to the crystallization of the side chains when n > 10. A single permeation jump is observed as the melting temperature of the side-chain crystallites is transgressed. Likewise, poly(*n*-alkyl acrylate –co– *m*-alkyl acrylate) random copolymers with some degree of crystallinity were found to co-crystallize, thus, exhibiting a single endothermic peak[1]. The peaks observed for copolymers were broader due to an increased crystallite distribution which generally led to a wider breadth of the permeation jump due to more gradual melting of the crystallites. A similar correlation is observed for poly (*n*-alkyl acrylate)/ poly(*m*- alkyl acrylate) blends with side-chain lengths greater than ten, *n* and *m* > 10. Two endothermic peaks are observed in blends which suggest the blend components crystallize independently of one another[2]. As expected, the blends exhibit two permeation jumps that correspond to the melting temperature of the side-chain crystallites of each component. In addition, crystallinity typically gives some insight about the magnitude of the permeation jump. Thermal analysis is a reliable predictor of permeability-temperature trends for poly (*n*-alkyl acrylate) homopolymers, copolymers and blends.

BLENDS OF POLY(N-ALKYL ACRYLATE)S AND N-ALIPHATICS

Poly (*n*-alkyl acrylate)s are used as flow-index improvers and pour-point depressants for lubricating oils that are comprised of many alkane derivatives[3-5]. It is generally accepted that these polymers create this effect by co-crystallization or adsorption mechanisms[3, 4, 6]. Thermal and structural studies of methacrylate homopolymers and copolymers blended with fatty derivatives show that co-crystallization strongly depends on the blend composition. Rubin and Puglise investigated blends of poly (octadecyl methacrylate) with alkanes (n-dodecane and n-octadecane) where the side-chains were found to co-crystallize at high polymer compositions. Statistical random copolymers poly[(methyl methyl acrylate) –*stat*– (*n*-octadecyl methacrylate)] and poly[(methyl acrylate) –*stat*– (*n*-octadecyl acrylate)] with n-octadecyl side chains were also found to co-crystallize with *n*-octadecanoic acid at low fatty acid concentrations, below 24 wt%. It is expected from these findings that blends of poly (*n*-alkyl acrylate)s with materials that chemically resemble the side chain can lead to an array of possibilities. In particular, poly (octadecyl acrylate) (PA-18) is used here to examine blends with *n*-paraffins (*n*-octadecane ($C_{18}H_{38}$) and *n*-tetracosane ($C_{24}H_{50}$)), *n*-fatty alcohols (*n*-hexadecanol ($C_{16}H_{33}OH$) and *n*-octadecanol ($C_{18}H_{37}OH$)), and *n*-fatty acid (*n*-octadecanoic acid ($C_{17}H_{35}COOH$)). These materials are either similar in length of the octadecyl side chain or the melting temperature of PA-18.

Experimental: materials, film formation, and thermal analysis

The fatty compounds are of high purity, 98%, thus, the materials were used as received. PA-18 and the fatty compounds were mixed and solution cast using 10 wt% toluene solutions and allowed to solidify. The films were stored in a vacuum oven at elevated temperature for 48 hours to remove the final traces of solvent. Thermal analysis of the blends was conducted using a differential scanning calorimeter. Each blends sample was heated above the melting temperatures of both components and held for a time to remove any residual crystallinity, cooled at 5^oC/min below the crystallization temperature of each component to provide comparable thermal histories between samples, and then heated at 10^oC/min beyond the melting temperature of both components. Thermal properties for each sample were extracted from the second scan.

Results and discussion

Figure 4.1 shows the thermograms for blends of PA-18 and *n*-octadecane whose chemical structure is similar to the octadecyl side chain of PA-18. *N*-Octadecane has a melting point below that of PA-18. At low concentrations of *n*-octadecane, the blend exhibits a single peak near the melting temperature of PA-18, but depressed slightly, approximately 1.5°C. Table 4.1 shows the thermal properties extracted from these thermograms. The heat of fusion for the blend is about what would be expected by simple additivity of the blend components. Two endothermic melting peaks appear as the concentration of *n*-octadecane increases to 50 wt%. The lower-temperature peak is near that of pure *n*-octadecane, while, the second peak is closer to that of pure PA-18 albeit both peaks have depressed melting temperatures compared to the pure components. The heat of fusion of the *n*-octadecane component is 30% less than expected by simple additivity of the blend components.

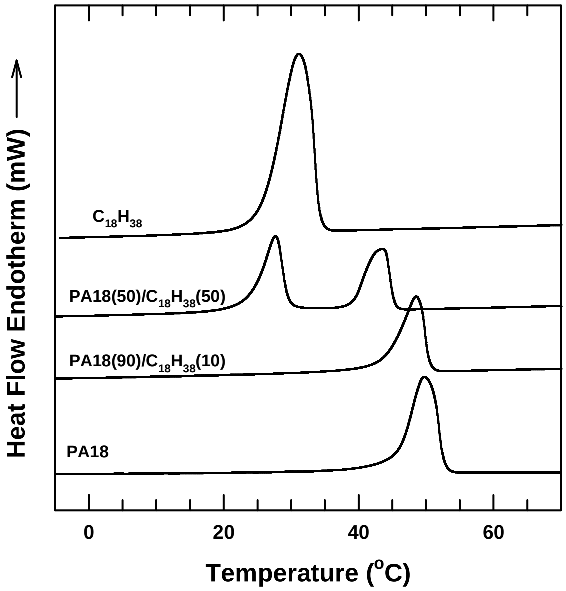

Figure 4.1: DSC scans of poly (octadecyl acrylate) and *n*-octadecane blends.

The PA-18 component has a higher heat of fusion than expected (12 cal/g) which suggests that *n*-octadecane increases crystallization or partially co-crystallizes with the *n*-octadecyl side chains of PA-18. Despite the increase in the heat of fusion experienced by the PA-18 due to co-crystallization, the crystallization of *n*-octadecane component is hindered by the presence of PA-18.

Table 4.1: Melting temperatures and heats of fusion of poly (octadecyl acrylate) and *n*-octadecane blends.

Polymer (wt%)	T_m (^oC)	ΔH_f (cal/g)	T_m (^oC)	ΔH_f (cal/g)
PA18	50.2	23.9	-	-
PA18(90)/$C_{18}H_{38}$(10)	48.5	26.4	-	-
PA18(50)/$C_{18}H_{38}$(50)	43.2	14.3	27.5	19.8
$C_{18}H_{38}$	-	-	31	57.9

The thermogram for blends of PA-18 and *n*-tetracosane are shown in Figure 4.2. *N*-tetracosane has a similar melting point as PA-18; however, a split melting peak is shown for the thermal history given; this is common behavior for some alkanes[7]. A single endothermic melting peak is observed for the PA-18 and *n*-tetracosane blends. Since the melting points are so close for the pure components, the single melting peak could arise due to peak overlap or co-crystallization. The melting peaks for the blends are depressed compared to that of the pure components as shown in Table 4.2. The 10 wt% *n*-tetracosane blend has a narrow peak compared to the pure materials and the 50/50 wt% blend and the heat of fusion is about what is expected from linear additivity. The heat of fusion for the 50/50 wt% blend is slightly lower than expected based on the pure materials added.

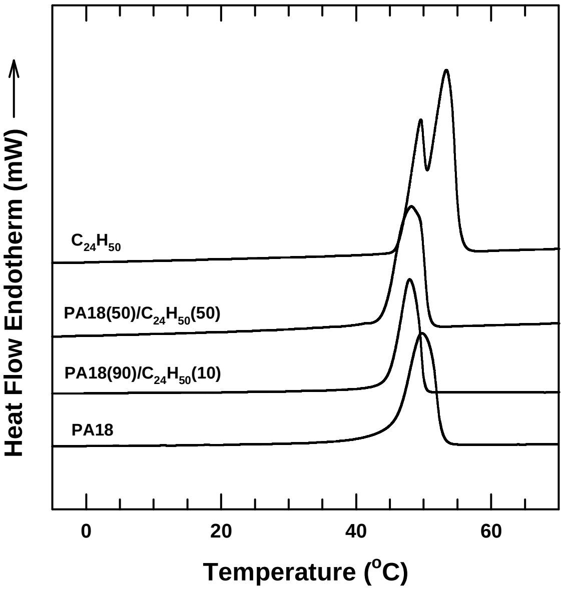

Figure 4.2: DSC scans of poly (octadecyl acrylate) and *n*-tetracosane blends

Table 4.2: Melting temperatures and heats of fusion of poly (octadecyl acrylate) and *n*-tetracosane blends.

Polymer (wt %)	T_m (°C)	ΔH_f (cal/g)	T_m (°C)	ΔH_f (cal/g)
PA18	50.2	23.9	-	-
PA18(50)/$C_{24}H_{50}$(50)	48.2	38.7		
PA18(90)/$C_{24}H_{50}$(10)	47.9	26.4		
$C_{24}H_{50}$(10)	-	-	49.5, 53.4	62.7

For both *n*-octadecane and *n*-tetracosane blends with PA-18, the heat of fusion of the blend is higher than that of the pure homopolymer. This suggests that an increased number of methylene units crystallize compared to the pure homopolymer due to this increased heat of fusion, i.e., crystallinity. Blends with greater than 10 wt% *n*-paraffins form films that are extremely brittle due to the low molecular weight of the paraffin components.

Figure 4.3 shows the thermograms for blends of PA-18 and *n*-octadecanoic acid. The DSC scans resemble those of the PA-18 and *n*-octadecane blends in Figure 4.1. The melting temperature for *n*-octadecanoic acid is higher than that of PA-18. Blends with high levels of the fatty acid show two endothermic peaks with positions similar to those of the pure components. At low concentrations, a single peak appears for the blend indicating co-crystallization. The heats of fusion are lower than theoretically possible had both components crystallized without hindrance, see Table 4.3.

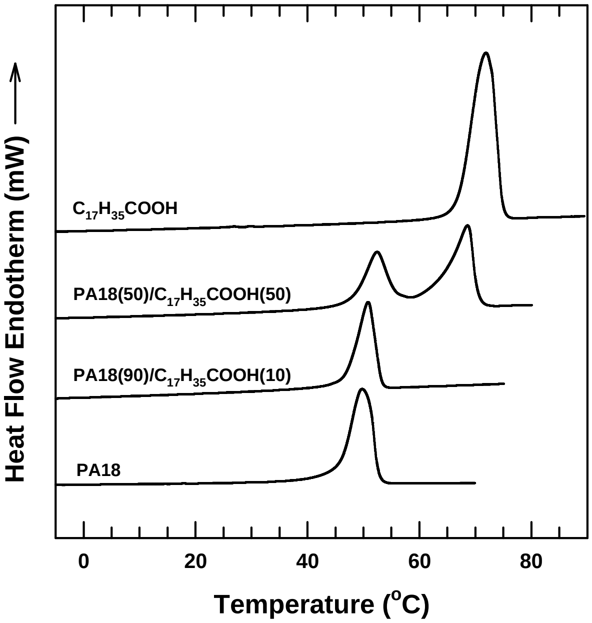

Figure 4.3: Figure DSC scans of poly (octadecyl acrylate) and *n*-octadecanoic acid blends.

Table 4.3: Melting temperatures and heats of fusion of poly (octadecyl acrylate) and *n*-octadecanoic acid blends.

Polymer (wt %)	T_m (°C)	ΔH_f (cal/g)	T_m (°C)	ΔH_f (cal/g)
PA18	50.2	23.9	-	-
PA18(90)/$C_{17}H_{35}COOH$(10)	50.9	27.8	-	-
PA18(50)/$C_{17}H_{35}COOH$(50)	52.4	13.2	68.5	20.8
$C_{17}H_{35}COOH$	-	-	71.9	55.6

The thermal properties of PA-18 blend with *n*-hexadecanol and *n*-octadecanol at 10 wt% are shown in Table 4.4. The fatty alcohol, *n*-hexadecanol has a similar melting temperature of PA-18 and *n*-octadecanol has a chemical structure similar to the octadecyl side-chain of PA-18. Each fatty alcohol blend has a single peak with heats of fusion that are lower than expected from linear additivity of the pure components.

Table 4.4: Melting temperatures and heats of fusion of poly (octadecyl acrylate) and n-octadecanoic acid blends.

Polymer	T_m (^oC)	ΔH_f (cal/g)
PA18	50.2	23.9
PA18(90)/$C_{16}H_{33}OH$(10)	48.9	25.8
$C_{16}H_{33}OH$	52.7	57.5
PA18(90)/$C_{18}H_{37}OH$(10)	50.7	25.7
$C_{18}H_{37}OH$	63.5	60.0

Blending low molecular weight fatty compounds with PA-18 show some promise to increase the crystallinity and possibly increase the magnitude of the permeation jump; however, only low amounts of these materials form suitable films. Due to low molecular weight of the fatty compounds the films were very brittle even at low concentrations, thus, permeability of these materials were not determined.

HOMOPOLYMER AND COPOLYMER POLY (N-ALKYL ACRYLATE) BLENDS

Homopolymer and copolymer blends are examined to compare their thermal behavior to binary homopolymer blends and to determine whether copolymers can help extend the homogeneity map established for binary homopolymers. The random copolymers were made by procedures established in this laboratory[1]. Blends were prepared by mixing the appropriate portions of the homopolymer and copolymer in a 10 wt% toluene solution. Polymer films were formed by solution casting and allowed to solidify in a fume hood by way of solvent evaporation. Films were placed in a vacuum oven at elevated temperatures to remove the remaining solvent. Thermal properties of selected films were examined by differential scanning calorimetry. The samples were heated through an initial heating cycle to remove any residual crystallinity, cooled at 5^{o}C/min, and then heated at 10^{o}C/min through a second heating cycle. Thermal properties were obtained from the second scan to ensure similar crystallization conditions.

Results and discussion

The thermal properties of the homopolymers and copolymers used in this investigation are shown in Table 4.5. The copolymers are represented by the molar ratio x_1/x_2 of respective monomers 1 and 2 present. The copolymers chosen for this investigation are of similar average side-chain length as the homopolymers. The average side-chain length of a copolymer is expressed as

$$\langle n \rangle = x_1 n_1 + x_2 n_2 \tag{1}$$

where x_1 is the mole fraction of monomer 1 with side-chain length n_1 and x_2 is the mole fraction of monomer 2 with side-chain length n_2[1]. The copolymers examined are all semi-crystalline except for P(A6-co-A12) 75/25 mol% which is amorphous at room temperature.

Figure 4.4 is a map of the macroscopic homogeneity between the homopolymers of side-chain length *n* and copolymers with an average side-chain length <*n*> for 50/50 wt% homopolymer/copolymer blend combinations. Comparing a similar map, Figure 3.1, for binary homopolymer blends shows that using copolymers does not extend or widen the limits of homogeneity. As expected from the binary homopolymer blends, there are no homogeneous mixtures comprised of amorphous and crystalline materials.

Table 4.5: Melting temperature and heat of fusion for homopolymers and copolymers of various side chain lengths cooled at 5°C/min.

Homopolymers	Side–chain length *n*	T_m (°C)	H_f (cal/g)
PA-18	18	50.0	23.9
PA-16	16	37.8	19.8
PA-14	14	22.3	14.9
PA-12	12	0.2	7.3
PA-10	10	-	-
Copolymers (mol %)	**Average side– chain length < *n* >**	**T_m (°C)**	**H_f (cal/g)**
P(A6-co-A22) 25/75%	18	56.2	30.9
P(A10-co-A18) 25/75%	16	38.7	17.6
P(A14-co-A18) 50/50%	16	32.5	18.4
P(A6-co-A22) 50/50%	14	50.5	20.3
P(A6-co-A12) 75/25%	7.5	-	-
P(A6-co-A22) 75/25%	10	33.0	11.5

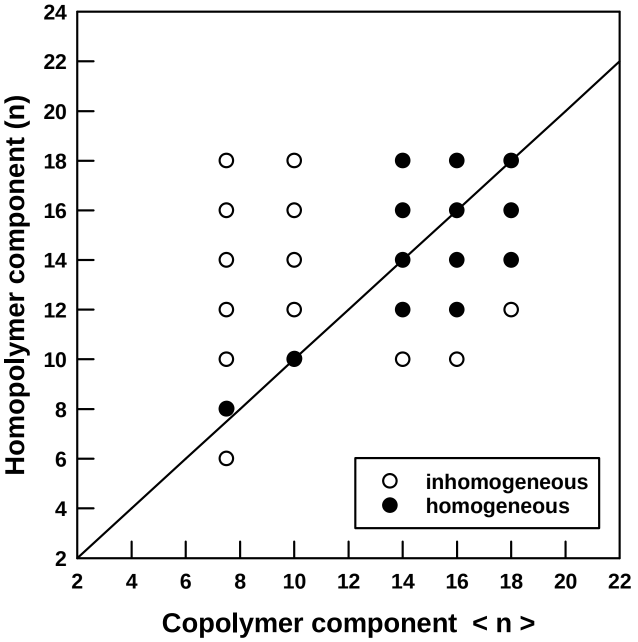

Figure 4.4: Map of film homogeneity for 50/50 weight poly(*n*-alkyl acrylate) homopolymer and copolymer blends with side-chain lengths n and <*n*>, respectively; the filled circles represent homogeneous mixtures while the open circles represent grossly heterogeneous mixtures.

Generally two endothermic peaks are observed for homopolymer and copolymer blends which is similar to what is observed for binary homopolymer blends. Figure 4.5 shows the typical thermogram for blends containing two semi-crystalline homopolymer and copolymer components; two homopolymers PA-16 and PA-18 are blended with equal weight of copolymer P(A6-co-A22) 25/75 mol%. The copolymer has an average side-chain length of 18 and a melting temperature higher than that of the homopolymers, PA-16 and PA-18, as seen in Table 4.5, thus, the peak corresponding to the copolymer appears as the higher melting component in Figure 4.5 for both blends.

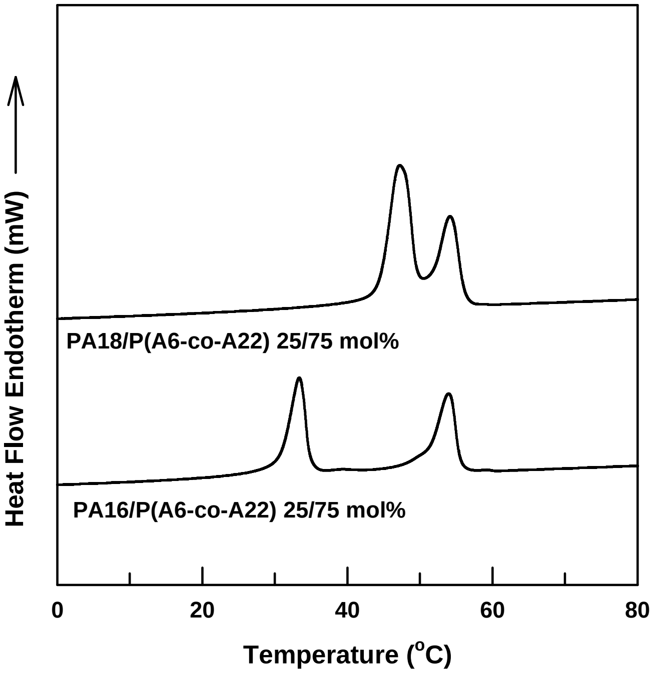

Figure 4.5: Thermograms for PA18 and PA16 homopolymers blend with copolymer P(A6-co-A22) at 25/75 mole percent of respective monomer.

Table 4.6: Melting temperatures and heats of fusion for selected 50/50 wt% blends of poly (*n*- alkyl acrylate) homopolymers and copolymers of various side chain lengths cooled at 5^{o}C/min.

Homopolymer/copolymer blends	Blend *n* /< *n* >	Homopolymer component		Copolymer component		Blend	
		T_m (^{o}C)	H_f (cal/g)	T_m (^{o}C)	H_f (cal/g)	H_f (cal/g) Exp	H_f cal/g) Theo
PA18/P(A6-co-A22) 25/75%	18/18	47.2	11.0	54.2	5.8	27.0	27.4
PA16/P(A6-co-A22) 25/75%	16/18	33.4	9.1	53.9	9.0	24.5	25.3
PA16/P(A14-co-A18) 50/50%	16/16	33.2	-	33.2	-	17.7	19.1
PA16/P(A10-co-A18) 25/75%	16/16	32.9	3.9	37.4	2.2	17.0	18.7

For the homogeneous blends consisting of homopolymer and copolymer components that are both semi-crystalline, typically the endothermic peaks are distinct unless the melting temperature of the components are similar such that the peaks overlap as seen for the PA18/P (A6-co-A22) 25/75 mol% blend in Figure 4.5. The melting temperature and heat of fusion for each component and the total heat of fusion for the blend are shown in Table 4.6 for the equal-weight PA18/P (A6-co-A22) 25/75 mol% blend and other selected homopolymer and copolymer blends. The experimental heat of fusion for the blend is computed by constructing a straight baseline encompassing the entire area of both endothermic peaks and the theoretical values are determined from linear additivity of the heats of fusion for the pure components present. The total heat of fusion for each blend is less than theoretically expected in the event that both components crystallize independently and without hindrance from one another.

The exception to these observations is the equal-weight PA16/P (A14-co-A18) 50/50 mol% blend that is characterized by a single endothermic peak as shown in Figure 6.6. The blend peak has a melting temperature between that of the pure components and of smaller breadth that suggests co-crystallization of the components. Although copolymer P (A10-co-A18) 75/25 mol % has an average side-chain length of 16 similar to P (A14-co-A18) 50/50 mol%, the equal-weight PA16/P(A10-co-A18) 75/25 mol % blend has two distinct peaks, characterized in Table 6.6. Structural studies are needed to verify that the narrow single peak is due to co-crystallization and not due to simple peak overlap.

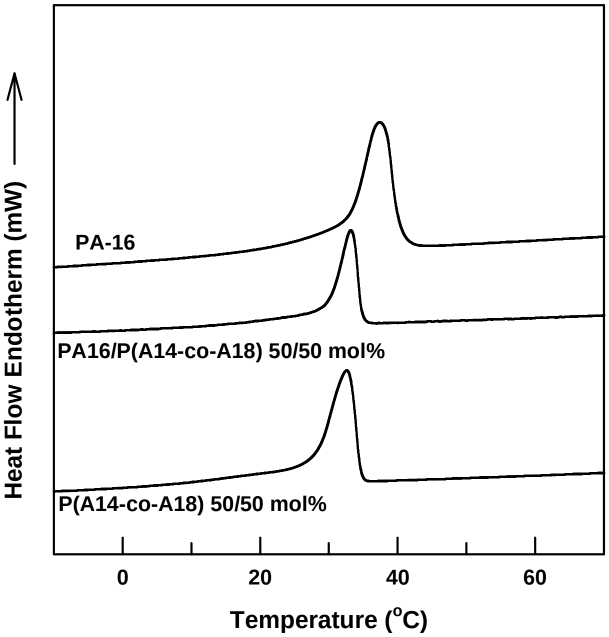

Figure 4.6: Thermograms for equal weight blend of PA16 and P(A14-co-A18) at 50/50 mole percent of the respective monomers and the pour components.

CONCLUSIONS

Poly (octadecyl acrylate) and fatty compound blends resulted in useful films at only low concentrations of the fatty materials. The crystallinity of the blend was slightly greater than that of the pure homopolymer suggesting that the permeation switch may be greater as suggested by trends seen for homopolymers, blends and copolymers. Permeation measurements were not conducted on these materials due to their very brittle nature and the mediocre increase in crystallinity.

Poly (*n*-alkyl acrylate) homopolymer and copolymer blends did not enable significantly different side-chain length materials to form homogeneous films so as to extend the homogeneity map of the binary homopolymers. The thermal behavior of homopolymer and copolymer blends is very similar to binary homopolymer blends with the exception of one blend, equal-weight PA16/P(A14-co-A18). Therefore, the permeation-temperature behavior for homopolymer and copolymer blends are expected to be similar to the binary homopolymer blends. From this cursory analysis, it is evident that poly (*n*-alkyl acrylate) homopolymer and copolymer blends can provide an alternative pathway to create thermally responsive membranes.

REFERENCES

1. O'Leary KA. Physical properties of poly (n-alkyl acrylate) copolymers. 2005. pp. 226 pp.
2. Kirkland BS and Paul DR. Gas transport in poly (n-alkyl acrylate)/ poly (m-alkyl acrylate) blends. The University of Texas at Austin.
3. Jordan EF, Jr., Smith S, Jr., Parker WE, Artymyshyn B, and Wrigley AN. Journal of Applied Polymer Science 1978;22(6):1509-1528.
4. Rubin ID and Pugliese RD. Angewandte Makromolekulare Chemie 1989;171:165-173.
5. Inomata K, Sakamaki Y, Nose T, and Sasaki S. Polymer Journal 1996;28(11):986-991.
6. Saikia PJ and Baruah SD. Journal of Applied Polymer Science 2007;104:1226-1231.
7. Mazee WM. The phase behavior of n-alkanes and some of their binary mixtures. Symposium on Recent Advances in the Chemical Thermodynamics of Hydrocarbons and Related Substances, vol. 3. Chicago, IL, 1958. pp. 35-47.

Chapter 5: Designing a modified atmosphere package

INTRODUCTION

Modified atmosphere packaging of fresh fruits and vegetables creates an optimal atmosphere to prolong shelf life by matching the produce respiration rate to the film permeation rate. However to achieve optimal O_2 and CO_2 concentrations using polymer films can require extensive experimental trials. Modeling the system allows prediction of the concentrations inside an MA package design, i.e., for a particular produce and package design. Models such as the Paul-Clarke retail model can be extremely useful for cursory and detailed examinations for produce and package considerations. Produce respiration and polymer permeation are the major processes considered that require some experimental or analytical representation to assist with predicting the gas concentration inside the package. In this chapter the effects of oxygen and carbon dioxide, and temperature on the respiration rates are reviewed along with the dynamic interaction of the respiration and permeation process in MA packaging. In addition, temperature effects have been incorporated into the Paul and Clarke model to predict package concentrations as a function of temperature.

THE INFLUENCE OF REDUCED O_2 AND ELEVATED CO_2 ON THE RESPIRATION RATE OF PRODUCE

Respiration is an oxidative process whereby substrates are broken down into simpler molecules such as O_2 and CO_2 as represented by the overall reaction, Equation 2.9. The respiration rate is a measure of this metabolic activity. Generally, respiration rates decrease as produce mature[1]. Post harvest, climacteric produce such as bananas, melons (cantaloupe, watermelon, and honeydew), apples and tomatoes experience a natural or climacteric rise, in its respiration rate that is normally accompanied by an increase in endogenous ethylene, the natural ripening hormone, production and then decreases as normal over time. Non-climacteric produce do not experience this rise in respiration rate. Many have found that lowered O_2 and elevated CO_2 concentrations of both climacteric and non-climacteric help extend the shelf life by lowering respiration rates, i.e., the shelf-life is inversely proportional to the respiration rate[2-6]. Platenius showed that low oxygen concentrations reduce the O_2 consumption rate for asparagus, spinach, snap beans, shelled peas, and carrots[6]. Kidd and West[3] found that O_2 and CO_2 significantly affected the climacteric rise in apples. The absence of oxygen eliminated the climacteric peak for pre-climacteric apples and post-climacteric studies showed that ethylene production is continuous, but in the absence of oxygen inhibits its stimulatory effect that induces ripening; high carbon dioxide concentrations induced a delayed climacteric rise. This climacteric nature of some produce enables some additional control over the ripening process. It is standard commercial practice to harvest some climacteric produce at the beginning of the maturation stage so that the introduction of exogenous ethylene can initiate the ripening process at a desired time. Although Kidd and West conducted experiments in the absence of oxygen, concentrations of oxygen must be maintained above the extinction point, below which anaerobic respiration tends to dominate and cause increased production of fermentation products such as ethanol and acetaldehyde. These products can cause undesirable odors and flavors making the produce inedible. The extinction point varies due to substrate type and temperature[7] making it difficult to design a versatile MA package capable of reaching optimal conditions over a range of temperatures. Like the extinction point, optimal O_2 and CO_2 concentrations depend on produce type, variety, maturity, and pre-harvest handling conditions as shown in Table 5.1. Short excursions away from the optimal concentrations are usually not detrimental to the produce quality; however, produce stored outside of the range for long periods can result in physiological damage.

Table 5.1: MA and CA recommendations for selected produce. The Post harvest Technology Research and Information Center of the Department of Plant Services' web site (http://postharvest.ucdavis.edu) is a repository of recommended storage conditions for a wide range of fruits and vegetables.

Produce	Temperature (°C)	Atmosphere	
		% O_2	% CO_2
apple, cultivars	0 – 2.5	1 – 2	1 – 3
apple, red delicious	0	1.6	1.8
banana	12 – 16	2 – 5	2 – 5
blueberry	0 – 5	2 – 5	12 – 20
broccoli, florets	0 – 5	2 – 3	6 – 7
broccoli	0 – 5	1 – 2	5 – 10
cantaloupe	2 – 7	3 – 5	10 – 20
cauliflower	0 – 5	2 – 3	3 – 4
celery	0 – 5	1 – 4	3 – 5
lettuce, head	0 – 5	1 – 3	0
lettuce, shredded	0 – 5	1 – 5	5 – 20
tomatoes, green	12 – 20	3 – 5	2 – 3
tomatoes, ripe	10 – 15	3 – 5	3 – 5
cherry, sweet	0 – 5	3 – 10	10 – 15
fig	1 – 5	5 – 10	15 – 20
grapefruit	10 – 15	3 – 10	5 – 10
mango	10 – 15	3 – 7	5 – 8
strawberry	0 – 5	5 – 10	15 – 20

MEASURING AND MODELING RESPIRATION RATES

Respiration rates are measured via non-destructive methods using closed, flow through, or permeable systems. Closed systems are good for measuring low respiring produce that are enclosed in an impermeable, airtight container of known volume where gas concentrations are sampled as a function of time. Respiration rates obtained with this method are measured at high O_2 / low CO_2 and low O_2 / high CO_2 concentrations therefore some care should be taken when applying analytical expressions obtained using this method. The flow through method encloses produce in an impermeable container with piping or tubing into and out of the container to flow a gas stream of known O_2 and CO_2 concentration. The gas concentration of the outlet can be measured at steady state to directly compute the respiration rate knowing the difference in O_2 and CO_2 concentrations between the inlet and outlet. The flow through method enables use of various O_2 and CO_2 ranges, but respiration rates must be high enough to provide noticeable changes between the inlet and outlet concentrations for accurate measurement. In the permeable method, produce is enclosed in a permeable package and the concentration of the package free volume or head space is examined as a function of temperature and/or at steady state with the use of accessible ports[8]. Although the permeable method is the least accurate due to the number of unknown variables such as film permeability and geometrical parameters (area and thickness), it is the best way to examine the performance of an actual MA package with respiring produce enclosed. When attempting to model concentrations inside a package enclosing a particular produce, it is important to know the method used to obtain the respiration rate.

The aerobic respiration process involves several complex metabolic pathways, glycolysis, tricarboxylic acid cycle and the electron transport system[1]. Therefore, modeling the respiration rate can become very complex depending on the factors considered. Since each produce type has different respiration rates that depend on the substrate, several individual respiration rate models have been developed for various produce [4, 5, 7, 9-24]. Analytical expressions relating the O_2 and CO_2 concentrations to the respiration rate, O_2 consumed or CO_2 produced, results in multiple parameters to fit the empirical data which are useful only for concentration ranges examined during measurement[9-11]. Lee[12] introduced an approach based on enzyme kinetic theory to determine respiration rates from the suggestion of a previous empirical model[9]. Lee implemented a Michaelis–Menten type equation to model the respiration of fresh produce because it is an enzymatic process regulated by allosteric enzymes; the respiration rate of microorganisms has also been modeled successfully using the Michaelis–Menten type equation[12]. For enzyme based respiration rate models, CO_2 is considered the inhibitor while O_2 is considered the substrate. In the absence of carbon dioxide, respiration rates per mass of produce, r_i, of gas *i* can be modeling using the following form

$$r_i = \frac{V_m[\mathrm{O_2}]}{K_m + [\mathrm{O_2}]} \tag{5.1}$$

where V_m is the maximum O_2 consumption rate per mass of produce, $[O_2]$ is the concentration of O_2 (%), and K_m is a Michaelis constant for oxygen consumption (% O_2). Carbon dioxide can influence the rate of respiration of produce to varying degrees. There are various types of CO_2 inhibition, competitive, uncompetitive, a combination of competitive and uncompetitive, and non-competitive, can be accounted for using the enzyme kinetic model[13, 14]. A competitive inhibition model is necessary when both the inhibitor (CO_2) and the substrate (O_2) compete for an active enzyme site and can be represented by the following expression

$$r_i = \frac{V_m[\mathrm{O_2}]}{[\mathrm{O_2}] + K_m\left(1 + \frac{[\mathrm{CO_2}]}{K_c}\right)} \tag{5.2}$$

The parameter K_c is a Michaelis constant for competitive inhibition with units of % CO_2 and $[CO_2]$ is the carbon dioxide concentration (%). When the inhibitor (CO_2) reacts with the enzyme-substrate complex and does not react with the enzyme, the inhibition mechanism is uncompetitive inhibition that can be represented by

$$r_i = \frac{V_m[\mathrm{O_2}]}{K_m + [\mathrm{O_2}]\left(1 + \frac{[\mathrm{CO_2}]}{K_u}\right)} \tag{5.3}$$

The parameter K_u is the Michaelis constant for uncompetitive inhibition with units of % CO_2. The model combining the influence of the competitive and uncompetitive inhibition accounts for the relative activity of each inhibition mechanism is expressed as follows

$$r_i = \frac{V_m[O_2]}{K_m\left(1+\frac{[CO_2]}{K_c}\right)+[O_2]\left(1+\frac{[CO_2]}{K_u}\right)} \tag{5.4}$$

Non-competitive inhibition is also a combination of completive and uncompetitive inhibition assuming both are equally active where the respiration rate is represented by

$$r_i = \frac{V_m[O_2]}{(K_m+[O_2])\left(1+\frac{[CO_2]}{K_n}\right)} \tag{5.5}$$

and K_n is the Michaelis non-competitive inhibition constant (% CO_2). Peppelenbos[13] evaluated the use of competitive, uncompetitive and non-competitive, and the combination inhibition methods to model the respiration rate of broccoli and other produce. Each inhibition method provided a good fit to the experimental data, but a single inhibition model that best fit the data was not found. Thus, the inhibition model generating the simpler expression is preferred for modeling. Although the enzyme based model provide great fits to the experimental data, the model parameters V_m, K_m, K_c, K_u, and K_n are considered empirical parameters that describe the respiration of fruits and vegetables phenomenologically rather than theoretical parameters of some physical meaning[13, 14]. The aforementioned model parameters must be determined for each gas i depending on the respiration rate, r_i , being sought and temperature being evaluated; these parameters should not be interpolated as they generally do not vary linearly with concentration or temperature. When predicting gas concentrations inside a MA package, respiration rates are better expressed as functions of mole fractions of oxygen and carbon dioxide, x_{O_2} and x_{CO_2} rather than as percent concentrations, [O_2] or [CO_2]. For example, the gas concentrations in Equations 5.1 – 5.5 can be expressed as a mole fractions of oxygen and carbon dioxide, x_{O_2} and x_{CO_2}, using the simple relation

$$x_i = \frac{[\mathrm{O}_2]}{100} \tag{5.6}$$

Literature[4, 5, 7, 9-12, 15-26] shows that most respiration rate models developed for MA package modeling have used either the closed or flow through system to model the respiration rate using the enzymatic kinetic theory. The enzyme based respiration rate expressions are then verified by conducting permeable method experiments and comparing the measured respiration rates to those computed from the previously determined respiration rate expression.

It takes much effort to determine the respiration rate of produce using enzyme kinetic theory as a basis. For example, the closed system is used to gather data in the transient state where O_2 and CO_2 concentrations are measured as a function of time. Generally this data is best fit with functions that have the lowest error through non-linear regression analysis. Hagger[19] found expressions for both oxygen and carbon dioxide concentrations for respiring broccoli that are generally used that

$$[\mathrm{O}_2] = 21 - \frac{t}{(A_1 t + B_1)C_1} \tag{5.7}$$

adequately represents for the oxygen concentration where *t* is the time from the start of the experiment to the point at which the overhead space is sampled and A_1, B_1, and C_1 are all constants. A similar expression is obtained for the CO_2 concentration

$$[CO_2] = \frac{t}{(A_2 t + B_2)C_2} \tag{5.8}$$

where A_2, B_2, and C_2 are all constants. The respiration rate of gas *i* per mass, W, of produce in a package of the constant free volume, V, is the amount or moles, n_i, of gas *i* consumed or evolved by the produce as a function of time that can be expressed as

$$r_i = \frac{d[\mathrm{i}]}{dt}\frac{p_t V}{WRT} \tag{5.9}$$

assuming that gas *i* is ideal (n_i = [i]PV/RT) where p_t is the total pressure that is atmospheric both inside and outside the package, *R* is the molar gas constant and *T* is the absolute temperature of these system. The following is obtained by taking the time derivative of Equations 5.7 and 5.8[19]

$$\frac{d[\mathrm{O_2}]}{dt} = A_1 C_1 t(A_1 t + B_1)^{(-1-C_1)} - (A_1 t + B_1)^{-C_1} \tag{5.10}$$

and

$$\frac{d[\mathrm{CO_2}]}{dt} = -A_2 C_2 t(A_2 t + B_2)^{(-1-C_2)} + (A_2 t + B_2)^{-C_2} \tag{5.11}$$

The respiration rate of oxygen and carbon dioxide can be obtained by combining the respective Equations 5.10 and 5.11 with Equation 5.9

$$r_{O_2} = -\left(A_1 C_1 t(A_1 t + B_1)^{(-1-C_1)} - (A_1 t + B_1)^{-C_1}\right)\frac{p_t V}{WRT} \tag{5.12}$$

and

$$r_{CO_2} = \left(- A_2 C_2 t(A_2 t + B_2)^{(-1-C_2)} + (A_2 t + B_2)^{-C_2}\right)\frac{p_t V}{WRT} \tag{5.13}$$

The respiration rate of O_2 is preceded by a negative sign due to its consumption by the produce. For the closed system method, model parameters are determined by estimating the respiration rates using Equations 5.12 and 5.13 and using multiple linear regression. Linearization of the various enzyme based respiration rate functions, Equations 5.1 – 5.5, results in the following for the Michaelis – Menten type

$$\frac{1}{r_i} = \frac{1}{V_m} + \frac{K_m}{V_m}\frac{1}{[\mathrm{O_2}]} \tag{5.14}$$

competitive inhibition

$$\frac{1}{r_i} = \frac{1}{V_m} + \frac{K_m}{V_m}\frac{1}{[\mathrm{O_2}]} + \frac{K_m}{V_m K_c}\frac{[\mathrm{CO_2}]}{[\mathrm{O_2}]} \tag{5.15}$$

uncompetitive inhibition

$$\frac{1}{r_i} = \frac{1}{V_m} + \frac{K_m}{V_m}\frac{1}{[\mathrm{O_2}]} + \frac{1}{V_m K_u}[\mathrm{CO_2}] \tag{5.16}$$

combination of competitive and uncompetitive

$$\frac{1}{r_i} = \frac{1}{V_m} + \frac{K_m}{V_m}\frac{1}{[\mathrm{O_2}]} + \frac{K_m}{V_m K_c}\frac{[\mathrm{CO_2}]}{[\mathrm{O_2}]} + \frac{1}{V_m K_u}[\mathrm{CO_2}] \tag{5.17}$$

and non-competitive inhibition

$$\frac{1}{r_i} = \frac{1}{V_m} + \frac{K_m}{V_m}\frac{1}{[\mathrm{O_2}]} + \frac{K_m}{V_m K_n}\frac{[\mathrm{CO_2}]}{[\mathrm{O_2}]} + \frac{1}{V_m K_n}[\mathrm{CO_2}] \tag{5.18}$$

It is clear from the expression for a combination of competitive and uncompetitive inhibition, Equation 5.17, and non-competitive inhibition, Equation 5.18, that both mechanisms are combinations of the competitive and uncompetitive inhibition models. However, the combination inhibition equally adds the effects of the competitive and uncompetitive mechanisms whereas the non-competitive adds their relative activity via the Michaelis constant K_n. When modeling, the respiration rates are linearized using the simplest expression, commonly the uncompetitive inhibition form, which provides a good fit of the experimental data to the enzyme based model. Multiple linear regression is also used for steady state data obtained via the flow through system. Table 5.2 shows the model parameters obtained using a closed system to measure the consumption rate of O_2 for broccoli[19]; similar parameters where obtained for the respiration rate of CO_2. The model parameters were obtained for four different temperatures. As stated earlier, the Michaelis parameters are normally verified by comparing the respiration rates predicted using the enzyme based respiration rate of O_2 and /or CO_2 to their respective rate that is experimentally determined from the permeable method.

Table 5.2: Michaelis parameters estimated for an enzyme based O_2 respiration rate model for the respiration of broccoli using an uncompetitive CO_2 inhibition model.

Temperature (^oC)	V_m (mg/kg h) [a]	K_m (% O_2) [a]	K_u (% CO_2) [a]
0	59.22	2.18	5.07
7	210.30	0.57	2.26
13	380.54	1.40	2.20
24	676.52	3.19	3.96

[a] From ref[19]

From a design perspective, the oxygen and carbon dioxide concentrations inside the permeable package can also be predicted by assuming the system is at steady state and conducting a material balance to account for the respiration and permeation processes are balanced. The sum of the flow rate of gas *i* through the packing film and the consumption or evolution of gas *i* via respiration of the produce is equal to the amount of gas *i* accumulated which is zero at steady state

$$\left\{\begin{matrix} \textit{rate of gas i} \\ \textit{generated by} \\ \textit{the produce} \end{matrix}\right\} + \left\{\begin{matrix} \textit{rate of gas i} \\ \textit{consumed by} \\ \textit{the produce} \end{matrix}\right\} + \left\{\begin{matrix} \textit{rate of gas i} \\ \textit{permeating} \\ \textit{into package} \end{matrix}\right\} = \left\{\begin{matrix} \textit{rate of} \\ \textit{accumulation} \\ \textit{of gas i} \end{matrix}\right\} \tag{5.19}$$

The rate of gas i permeating the polymer film comprising the package can be represented as

$$\{\, \textit{permeation rate of gas i} \,\} = \frac{P_i A_p p_t (x_{i,o} - x_{i,i})}{\ell_p} \tag{5.20}$$

where P_i is the permeability coefficient for gas i through the total area, A_p, of the polymer film with a thickness ℓ_p, p_t is the total pressure outside and inside the package that is maintained at constant atmospheric pressure, $x_{i,o}$ and $x_{i,i}$ are the mole fractions of gas i

outside and inside the package, respectively. Outside the package the atmosphere is that of fresh air ($x_{O_{2,o}} = 0.21$, $x_{CO_{2,o}} = 0$ and $x_{O_{2,o}} = 0.79$). The balance of the respiration and permeation processes, Equation 5.19, for gas *i* combined with Equation 5.20 can be written as

$$r_i W + \frac{P_i A_p p_{\mathrm{t}} (x_{i,o} - x_{i,i})}{\ell_p} = 0 \tag{5.21}$$

The preceding equation is used to solve for the concentration of gas *i* inside the package and is the most commonly used mathematical MA model used throughout literature. To determine the oxygen concentration inside a package using Equation 5.21, a respiration rate model must be chosen. For the simplest case, the Michaelis – Menton type expression from Equation 5.1 is used to obtain a quadratic expression for the oxygen concentration, $x_{O_2,i}$

$$a x_{O_2,i}^2 + b x_{O_2,i} + c = 0 \tag{5.22}$$

where the constants a, b and c are

$$a = 1$$

$$b = \left[\frac{1}{100} \left(K_m - 21 \right) + \frac{W \ell_P V_m}{P_{O_2} A_p p_t} \right]$$

$$c = -\frac{21}{100} K_m$$

The CO_2 concentration inside the package may be determined in a similar fashion. To develop explicit expressions for $x_{O_2,i}$ or $x_{CO_2,i}$ inside the package using a respiration rate function with CO_2 inhibition requires that both oxygen and carbon dioxide material balances be solved simultaneously. This further complicates the process and is beyond the scope of this discussion.

This simple calculation to determine the concentration of O_2 and CO_2 surrounding the produce inside the package is an MA package model with a simple package design.

MA models for retail packages with more sophisticated designs consisting of pores or perforations have been developed to change the CO_2 to O_2 permselectivity of the package or a high-flux membrane label by adjusting the relative permeation through the non-selective membrane to the selective membrane[16, 27-29]. The process determining the concentration inside the package is summarized in the flow diagram in Figure 5.1. For a given produce choice, the optimal storage temperature and the O_2 and CO_2 gas concentration targets, similar to the ranges shown in Table 5.1, are defined. It is evident from this commonly used mathematical MA model that the respiration of produce and the permeation of the packaging film are dependent on concentration of O_2 and CO_2 inside the package, but both are also functions of temperature.

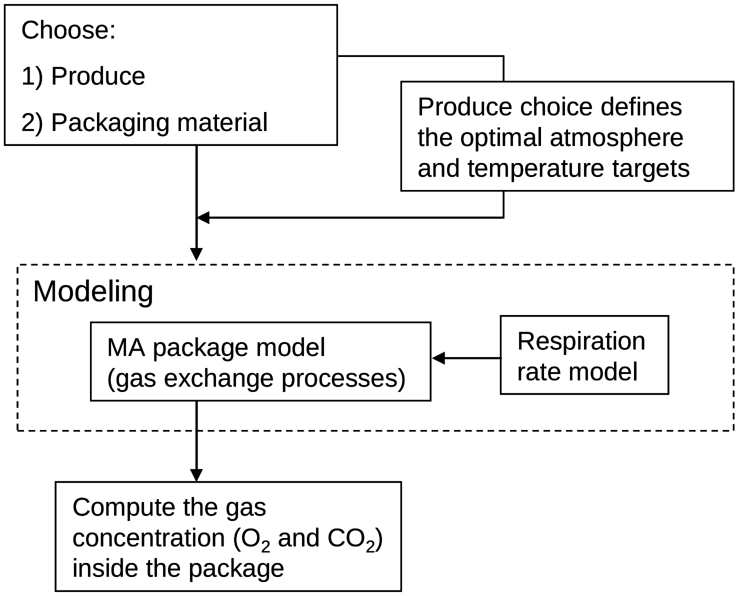

Figure 5.1: A flow diagram illustrating the process to develop a model to predict the concentration of the modified atmosphere for a system consisting of a particular package design and produce.

EFFECT OF TEMPERATURE ON THE RESPIRATION RATE OF PRODUCE

Although reduced O_2 and elevated CO_2 levels help extend produce shelf life, low temperature storage has the largest influence on reducing metabolic activity, i.e., respiration rates[2, 7, 10]. Precise temperature control is ideal throughout the distribution chain of produce, but temperature fluctuations are inevitable. Therefore, it is essential to understand how the respiration rate varies with temperature. The respiration rate, r_i is often found to have an Arrhenius relationship with temperature

$$r_i = r_{o,i} \exp(-E_{R,i} / RT) \qquad (5.23)$$

where $r_{o,i}$ is the respiration pre-exponential factor for gas i, and $E_{R,i}$ is the activation energy for respiration of gas i, R is the molar gas constant and T is the absolute temperature. This form is useful for determining the respiration rate of produce stored at different temperatures given the necessary parameters, i.e., $r_{o,i}$ and $E_{R,i}$. The effects of temperature on the respiration rate of produce has been widely measured and found to follow this Arrhenius relationship for a particular gas concentration. Some reports[17, 19] have shown that a given produce type has universal Arrhenius parameters, while, others[7, 30] contend that the parameters vary as a function of O_2 and CO_2 concentrations and are not universal. Some typical activation energies of respiration for broccoli, pre-climacteric bananas, blueberries, and raspberries are shown in Table 5.3. There is some ambiguity as to whether this Arrhenius relationship is indeed universal for all concentrations; therefore, this form is not exactly useful for modeling respiration rates for use in a MA package model.

Table 5.3: Activation energies for the respiration of selected produce in the temperature ranges specified.

Produce	Temperature range (^{o}C)	$E_{R,O_2}(kcal/mol)$	$E_{R,CO_2}(kcal/mol)$	Reference
Broccoli	0 – 13	15.0	15.8	[19]
Bananas (pre- climacteric)	2.5 – 37	13.8	13.8	[5]
Blueberries	5 – 25	35.2	39.0	[17]
Raspberries	0 – 20	10.7	13.3	[31]

Early on the influence of temperature on the respiration rate was quantified by a temperature coefficient called the Q_{10}. Biological reactions such as those involved with the respiration process have a physiological temperature range in which the systems strive to reach some homeostasis by increasing or decreasing in activity. The Q_{10} is a measure of the increase of the respiration rate over a 10^{o}C temperature interval that can be expressed by the following

$$Q_{10} = \left(\frac{R_2}{R_1}\right)^{10/(T_2-T_1)} \tag{5.24}$$

where R_2 is the respiration rate at temperature T_2 and R_1 is the respiration rate at temperature T_1. Similar to the Arrhenius relationship, the Q_{10} enables the determination of the respiration rate at any temperature within a 10^{o}C interval. The Q_{10} for vegetables ranges from 1 to 4 over temperature ranges from 0 to 40^{o}C[1]. As temperature increases, the Q_{10} values per 10^{o}C intervals have been shown to decrease; therefore, prior to using Q_{10} values, it is important to know over what temperature range Q_{10} is reported for proper extrapolation.

RESPIRATION RATES OF PRODUCE VERSUS PERMEATION RATES OF POLYMERS

The goal of a MA package is to create an optimal atmosphere inside the package by balancing the amount out O_2 entering and CO_2 leaving the package such that optimal gas concentrations are maintained while the produce continues to consume O_2 and generate CO_2. This passive technique requires that the respiration rate of the produce and the permeation rate of the package film be appropriately balanced so that the desired gas concentrations at minimum are maintained. If produce is packaged without gas flushing, it may take several days to reach the desired gas concentration; therefore, it is common practice to flush the package with a desired gas concentration prior to sealing. The challenge to implementing MA packaging has been due to the availability of polymers with the necessary characteristics to balance respiration rates of produce. Often the selectivity of CO_2 to O_2 for common polymers, like those shown in Table 4.4, are high such that only low CO_2 concentration are attained, whereas, others have low selectivities such that only high CO_2 concentrations are reachable. The selectivities of most polymers do not have the necessary selectivity requirements to maintain the desired O_2 and CO_2 concentrations, therefore, packages are designed around the optimal oxygen concentration to prevent anoxic conditions. In addition to film CO_2 to O_2 permselectivity shortcomings, temperature changes present an even more difficult problem. As temperature increases, the respiration rate of produce increases at a greater rate than the gas transmission rate of most polymer films. Comparing the activation energies of respiration for the produce in Table 5.3 to the permeation for common polymers in Table 5.4, shows that the rate of increase is generally greater for the respiration process. As shown in Chapter 3, poly(*n*-alkyl acrylates) can be used to overcome this problem for some produce. Predicting the effects that temperature fluctuations have on the gas concentration inside the package can aid in designing safe MA package designs.

Table 5.4: Comparison of permeability coefficients (Barrers) at 25°C, activation energies (kcal/mol) for permeation of O_2, CO_2 and N_2 and selectivities for selected polymers.

Polymer	P_{O_2}	P_{CO_2}	P_{N_2}	E_{P,O_2}	E_{P,CO_2}	E_{P,N_2}	CO_2/O_2 Selectivity	O_2/N_2 selectivity
Low density Poly(ethylene) [a,b]	2.93	12.66	0.97	10.2	9.3	11.8	4.3	3.0
Poly(butadiene) [a]	18.96	138.08	6.41	7.1	5.2	8.2	7.3	3.0
Poly(butadiene-styrene) [c]	17.90	129.43	–	7.3	5.7	–	7.2	–
Poly(vinylidene chloride) (Saran) [a]	0.0024	0.031	0.0006	15.9	12.3	16.8	13.3	4.1
Natural rubber [a]	23.35	152.64	–	7.0	5.2	–	6.5	–
Silicone rubber [c]	124.1	661.9	–	2.0	0.0	–	5.3	–

[a] Data from ref[32]
[a] Data from ref[33]
[c] Data from ref[34]

MODIFICATION OF THE PAUL-CLARKE MA RETAIL PACKAGE MODEL TO ACCOUNT FOR TEMPERATURE AFFECTS

As seen in Chapter 2, the Paul-Clarke MA package model resulted in expressions for the composition inside a retail package through a series of material balances. It is assumed that the package is held at constant temperature. However, during the distribution chain, produce may undergo a range of temperature changes and especially from retail to the consumer's table. It is important to be able to predict the changes in the composition of the modified atmosphere that occur as a result of temperature fluctuations to ensure that the atmosphere surrounding the produce remain in a safe operating range, above the extinction point.

The composition inside the package is given by Equations 2.10 and 2.11 where the respiration rate and permeation coefficients are both a function of temperature, although it is not explicitly shown. Temperature effects are incorporated into the Paul-

Clarke model using the fact that permeation follows an Arrhenius relationship with temperature; therefore, the permeation coefficients can be expressed as a function of temperature. For the following analysis, the MA package consists of a polymer film with a high-flux membrane label, with the option of including holes or pores. Gas permeation is much greater through the membrane label than through the package; therefore, the parameter K_i for each gas *i* which describes parallel permeation into the package is simplified to

$$K_i = A_m\left(\frac{P_{mi}}{\ell_m}\right) \tag{5.25}$$

where P_{mi} is the permeability coefficient for the membrane label with thickness ℓ_m and area A_m. The following equation can be used to express K_i at temperature *T*

$$(K_i)_T = (K_i)_{ref}\exp\left[-\frac{E_{P,i}}{R}\left(\frac{1}{T}-\frac{1}{T_r}\right)\right] \tag{5.26}$$

where $(K_i)_T$ is the value of K_i at *T* and $(K_i)_{ref}$ is the value at a chosen reference temperature, T_r. For convenience we will define a parameter ΔT_r

$$\Delta T_r = \frac{1}{T}-\frac{1}{T_r} \tag{5.27}$$

An expression for the ratio of K_i to K_j is also useful

$$\frac{(K_i)_T}{(K_j)_T} = \frac{(P_{Pi})_{ref}}{(P_{Pj})_{ref}}\exp\left[-\left(\frac{E_{P,i}-E_{P,j}}{R}\right)\Delta T_r\right] \tag{5.28}$$

where $(P_{pi})_{ref}$ and $(P_{pj)})_{ref}$ are evaluated at the reference temperature. The ratio of the mass transfer coefficients for diffusive transport through the non-selective pores, *H*, to the O_2 permeating through the selective membrane, K_{O_2}, is represented by β

$$\beta = \frac{H}{K_{O_2}} = \frac{nA_hD_{im}}{\ell_{eff}RT(K_{O_2})_T} \tag{5.29}$$

The diffusive parameter *H* contains variables that describe the system such as *n* the number of holes of area A_h with an effective length ℓ_{eff} and the binary diffusion coefficient *D*$_{\mathrm{im}}$. It is assumed that the binary diffusion coefficients are very similar, thus, any selectivity of diffusive transport thought the holes, $D = D_{\mathrm{im}}$ is ignored. The binary diffusion coefficient is also a function of temperature; however, the change in the diffusion coefficient due to temperature fluctuations experienced during the transport of MA packaged produce are smaller than those due to selectivity of diffusive transport, see Table 5.5. For all practical purposes $\mathrm{D_{im}}$ is assumed constant with temperature.

Table 5.5: Binary diffusion coefficients at temperatures that are common during produce transport[a].

Temperature ($^{\mathrm{o}}$C)	D_{O_2/N_2} (cm^2/s)	D_{O_2/CO_2} (cm^2/s)	D_{N_2/CO_2} (cm^2/s)
0	0.17	0.13	0.13
10	0.19	0.14	0.14
20	0.20	0.15	0.15
25	0.20	0.15	0.15
30	0.21	0.16	0.16

[a] Data calculated from the kinetic theory of gases [35].

The ratio β can now be expressed as a function of temperature

$$\beta_T = \beta_{ref} \frac{T_{ref}}{T} \exp\left(\frac{E_{P,O_2}}{R} \Delta T_r \right) \tag{5.30}$$

where β_{ref} is

$$\beta_{ref} = \frac{H_{ref}}{(K_{O_2})_{ref}} \tag{5.31}$$

Now the concentration of O_2 and CO_2 inside the package can be expressed as a function of temperature

$$x_{CO_2} = \frac{W r_{O_2} RQ}{\left(A_m \middle/ \ell_m \right) (P_{m,O_2})_{ref} \exp\left(-\frac{E_{P,O_2}}{R} \Delta T_r \right) \left[\frac{(K_{CO_2})_T}{(K_{O_2})_T} + \beta_T \right] p_t} \tag{5.32}$$

where *W* is the mass of produce, r_{O_2} is the rate of O_2 consumed by the produce, *RQ* is the respiratory quotient and p_t is the total pressure that is atmospheric pressure inside and outside the package. The O_2 composition can also be expressed as a function of temperature

$$x_{O_2} = 0.21\left[1 - \frac{x_{CO_2}}{(x_{CO_2})_0}\right] \tag{5.33}$$

where $(x_{CO_2})_0$ is the fraction of CO_2 when the O_2 concentration is zero. The parameter $(x_{CO_2})_0$ is a useful mathematical quantity that has no real physical significance

$$(x_{O_2})_0 = 0.21\left[\frac{1 + \dfrac{1}{0.79}\beta_T + \dfrac{0.21}{0.79}\left(\dfrac{(K_{N_2})_T}{(K_{O_2})_T}\right)}{\dfrac{1}{RQ}\left(\dfrac{(K_{CO_2})_T}{(K_{O_2})_T} + \beta_T\right) + \dfrac{0.21}{0.79}\left(\dfrac{(K_{N_2})_T}{(K_{O_2})_T} + \beta_T\right)}\right] \tag{5.34}$$

Each ratio K_i / K_j can be evaluated at *T* using Equation 5.28 and β_T is computed using Equation 5.30. The gas composition inside the package, x_{O_2} and x_{CO_2}, is now explicitly expressed as a function of temperature; therefore, it is possible to predict the gas composition changes as a result of temperature fluctuations.

PREDICTING THE CONCENTRATION OF A MA PACKAGE WITH TEMPERATURE CHANGES

The following analysis examines a MA package with a high-flux membrane label made of poly (dimethylsiloxane) (PDMS). The transport properties of PDMS are shown in Table 5.6. The package is designed to maintain an optimal atmosphere (2 – 3 % O_2 and 6 – 7 % CO_2) for cut broccoli. The target for this analysis is to maintain a gas composition of 2.5 % O_2 and 6.0 % CO_2. It is often difficult to maintain the optimal concentration for both O_2 and CO_2 due to the difference in selectivity of the polymer and the relative rates that CO_2 is generated and O_2 is consumed by the produce.

Table 5.6: Permeability coefficient and activation energies of PDMS for O_2, N_2 and CO_2 from ref[36]

Gas	P (Barrers)	E_P (kcal/mol)
O_2	820	1.74
CO_2	390	0.23
N_2	3800	2.03

Hagger's[19] enzyme kinetics based respiration rate model with uncompetitive CO_2 inhibition is used to estimate the respiration rate as a function of gas composition and temperature. The model parameters were determined for four temperatures 0, 7, 13 and 24°C; thus, the package is optimized for 7°C to examine small temperature changes above and below the design temperature. The mass of broccoli, W = 0.130 kg, for this analysis is similar to that used in the MA package experiments conducted by Hagger. Figure 5.2 shows the respiration rate for O_2 and CO_2 of cut broccoli as a function of temperature. The lines representing the respiration rates are not exactly linear due to the use of the empirical respiration rate model at each temperature. At higher temperatures, the O_2 respiration rate slows slightly while the rate of CO_2 generation increases steadily; as a result, the RQ increases at elevated temperatures. Similar to most polymer/produce combinations, the rate of respiration increases more with temperature than does the rate of permeation, i.e., the activation energy for the respiration process is greater than that of the permeation process. Therefore a MA package designed to maintain a defined gas composition at one temperature will be unable do so at other temperatures.

The current analysis uses a package with a high-flux PDMS membrane label that is designed to maintain a MA atmosphere of 2.5 % O_2 and 6.0 % CO_2 at 7°C. Specifying the produce defines the respiration rate, RQ and the target gas compositions thus $(x_{CO_2})_0$ may be computed from Equation 5.33. The choice of polymer material to form the high-flux membrane label defines the transport properties P_i for each gas *i*. Now from the equations for x_{CO_2} and x_{CO_2}, the design requirements such as the ratio of the membrane area to its thickness A_m / ℓ_m and the necessary non-selective transport via β are determined. A package equipped with a high-flux membrane label made of PDMS requires a membrane area to thickness ratio A_m / ℓ_m of 795 cm^2/cm to maintain an optimal gas composition for 0.130 kg of cut broccoli. In addition, a value of $\beta = 1.2$ is required to achieve optimal conditions for this polymer/produce combination. Figure 5.4 shows the gas composition that is predicted using Equations 5.32 and 5.33 at 0, 7 and 13^{o}C. As temperature increases, the O_2 concentration decreases due to more oxygen being consumed by broccoli than the amount permeating into the package.

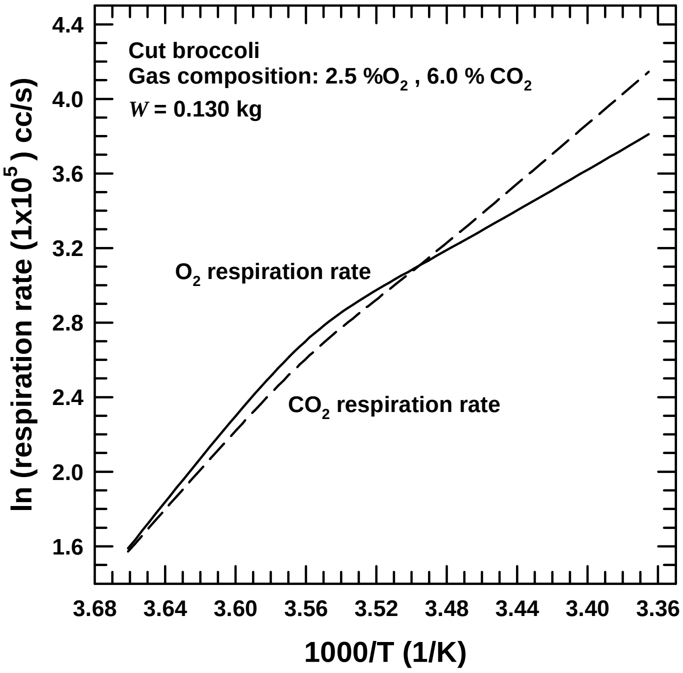

Figure 5.2: Respiration rate of O_2 and CO_2 for cut broccoli at 2.5 % O_2 and 6.0 % CO_2.

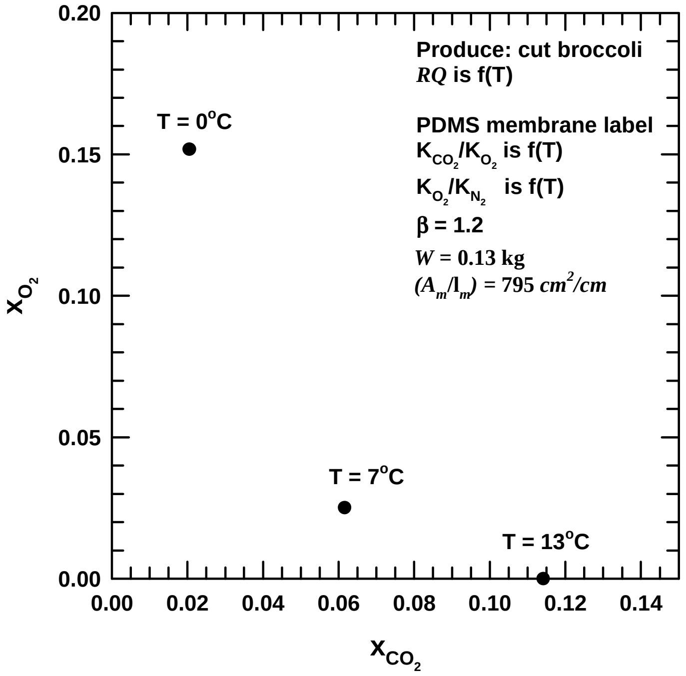

Figure 5.3: Predicted gas composition of a MA package with a PDMS membrane label (designed for 2.5 % O_2 and 6.0 % CO_2 at 7°C) for cut broccoli at 0, 7 and 13°C.

The opposite is true as the temperature decreases; the O_2 concentration increases due to less oxygen being consumed by broccoli than the amount permeating into the package. Similar trends of gas composition changes with temperature have been observed experimentally for several polymer/produce combinations[10, 15, 23, 37] with increases in temperature. Nevertheless, decreasing the temperature to 0°C or increasing to 13°C causes the gas composition inside the package to move outside of the narrow range of recommended O_2 and CO_2 concentrations for storage of cut broccoli. At the higher temperature of 13°C, the gas composition inside the package has reached unacceptable anaerobic conditions. Polymers with more temperature responsiveness must be used, i.e.

higher activation energies of permeation, to maintain optimal O_2 concentrations over a wider range of temperatures.

As seen in Chapter 3, side-chain crystalline poly (*n*-alkyl acrylate)/poly (*m*-alkyl acrylate) blends provide such a pathway to increase the activation energy that more appropriately match the temperature dependency of produce respiration rates over wider temperature ranges for some produce. There are many challenges to designing a MA package that can perform over the range of temperatures normally experienced through the distribution process of produce. Certainly, designing membranes with permeation rates that vary more with temperature than respiration rates help reduce the large composition changes observed with changes in temperature. Pores are generally introduced for use in parallel with a selective material to help maintain constant pressure, i.e. prevent package shrinkage, and to decrease the CO_2 to O_2 selectivity of the selective material so that higher CO_2 concentrations can be reached. However, the inclusion of pores reduces the temperature responsiveness of the package as permeation through the non-selective pores increase. The activation energy of permeation through holes is expected to be approximately 1.2 kcal/mol for O_2 and CO_2 that is low compared to common polymers (see Tables 5.4 and 5.5)[38]. The design of a MA package requires a delicate balance of these temperature and permselectivity considerations that are unique for each produce.

Altering variables like the produce weight, film area or thickness can change the absolute rate of respiration and permeation as seen from the simple MA model described by Equation 5.21. Numerous case studies may be conducted changing these variables or the transport parameters to evaluate the effect on gas composition but is beyond the scope of this discussion.

CONCLUSIONS

The design of a MA package requires information about the respiration rate of the produce being packaged and the permeability of the polymer used to regulate gases into and out of the package. Respiration rate models developed based on the enzyme kinetic theory has provided the best method to estimate the respiration rate of produce for MA package modeling. The choice of produce defines the desired gas concentration. The choice of polymer to form the membrane and the package design will depend on the optimal conditions. The mathematical expressions developed by Paul and Clarke allows predication of gas composition inside the package, but modifying the Paul-Clarke model to account for temperature effects further expands the use of the model. This modification allows the estimation of gas composition changes in the modified atmosphere as a function of temperature. The gas compositions predicted for a package with a high-flux PDMS membrane label enclosing cut-broccoli show similar trends to experimental observations reported in literature[10, 15, 23, 37].

REFERENCES

1. Kader AA. Respiration of Gas Exchange of Vegetables. In: Weichmann J, editor. Postharvest physiology of vegetables. New York: Marcel Dekker, Inc., 1987. pp. 25-43.
2. Fidler JC and North CJ. The Journal of Horticultural Science 1967;42:189-206.
3. Kidd F and West C. Plant Physiology 1945;20(4):467-504.
4. Jurin V and Karel M. Food Technology 1963;17(6):104-108.
5. Karel M and Go J. Modern Packaging 1964;37:123-127.
6. Platenius H. Plant Physiology 1943;18(4):671-684.
7. Cameron AC, Beaudry RM, Banks NH, and Yelanich MV. Journal of the American Society for Horticultural Science 1994;119(3):534-539.
8. Lee DS. Journal of Food Engineering 1996;27:297-310.
9. Yang CC and Chinnan MS. Transactions of the ASAE 1988;31(3):920-925.
10. Talasila PC, Chau KV, and Brecht JK. Transactions of the ASAE 1992;35(1):221-224.
11. Gong S and Corey K. Journal of the American Society for Horticultural Science 1994;119(3):546-550.
12. Lee DS, Haggar PE, and Yam KL. Journal of Food Science 1991;56(6):1580-1585.
13. Peppelenbos HW and Leven JV. Postharvest Biology and Technology 1996;7:27-40.
14. Fonseca SC, Oliveira FAR, and Brecht JK. Journal of Food Engineering 2002;52(2):99-119.
15. Ying L. Journal of Southeast University 2005;21(3):314-318.
16. Edmond JP, Chau KV, and Brecht JK. Modeling respiration rates of blueberry in a perforation-generated modifeid atmosphere package. Proceedings from the Sixth International Controlled Atmosphere Research Conference. Cornell University, Ithaca, New York, 1993. pp. 134-144.

17. Song Y, Kim HK, and Yam KL. Journal of American Society of Horticultural Science 1992;117(6):925-929.
18. Fonseca SC, Oliveira FAR, Frias JM, Brecht JK, and Chau KV. Journal of Food Engineering 2002;54(4):299-307.
19. Hagger PE, Lee DS, and Yam KL. Journal of Food Process Engineering 1992;15:143-157.
20. Peppelenbos HW. The influence of O_2 and CO_2 on the quality of fresh mushrooms. Proceedings from the Sixth International Controlled Atmosphere Research Conference, vol. 2. Cornell University, Ithaca, New York, 1993. pp. 746-758.
21. McLaughlin CP and O'Beirne D. Journal of Food Science 1999;64(1):116-119.
22. Smyth AB, Song J, and Cameron AC. Journal of Agricultural and Food Chemistry 1998;46(11):4556-4562.
23. Beaudry RM, Cameron AC, Shirazi A, and Dostallange DL. Journal of the American Society for Horticultural Science 1992;117(3):436-441.
24. Cameron AC, Boylan-Pett W, and Lee J. Journal of Food Science 1989;54(6):1413-1416.
25. Andrich G, Fiorentini A, Tuci A, Zinnai A, and Sommovigo G. Journal of the American Society for Horticultural Science 1991;116(3):478-481.
26. Makino Y, Iwasaki K-i, and Hirata T. Journal of Agricultural Engineering Research 1997;67:47-59.
27. Paul DR and Clarke R. Journal of Membrane Science 2002;208(1-2):269-283.
28. Fonseca SC, Oliveira FAR, Lino IBM, Brecht JK, and Chau KV. Journal of Food Engineering 2000;43(1):9-15.
29. Silva FM, Chau KV, Brecht JK, and Sargent SA. Applied Engineering in Agriculture 1999;15(4):313-318.
30. Lakakul R, Beaudry RM, and Hernandez RJ. Journal of Food Science 1999;64(1):105-110.

31. Joles DW, Arthur C. Cameron, Ahmad Shirazi, Peter D. Petracek, and Randolph M Beaudry. Journal of the American Society for Horticultural Science 1994;119(3):540-545.
32. Pauly S. Permeability and Diffusion Data. In: Brandrup J, Immergut EH, and Grulke EA, editors. Polymer Handbook. New York: Wiley-Interscience, 1999. pp. 543-569.
33. Michaels AS and Bixler HJ. Journal of Polymer Science 1961;50:413-439.
34. Exama A, Arul J, Lencki RW, Lee LZ, and Toupin C. Journal of Food Science 1993;58(6):1365-1370.
35. Bird RB, Stewart WE, and Lightfood EN. Transport Phenomena: Wiley, 2002.
36. Senthilkumar U and Reddy BSR. Journal of Membrane Science 2007;292(1-2):72-79.
37. Clarke R and De Moor CP. The future in film technology: A tunable packaging system for fresh produce. In: Gorny JR, editor. Proceedings of the 7th International Controlled Atmosphere Research Conference, vol. 5. University of California, Davis, 1997. pp. 68-75.
38. Cameron AC, Talasila PC, and Joles DW. Hortscience 1995;30(1):25-34.

Chapter 6: A steady-state model for attaining a modified atmosphere of produce in a bulk container using selective and non-selective membranes

INTRODUCTION

Consumer demand for a wide variety of fresh produce drives the need for improved methods of storing, shipping and marketing of fruits and vegetables[1]. Post harvest, the shelf life of produce depends on external factors such as temperature and composition of the surrounding atmosphere. Storage at low temperatures throughout the distribution chain is a well-known method to keep respiration rates, i.e., metabolic activity, low; however, modifying the composition of the surround atmosphere further supplements low temperature management to minimize the loss of produce throughout the distribution chain[2-4]. It has long been known that reduced O_2 and elevated CO_2 slows the metabolic activity of produce and delays senescence thereby extending shelf life. Two common techniques are used to modify the atmosphere surrounding produce. For bulk storage or transport, controlled atmosphere storage (CAS) uses traditional air separation technologies, including membranes, to alter the chamber atmosphere; here, a gas mixture of any desired composition, created by an external process, is purged through the storage container. Modified atmosphere packaging (MAP) passively establishes the composition of the surrounding atmosphere through the interaction of the produce respiration and gas transmission through the packaging material or a membrane patch. The optimal O_2 and CO_2 composition for maintaining freshness varies from one type of produce to another. The composition achieved, at steady state, inside such a package depends on many factors including the produce respiration rate, the membrane permselectivity characteristics, and the ratio of produce mass to membrane area. Often, the permeation characteristics of available membrane materials do not meet the requirements necessary to adequately maintain the modified atmosphere in the optimal ranges[2, 5]. There are two issues regarding the permselectivity characteristics of membrane materials for such applications. Typical polymeric materials available for developing membranes for this application have a relatively narrow range of CO_2/O_2 selectivity[6]. For some types of produce, like pears and apples, this selectivity is not high enough to create the low CO_2 levels needed in the package. This issue must be addressed by searching for membranes with a higher CO_2/O_2 selectivity. On the other hand, conventional membranes are too selective for CO_2 over O_2 to create the higher levels of CO_2 some produce require. This can be resolved by using combinations of a selective membrane and a non-selective membrane (or perforations)[6].

Numerous models have been developed to predict the composition of the modified atmosphere for given cultivars and package designs[6-13]. Paul and Clarke[6] developed a versatile model to determine the O_2 and CO_2 concentrations inside a package containing produce using a selective membrane in combination with non-selective perforations. The focus of this model was small retail packages and demonstrated how to achieve the desired atmosphere (for a given type of produce) by using the proper combination of selective and non-selective gas exchange.

In this chapter, a similar model will be developed for bulk MA storage when the storage chamber is outfitted with both a selective membrane and non-selective membrane with fixed areas. By varying the air flow across the non-selective membrane the concentration inside the chamber can be controlled within wide limits to achieve the desired atmosphere for the given produce. In this way, the same chamber with its fixed membranes can be used at different times to store a wide range of produce types.

CHEMISTRY OF POST-HARVEST PRODUCE

Post harvest, produce continues to respire in contrast to other perishable goods, like meats, nuts, etc. The normal aerobic respiration of produce is an oxidative process involving biochemical reactions that is not problematic so long as the cell structure and organization is maintained. The respiration process is comprised of several complex metabolic pathways through which oxygen is consumed and carbon dioxide is generated; however, for simplicity the respiration process has been represented by a simple overall reaction, Equation 2.15, symbolizing the breakdown of substrates into simpler molecules. At the time of harvest, produce has completed the growth phase of development and has entered the maturation stage. Although aiding in sustaining cell structure, respiration is the primary contributing factor to the ripening and senescence phases of post-harvest produce. The objective has been to find methods of depressing the respiration process and, thus, delaying senescence. The respiration rate, the rate that O_2 is consumed or the rate of CO_2 is produced, is a reflection of destructive metabolic changes and quality deterioration of the produce. In addition to the absolute respiration rate, the relative rate of CO_2 generation to O_2 consumption represented by the respiratory quotient, RQ,

$$RQ = \frac{rate\, of\ CO_2\ generated\ by\ the\ produce}{rate\, of\ O_2\ consumed\ by\ the\ produce} = \frac{r_{CO_2}}{r_{O_2}} \tag{6.1}$$

is an important factor. As with respiration rate, the RQ also depends on the type of substrate that comprises the produce. Most fruits and vegetables have RQ values between 0.7 and 1.3. Typically, carbohydrates have an RQ value near 1, lipids have values that are less than or equal to 1, and organic acids have values that are greater than 1[14].

Storage temperature and the surrounding gas concentration have significant effects on respiration rates. Lower temperatures reduce the absolute value of respiration rates most; therefore, primary efforts have been to control storage temperature. Platenius[15] examined the effect of O_2 concentration on the respiration of several vegetables and found that the respiration rate was reduced at low levels of O_2 where the Pasteur effect also takes place. Figure 6.1 shows the normal trends during aerobic respiration. It is crucial to remain above the extinction point, i.e., the oxygen concentration below which anaerobic respiration occurs. This point is normally marked by increased CO_2 production, absent O_2 consumption, due to the decarboxylation of pyruvate; therefore, the RQ rises and where this occurs is commonly referred to as the RQ breakpoint. In the anaerobic region, fermentative metabolism is induced resulting in products such as ethanol and acetaldehyde that can cause offensive odors and flavors usually rendering the produce inedible. Some produce can tolerate a degree of fermentation and still remain of acceptable quality for human consumption. Retail packages of salad greens from a local supermarket showed that aerobic conditions had been compromised by the presence of fermented odors and flavors; however the produce may still be edible with the addition of salad dressing[16].

Elevated CO_2 concentrations help to reduce respiration rates and inhibit some harmful bacterial pathogens. Clostridium botulinum raises particular concern for MA applications as it tends to thrive well at low O_2 concentrations and at low temperatures[17, 18]. On the other hand, elevated CO_2 concentrations may also induce physiological injury to the produce and render them inedible. As shown in Chapter 5, investigations on the effect of reduced O_2 and elevated CO_2 levels have repeatedly shown that significant reduction of respiration rates and further extension of produce freshness[15, 19-21]. The modified atmosphere necessary for optimal storage is different for each type of produce and variety.

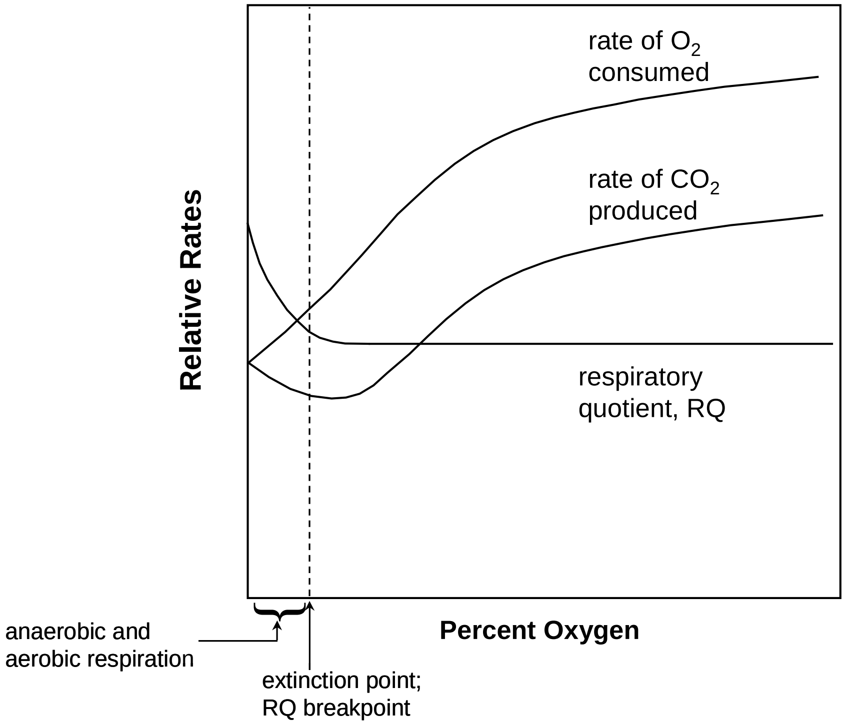

Figure 6.1: The effect of oxygen concentration on respiration rates and respiratory quotient.

Much effort has been placed on experimentally determining optimal temperatures, and O_2 and CO_2 concentrations to store produce to ensure quality products. Each type of produce has optimal O_2 and CO_2 concentration ranges as shown in Figure 6.2, using data from Table 5.1. Some produce, apples and bananas, require low O_2 and low CO_2 concentrations whereas others, strawberries and blueberries, need moderate O_2 and high CO_2 concentrations. Damage to cells, such as cutting or shredding, as shown on this map can further restrict the optimal range for depressing respiration, e. g., cut broccoli requires a reduced concentration range compared to whole broccoli.

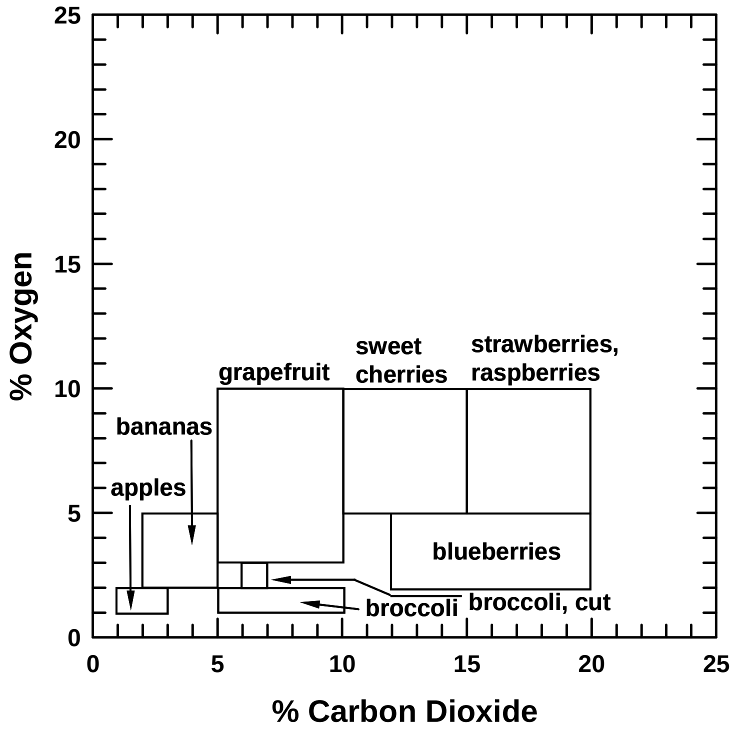

Figure 6.2: Optimal oxygen and carbon dioxide ranges for selected produce adapted from Paul and Clarke[6]. The Post harvest Technology Research and Information Center of the Department of Plant Services' web site (*http://postharvest.ucdavis.edu*) is a repository of recommended storage conditions for a wide range of fruits and vegetables.

GENERAL DESIGN CONSIDERATIONS

As discussed in Chapter 5, the respiration process typically follows an Arrhenius relationship. The respiration rate varies more with temperature than does the permeation rate of most common polymers. At a specific temperature, it is possible to design packages with common polymers to maintain the defined gas concentration. However, as temperature increases, particularly during distribution or storage, it is possible to reach regions where the produce is consuming more O_2 than the package can replenish and emitting more CO_2 than the package can transmit, thus, giving rise to anaerobic conditions which can be physiologically injurious. MA packaging techniques require that individual packages are properly designed prior to implementation to preclude such conditions.

As discussed above, for a given polymer material, adding a parallel pathway for gas exchange via non-selective perforations (holes), enable operation in regions of moderate O_2 and high CO_2 concentrations, suitable for strawberries and blueberries, and provide gas pressure equalization for flexible and permeable packages to prevent distortion[8, 22]. Edmonds developed a perforation model for blueberries that predicted high CO_2 ranges that can be altered by various hole dimensions[8]. The Paul-Clarke model shows that the gas concentration inside retail packages comprised of a selective membrane label or patch and non-selective perforations is capable of attaining a wide range of CO_2 concentrations. In such designs, the permeation through the membrane and the perforations is much higher than that through the polymer film making up the package. Figure 6.3 shows the accessible ranges of O_2 and CO_2 concentrations using such a design for typical produce, RQ of 1.2, where the membrane label has a CO_2 to O_2 selectivity $\alpha_1 = 4$ and an O_2 to N_2 selectivity $\alpha_2 = 3$. When all the gas permeation occurs through the selective membrane, the O_2 and CO_2 concentrations that can be achieved by such a membrane is indicated by the dashed line at the left. This case assumes there is a small perforation that allows convective exchange of gas so that the package volume (or pressure) remains constant. The permselectivity characteristics of commonly available polymers do not permit much variation of this line. The dashed line to the right illustrates the case where all the gas exchange occurs by non-selective permeation through the perforations. This allows access to regions of much higher CO_2 concentrations. When the gas exchange occurs by some combination of selective and non-selective permeation, the operating line can be any where in between these limits.

For a given design, a solid line similar to the one shown in Figure 6.3 defines the gas concentrations that are possible within a package.

The same concept is used here to develop a bulk MA design. Contrary to retail packages, varying the pore characteristics of the non-selective membrane intended for multiple uses to transport different types of produce is not a practical alternative. We will examine a bulk MA design that allows control of the gas exchange through the pores (i.e., retain the versatility of the Paul-Clarke concept to reach a wide range of gas concentrations simply by altering the membrane/perforation ratio) by adjusting the air feed upstream of the non-selective membrane.

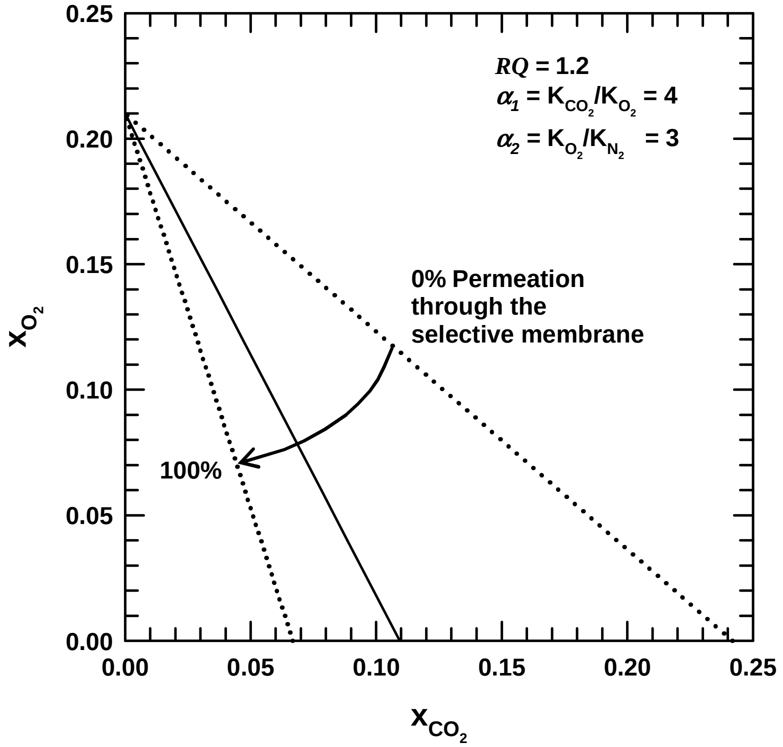

Figure 6.3: O_2 and CO_2 concentration ranges obtainable with Paul-Clarke MA retail package design (schematic adapted from Paul and Clarke[6])

PROPOSED BULK MODIFIED ATMOSPHERE STORAGE DESIGN

Figure 6.4 shows the respiring produce inside a rigid bulk storage or transport chamber with three compartments. The produce compartment is separated from the bottom section by a selective membrane that helps regulate the O_2 entering and the CO_2 leaving the main produce compartment. The selectivity characteristics of this membrane are fixed and cannot be changed except by choosing a membrane made from a different polymer. The absolute gas transmission rates through this permselective membrane can be adjusted by changing the geometrical parameters (area and thickness); however, these parameters also become fixed once the design is specified. Fresh air is pumped into the lower chamber in sufficient excess that its composition is effectively unchanged by O_2 and CO_2 exchange with the produce chamber across the selective membrane. The composition of the fresh air is expressed as mole fractions, i.e., $(x_{O_2})_{air} = 0.21$, $(x_{CO_2})_{air} = 0$, and $(x_{N_2})_{air} = 0.79$).

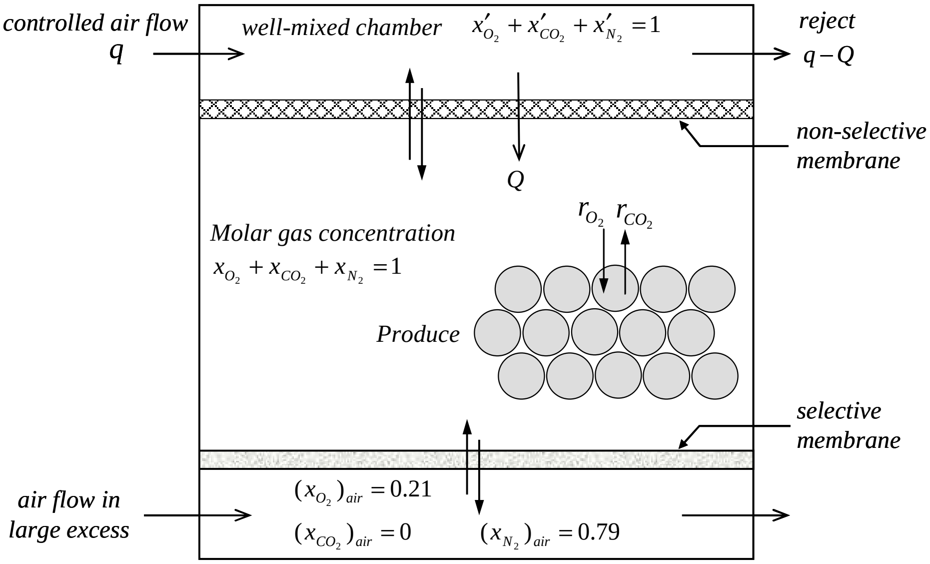

Figure 6.4: Illustration of produce in a bulk modified atmosphere storage or transport chamber with both selective and non-selective membranes.

Ideally this membrane will have a high CO_2/O_2 selectivity such that it will be able to maintain the lowest mole fractions of CO_2, x_{CO_2}, inside the produce chamber required by any type of produce to be stored in this unit. However, other types of produce that require a higher x_{CO_2} may also be accommodated by adding the porous, non-selective membrane between the produce chamber and the upper chamber. This non-selective membrane serves two purposes. First, it allows convective exchange of gas to accommodate any difference in the rate of O_2 in and CO_2 out caused by permeation that would tend to alter either the volume or total pressure within the produce chamber. The amount of this convective flow is Q and its direction is usually into the produce chamber; however, under some conditions the direction can be reversed, i.e., Q becomes negative. Second, the non-selective membrane transmits O_2, CO_2, and N_2 by permeation albeit non-selectively. This provides a way of modulating the CO_2/O_2 selectivity downward from that of the selective membrane. These two functions are provided by the perforations in the Paul-Clarke model. However, in this design, the relative amount of selective and non-selective permeation of gases into and out of the produce chamber can be regulated by adjusting the air flow rate, q, to the upper chamber without altering any hardware. In this way, the needs of any type of produce can be met by simply adjusting q. The physical layout shown in Figure 6.4 is only for conceptual purposes. In practice the two membranes may be in module form (allowing for hollow-fiber or spiral-wound membranes) connected to the produce storage chamber by appropriate piping, see Figure 6.5.

To facilitate the development of a mathematical model for this conceptual design, the gas in the chamber upstream of the non-selective membrane is assumed to be well-mixed such that the mole fractions x'_{O_2}, x'_{CO_2} and x'_{N_2} are constant throughout this gas space. The gas flow out of this chamber is $q - Q$. The composition of the gas inside the produce chamber is also assumed to be uniform throughout this space, i.e., well-mixed, at the values of x_{O_2}, x_{CO_2}, and x_{N_2}. This is a steady-state model so these values do not change with time. The oxygen consumption and carbon dioxide production of the stored produce are given by r_{O_2} and r_{CO_2} that are assumed constant for a given temperature and atmospheric concentration.

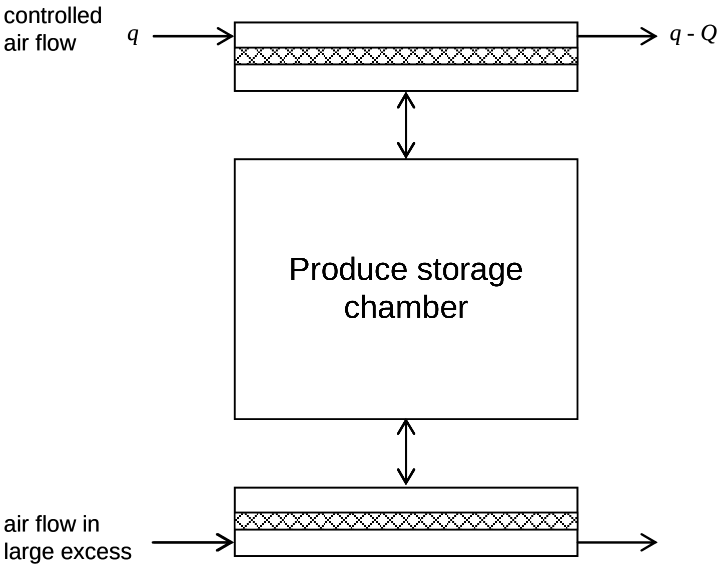

Figure 6.5: Practical produce storage chamber designed with traditional membrane modules

The model for this bulk MA storage system, see Figure 6.4, involving the use of both a selective and a non-selective membrane allows one to predict, for a fixed equipment design, the relationship between x_{O_2} and x_{CO_2} as q is varied for a fixed produce type and amount and a given operating temperature. By varying q, different atmospheres, i.e., x_{O_2} and x_{CO_2}, can be created such that this unit can be used to meet the optimum storage conditions needed for a wide range of produce as will be shown. In principle, this concept can be used to compensate for changes in storage temperature by controlling q;

however, this function will not be considered here. As noted earlier both respiration and transpiration processes continue to take place in produce after harvesting. This model will take into account the O_2, CO_2 and N_2 exchange processes between the produce and the external air regulated by the membranes shown in Figure 6.4. It is assumed that the gases in all three compartments and the fresh air feeds are saturated or of the same humidity; therefore, there is no H_2O exchanged by permeation or convection. The nomenclature for the present bulk MA model will be the same as that used in the Paul-Clarke model[6].

The rate of a gas *i* permeating the selective membrane can be represented by the following expression

$$\{\, permeation\ rate\ of\ i \,\} = K_i p_t \left[(x_i)_{air} - x_i \right] \tag{6.2}$$

where p_t is the total pressure inside and outside of the system, $(x_i)_{air}$ is the mole fraction of gas *i* in the lower fresh-air chamber, and x_i is the mole fraction of gas *i* inside the main produce chamber. The quantity K_i describes the permeation through the selective polymer membrane and is given by

$$K_i = \frac{A_m P_{mi}}{\ell_m} \tag{6.3}$$

where A_m is the membrane area, ℓ_m is the thickness of the membrane, and P_{mi} is the permeation coefficient for gas *i* through the membrane. At a given temperature, the membrane has an inherent and fixed permselectivity, K_i / K_j , that is the ratio of the permeation coefficients for gas *i* to gas *j*. Polymers used for MA applications have a range of permselectivities for binary combinations of O_2, CO_2, and N_2. The most important permselectivity parameter for MA packaging applications is K_{CO_2} / K_{O_2} which dictates how the gases are regulated. For modeling purposes, we will assume permselectivities of K_{CO_2} / K_{O_2} between 2 to 10 and K_{O_2} / K_{N_2} between 2 and 6[6].

However, polymers from which membranes are typically made for this application have permselectivities of K_{CO_2}/K_{O_2} that are in a narrower range, i.e., commonly between 3 to 7 and K_{O_2}/K_{N_2} between 3 and 5[5, 9] as shown later in Table 6.1. It is often desirable to have permselective membranes with CO_2/O_2 selectivities lower than 3 for respiring produce that require high concentrations of CO_2 for optimum shelf life. For produce requiring low CO_2 concentrations, e.g., less than 3% CO_2, higher CO_2/O_2 permselectivities are needed than are currently available with polymers that can be conveniently formed into high-flux membranes with current technology.

PAUL-CLARKE MODEL FOR GAS EXCHANGE THROUGH HOLES APPLIED TO BULK MA MODEL

Gases are transmitted through the holes (or pores) of the non-selective membrane in Figure 6.4 by both diffusion along concentration gradients and convection along a small total pressure gradient. In the Paul-Clarke model, the gas phase within the pores was treated as a pseudo-binary mixture. The total flux, N_{iz}, of gas i through a pore can be represented by the unidimensional form of Fick's first law given that the binary diffusion coefficients of the gases (O_2, N_2, and CO_2) being considered are very similar[6].

$$N_{iz} = x_i \sum_{j=1} N_{jz} - cD_{im} \frac{dx_i}{dz} \tag{6.4}$$

The first term is due to convection and the second term due to diffusion; where the convective flux, $\widehat{Q}$, through a pore is giving by the term $\sum_{j=1} N_{jz}$, where c is the total molar gas concentration and D_{im}, is the binary diffusion coefficient of gas i in the mixture. As shown in Figure 6.5 all transport occurs in the z-axial direction. The Paul-Clarke model used a longer effective length, ℓ_{eff}, of the pore to account for end effects at the entrance and exit of the hole.

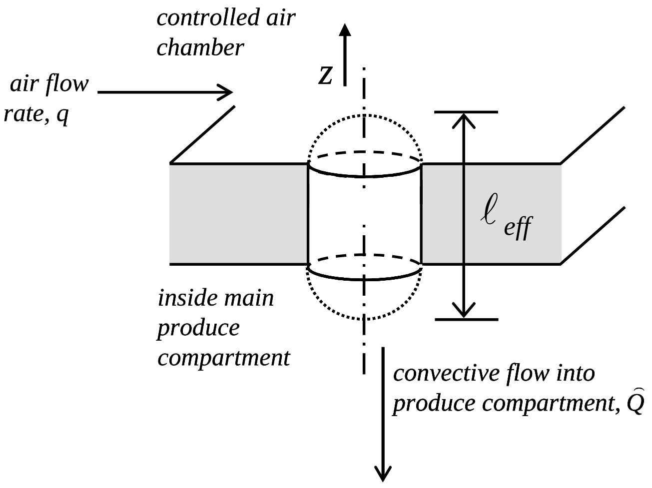

Figure 6.6: Schematic of a hole (or pore) and geometry used to model diffusive and convective transport.

Equation 6.4 is integrated over the effective length of the pore such to satisfy the conditions inside the main produce chamber where the mole fraction is x_i and inside the upper air flow-controlled compartment where the mole fraction of gas *i* is x_i' to obtain the following expression

$$\frac{N_{iz} - (x_i)\hat{Q}}{N_{iz} - (x_i')\hat{Q}} = \exp\left(\frac{\hat{Q}\ell_{eff}}{cD_{im}}\right) = \xi \tag{6.5}$$

This expression was simplified by using a series expansion for the exponential term and assuming the third and higher terms can be neglected. The resulting expression can be obtained for the total flux for gas *i* through a pore

$$N_{iz} = \frac{cD_{im}}{\ell_{eff}}\left(x_i' - x_i\right) + x_i'\hat{Q} \tag{6.6}$$

The total flux for gas *i* through all pores can be accounted for by multiplying Equation 6.6 by the total hole area, nA_h, (n is the number of pores with an area of A_h) permeated. For the temperatures and pressures experienced during transport and the gases considered, the gas phase is assumed to be ideal ($c = p/RT$ where R is the gas constant and T is the absolute temperature). With some rearrangement the following expression for total gas flow through the pores is realized

$$N_{iz} = \frac{nA_h D_{im}}{\ell_{eff} RT}\left(p_i' - p_i\right) + x_i' Q \tag{6.7}$$

where the total convective flux, $nA_h\widehat{Q}$, is represented by Q. It is evident by comparing Equations 6.2 and 6.7 that the driving forces (i.e., concentration gradients) are different for diffusive and convective transport for this bulk design, unlike the previous individual MA model. From the Paul-Clarke model, the factored quantities from the diffusive term were collected and defined as H.

$$H \equiv \frac{nA_h D_{im}}{\ell_{eff} RT} \tag{6.8}$$

This term will be useful for developing the transport through the pores for the non-selective membrane. It is evident from Equation 6.7 that the diffusive transport contribution for gas through a pore is

$$N_{iz} = \frac{nA_h D_{im}}{\ell_{eff} RT}(p_i' - p_i) = Hp_t(x_i' - x_i) = Hp_t \Delta x_i \tag{6.9}$$

These general equations for transport through both the selective membrane and holes (or pores) provide the ground work needed to develop the mathematics for modeling the bulk produce storage or transport model.

STEADY STATE BULK MA MODEL

The objective here is to determine the concentration of the main produce chamber of the bulk MA design shown in Figure 6.4. We will assume that the upper air controlled chamber is well mixed and that the pressure is constant at atmospheric pressure throughout the storage unit. The focus here will be on the gases O_2, CO_2, and N_2; in addition, we ignore humidity effects on the gas transmission rates. In an effort to determine the concentrations of the produce chamber, the amount of each gas species *i* can be accounted for by examining a number of independent balances over the bulk storage unit. Specific balances, similar to Equation 6.10, can be obtained for each gas *i*

$$\left\{\begin{matrix}\text{rate of}\\ \text{accumulation}\\ \text{of gas } i\end{matrix}\right\} = \left\{\begin{matrix}\text{rate of gas } i\\ \text{generated by}\\ \text{the produce}\end{matrix}\right\} + \left\{\begin{matrix}\text{rate of gas } i\\ \text{permeating}\\ \text{into chamber}\end{matrix}\right\} + \left\{\begin{matrix}\text{rate of gas } i\\ \text{into chamber}\\ \text{by convection}\end{matrix}\right\} \tag{6.10}$$

Equations 6.11-6.13 are obtained by performing individual component balances, assuming steady state, over the entire storage unit

$$r_{O_2} - 0.21q - K_{O_2} p_t (0.21 - x_{O_2}) + x'_{O_2}(q - Q) = 0 \tag{6.11}$$

$$r_{CO_2} - x'_{CO_2}(q - Q) - K_{CO_2} p_t (x_{CO_2} - 0) = 0 \tag{6.12}$$

$$x'_{N_2}(q - Q) - 0.79q - K_{N_2} p_t (0.79 - x_{N_2}) = 0 \tag{6.13}$$

Similarly, a balance over the produce chamber results in the following equations:

$$r_{O_2} - x'_{O_2} Q - K_{O_2} p_t (0.21 - x_{O_2}) - Hp_t (x'_{O_2} - x_{O_2}) = 0 \tag{6.14}$$

$$r_{CO_2} + x'_{CO_2} Q - K_{CO_2} p_t (x_{CO_2} - 0) - Hp_t (x_{CO_2} - x'_{CO_2}) = 0 \tag{6.15}$$

$$x'_{N_2} Q - K_{N_2} p_t (x_{N_2} - 0.79) - Hp_t (x_{N_2} - x'_{N_2}) = 0 \tag{6.16}$$

An expression for the total convective flow, *Q*, through the porous, non-selective membrane can be obtained by combining Equations 6.13 and 6.16 to eliminate x'_{N_2}

$$Q = -\frac{Hp_t(K_{N_2} p_t) + q(K_{N_2} + H)p_t}{0.79q + Hp_t x_{N_2}}(0.79 - x_{N_2}) \tag{6.17}$$

Several dimensionless variables are defined for convenience

$$\beta = H / K_{O_2} \tag{6.18}$$

$$v = q/Hp_t \tag{6.19}$$

$$w = Q/Hp_t \tag{6.20}$$

$$\alpha_1 = K_{CO_2}/K_{O_2} \tag{6.21}$$

$$\alpha_2 = K_{O_2}/K_{N_2} \tag{6.22}$$

where β the ratio of the mass transfer coefficients for diffusive transport through the porous membrane to the O_2 permeating through the selective membrane, v and w represent the controlled feed of air to non-selective membrane, q, and the convective flow of gas, Q, through this membrane normalized by the mass transfer coefficient of this membrane, respectively, and α_1 and α_2 are the permselectivities of CO_2/O_2 and O_2/N_2, respectively. We can now write Q in its dimensionless form and in terms of the other aforementioned dimensionless variables

$$w = \left[\frac{(v+1)/\alpha_2\beta + v}{0.79v + x_{N_2}}\right](x_{N_2} - 0.79) \tag{6.23}$$

Next we solve for x'_{O_2} by combining the two oxygen balances, Equations 6.11 and 6.14

$$x'_{O_2} = \frac{0.21q + x_{O_2}Hp_t}{q + Hp_t} = \frac{0.21v + x_{O_2}}{v+1} \tag{6.24}$$

Likewise an expression for x'_{CO_2} can be obtained by combining the two CO_2 balances, i.e., Equations 6.12 and 6.15,

$$x'_{CO_2} = \frac{x_{CO_2}Hp_t}{q + Hp_t} = \frac{x_{CO_2}}{v+1} \tag{6.25}$$

Finally using the relations

$$x_{O_2} + x_{CO_2} + x_{N_2} = 1 \tag{6.26}$$

and

$$x'_{O_2} + x'_{CO_2} + x'_{N_2} = 1 \tag{6.27}$$

along with the two preceding Equations 6.24 and 6.25, an expression for x'_{N_2} results as follows

$$x'_{N_2} = \frac{0.79q + x_{N_2} Hp_t}{q + Hp_t} = \frac{0.79v + x_{N_2}}{v+1} \tag{6.28}$$

From Equations 6.24, 6.25, and 6.28 we can see that the gas concentration in the gas chamber upstream of the non-selective membrane is a direct function of the air flow rate entering this chamber, thus, the driving force for gas permeation through this membrane varies with the air feed rate *q*. As *v* increases to large values, the upper-compartment gas concentration approaches that of fresh air

$$\lim_{v \to \infty} x'_{O_2} = 0.21 \tag{6.29}$$

$$\lim_{v \to \infty} x'_{CO_2} = 0 \tag{6.30}$$

$$\lim_{v \to \infty} x'_{N_2} = 0.79 \tag{6.31}$$

Now we can develop equations for the gas composition inside the produce chamber, x_i, in terms of design or controllable parameters. It is useful to define

$$C \equiv \frac{0.21 - x_{O_2}}{x_{CO_2}} \tag{6.32}$$

and

$$\delta \equiv \frac{0.21 - x_{O_2}}{0.21} \tag{6.33}$$

Combining Equations 6.15 and 6.25 leads to the following

$$r_{CO_2} = x_{CO_2}(Hp_t)\left[\frac{\alpha_1}{\beta} + \frac{v - w}{v+1}\right] \tag{6.34}$$

Similarly, by combining Equations 6.14 and 6.24 the following is obtained

$$r_{O_2} = (0.21 - x_{O_2})(Hp_t)\left[\frac{1}{\beta} + \frac{1}{v+1}\left\{v + w\frac{0.21v + x_{O_2}}{0.21 - x_{O_2}}\right\}\right] \tag{6.35}$$

Since $RQ = r_{CO_2}/r_{O_2}$, dividing Equation 6.34 by Equation 6.35 and combining with Equation 6.23 the variable *w* can be eliminated. After much algebra, the result can be placed into the form of a quadratic equation

$$aC^2 + bC + c = 0 \tag{6.36}$$

where the constants are

$$a = RQ\left\{1 + 0.266\left(\delta + \frac{1-\delta}{\alpha_2}\right) + 1.266v\beta + \left[1 + \frac{0.266}{\alpha_2}\right]v\right\} \tag{6.37}$$

$$b = -\left[\alpha_1 + v\beta(1 + 0.266RQ) + 0.266\left(\delta RQ + RQ\left(\frac{1-\delta}{\alpha_2}\right)\right) + v\left(\alpha_1 + \frac{0.266RQ}{\alpha_2}\right) + 0.266\delta\left(\alpha_1 - \frac{1}{\alpha_2}\right)\right] \tag{6.38}$$

$$c = 0.266\delta\left(\alpha_1 - \frac{1}{\alpha_2}\right) \tag{6.39}$$

For a given selective membrane, i.e., fixed permselectivities α_1 and α_2 and non-selective membrane, i.e., fixed β, the quadratic equation, Equation 6.36, can be solved to find the two roots of C; however, only the positive root has physical meaning. Generally, C is a function of O_2 concentration, x_{O_2}, and the air feed rate, *v*. For a given *v*, sets of O_2 and CO_2 concentrations can be computed by assuming an oxygen concentration.

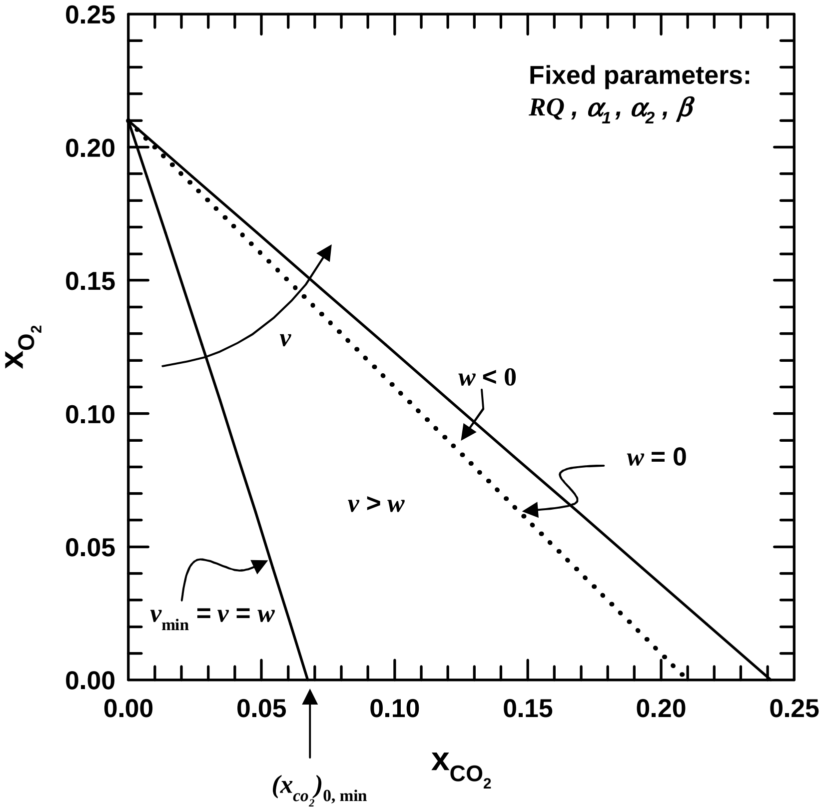

Figure 6.7: Schematic showing the steady-state relationships between oxygen and carbon dioxide concentrations inside the main produce compartment as the air feed rate in the upper compartment varies for this bulk design.

By assuming values of x_{O_2}, Equation 6.33 is used to obtain numerical values of δ to calculate the variable C. Once C is computed, Equation 6.36 is used to determine x_{CO_2} for the assumed O_2 concentration. This procedure was repeated over a range of O_2 concentrations corresponding to δ ranging from 0 to 1 to obtain results like those shown in Figure 6.7. Therefore, for each air feed rate v examined, sets of x_{O_2} and x_{CO_2} are determined throughout the composition range to generate operating lines like those shown in Figure 6.7. A point on an operating line is defined when the relative rates of gas exchange between the produce and the membrane are chosen by specifying the mass of the produce and the ratio of the membrane area to its thickness. Even though the equations for this model indicate that plots of x_{O_2} versus x_{CO_2} have some non-linearity, the sets of x_{O_2} and x_{CO_2} calculated from Equations 6.36 – 6.39, for various values of *v*, are effectively straight lines with an intercept of $x_{O_2} = 0.21$ for $x_{CO_2} = 0$. The lines intersect the axis where $x_{O_2} = 0$ at a value denoted as $(x_{CO_2})_0$; this is a convenient mathematical quantity that is useful for exploring how the design and operating parameters affect the composition of the gas phase surrounding the produce[6]. Equation 6.32 can be evaluated for $x_{O_2} = 0$ to obtain an expression for the quantity

$$C = \frac{0.21}{(x_{CO_2})_0} \tag{6.40}$$

On closer examination, plots of x_{O_2} versus x_{CO_2} are slightly curved at low *v*, e.g., where $(x_{CO_2})_0 < 0.07 - 0.10$; however, as *v* increases the plots of x_{O_2} versus x_{CO_2} are straight lines for all practical purposes. With this in mind, we will assume the solutions are practically linear. The attainable concentration region is bound by the two solid lines where *v* is at its lowest value and where *v* is sufficiently large the gas surrounding the produce no longer changes with increases in the dimensionless air feed rate *v*. The dotted line in this region corresponds to the situation where there is no convective flow through the non-selective membrane; above this line or as *v* continues to increase, the convective flow through the non-selective membrane is negative, i.e., the convective flow is out of the produce chamber. In the area encompassed by these two solid lines, the slopes of the lines decrease as the feed rate of air, *v* increases. The value of $(x_{CO_2})_0$ at the lower limit of *v* is denoted as $(x_{CO_2})_{0,\min}$. The lower limit, $v_{\min}$, is where the air flow to the non-selective membrane chamber equals the total convective flow through this membrane, i.e., $v_{\min} = v = w$. This would correspond to the case where the air flow to the upstream side of the non-selective membrane is just what is needed to keep the pressure in the produce compartment equalized with the outside air, i.e., $q = Q$. For the limit where q approaches Q; Equation 6.17 gives

$$\lim_{q \to Q} Q = -\frac{(K_{N_2}) p_t}{0.79}(0.79 - x_{N_2}) \tag{6.41}$$

As expected, this equation is identical to the Paul-Clarke model expression for convective flow when there is no permeation through the pores, i.e., $H = 0$. The value of $v_{\min}$ can be determined by substituting $v = w$ into Equation 6.23 and solving. This results in a quadratic equation

$$av^2 + bv + c = 0 \tag{6.42}$$

where the constants are

$$a = 0.79 \tag{6.43}$$

$$b = x_{N_2} + (0.79 - x_{N_2})\left(1 + \frac{1}{\alpha_2 \beta}\right) \tag{6.44}$$

$$c = \frac{0.79 - x_{N_2}}{\alpha_2 \beta} \tag{6.45}$$

As the air feed rate becomes sufficiently large, the composition of the gas in the upper chamber approaches that of the fresh air feed as shown from Equations 6.29 – 6.31. In this limit, the convective flow, Q, through the non-selective membrane expressed by Equation 6.17 results in the following

$$\lim_{q \to \infty} Q = -\frac{(K_{N_2} + H) p_t}{0.79}(0.79 - x_{N_2}) \tag{6.46}$$

The preceding equation for the convective flow is exactly the same as predicted by the Paul-Clarke model, as expected. From this equation it is now apparent that *w* or *Q* will be zero when $x_{N_2} = 0.79$ and when $(x_{CO_2})_0 = 0.21$ and $\delta = 1$. Under these conditions, the concentration of the main chamber is that of fresh air and there is no longer a driving force for permeation through the non-selective membrane. Figures 6.8 and 6.9 show x_{O_2} versus x_{CO_2} as the relative permeation rates through the non-selective and selective membranes are set to levels $\beta = 10$ and $\beta = 30$, respectively. Specific cases are examined given a typical permselective membrane where $\alpha_1 = 4$ and $\alpha_2 = 3$ for produce characterized by $RQ \approx 1.2$. The range of air feed rates, *v*, shown was chosen to obtain the full range of variation in x_{O_2} versus x_{CO_2} relationship between the lower and upper bound lines. Comparing Figures 6.8 and 6.9, the air flow rates, *v*, necessary to reach the full range of concentrations decrease as the permeation β through the holes increases. The produce chamber composition changes rapidly with *v* as more permeation occurs through the non-selective membrane relative to the selective membrane, i.e., as β increases.

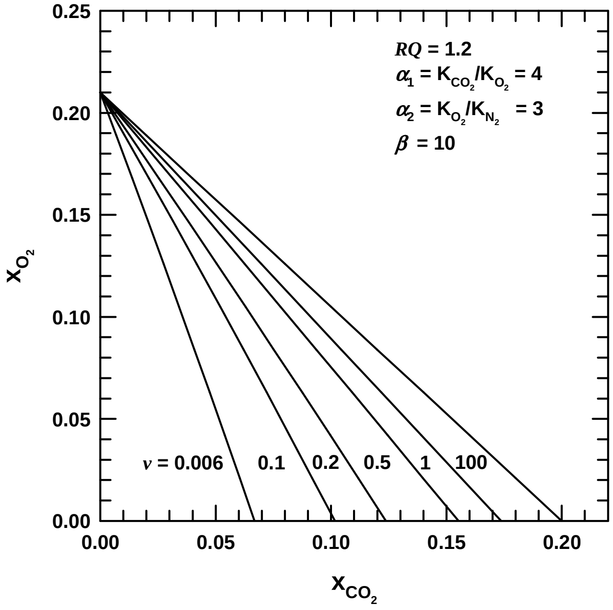

Figure 6.8: Steady-state relationships between O_2 and CO_2 concentrations in the produce compartment as the air flow rate, *v*, varies for $\beta = 10$.

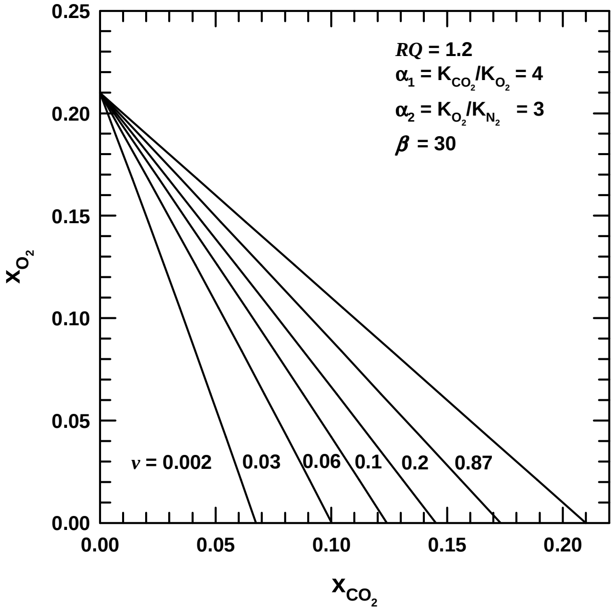

Figure 6.9: Steady-state relationships between O_2 and CO_2 concentrations in the produce compartment as the air flow rate, *v*, varies for $\beta = 30$.

As the air feed rate approaches the convective flow through the pores of the non-selective membrane, there is no permeation through the non-selective membrane. Thus, an explicit expression for $(x_{CO_2})_{0,\min}$ is obtained by evaluating the value of C under these conditions, i.e., $v = v_{\min}$, $\delta = 0$, and $\beta = 0$; the quadratic constants from Equations 6.37 – 6.39 are

$$a\Big|_{(x_{CO_2})_0,\min} = RQ\left\{1 + 0.266 + \left[1 + \frac{0.266}{\alpha_2}\right]v\right\} \tag{6.47}$$

$$b\Big|_{(x_{CO_2})_0,\min} = -\left[\alpha_1 + 0.266RQ + 0.266RQ + v\left(\alpha_1 + \frac{0.266RQ}{\alpha_2}\right) + 0.266\delta\left(\alpha_1 - \frac{1}{\alpha_2}\right)\right] \tag{6.48}$$

$$c\Big|_{(x_{CO_2})_0,\min} = 0.266\delta\left(\alpha_1 - \frac{1}{\alpha_2}\right) \tag{6.49}$$

From this exercise, it is clearly observed that $(x_{CO_2})_{0,\min}$ is a direct function of RQ, α_1, and α_2.

Figure 6.10 illustrates how $(x_{CO_2})_{0,\min}$ varies when different polymer films forming the selective membrane are used. As expected, $(x_{CO_2})_{0,\min}$ responds significantly to changes in the CO_2/O_2 permselectivity α_1; whereas, there is essentially no sensitivity to the O_2/N_2 permselectivity α_2. As α_1 increases or more carbon dioxide permeates the selective membrane, the value of $(x_{CO_2})_{0,\min}$ decreases which is consistent with lowering the concentration of CO_2 inside the produce chamber. Figure 6.11 shows how $(x_{CO_2})_{0,\min}$ varies with RQ of the produce stored in the chamber. As RQ increases, $(x_{CO_2})_{0,\min}$ increases owing to the increased rate of CO_2 production. A higher CO_2/O_2 permselective membrane, e.g. $\alpha_1 = 10$, is capable of reaching lower $(x_{CO_2})_{0,\min}$ values, near the inaccessible concentration region shown in Figures 6.8 and 6.9 than a material with a lower selectivity, e.g. $\alpha_1 = 4$. The choice of polymer for the permselective membrane primarily dictates the lower limit of $(x_{CO_2})_0$.

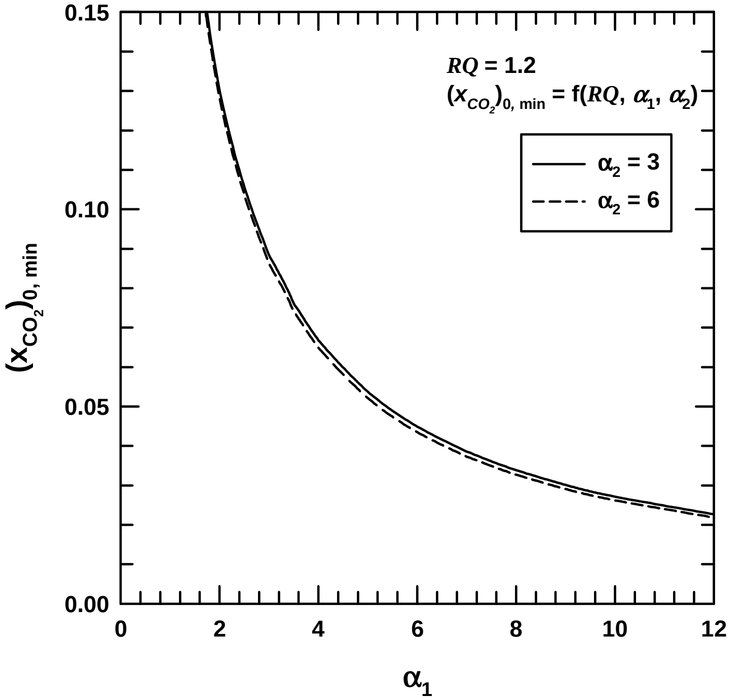

Figure 6.10: Sensitivity of lower limit of $(x_{CO_2})_0$ to different selective membranes

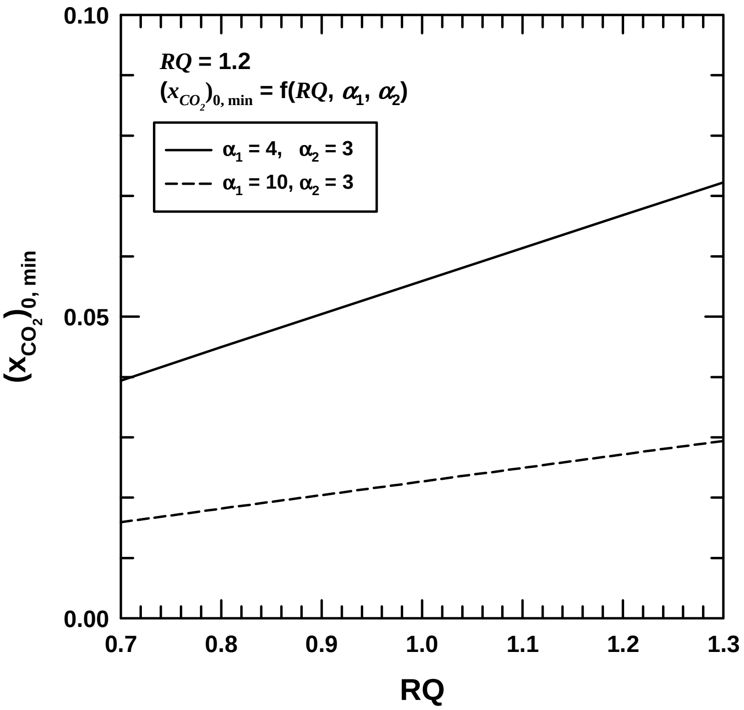

Figure 6.11: Illustrates the sensitivity of $(x_{CO_2})_{0,\min}$ for the storage of different produce (RQ) for the typical range of permselective materials currently available for MA application.

The entire region of $(x_{CO_2})_0$ values reachable with air feed rates from $v_{\min}$ and greater for various combinations of selective and non-selective membranes is explored in Figures 6.12 – 6.18 where $(x_{CO_2})_0$ is plotted versus the air feed rate, v. It was established earlier that $(x_{CO_2})_{0,\min}$ is not significantly influenced by α_2; therefore, few calculations altering α_2 were made. As the feed rate of air to the upper gas chamber increases, $(x_{CO_2})_0$ increases from the value at $v_{\min}$, $(x_{CO_2})_{0,\min}$, in a non-linear fashion and plateaus at high flow rates, v. There is no change in $(x_{CO_2})_0$ with further increases in v beyond the values shown. Similar to the x_{O_2} versus x_{CO_2}, the dashed line of the lower value of $(x_{CO_2})_0$ represents the case where $w = v_{\min}$ or the minimum air feed rate to equalize the pressure in the produce chamber and the dashed line at the higher value of $(x_{CO_2})_0$ is where the convective flow through the pores of the non-selective membrane is zero that occurs when $(x_{CO_2})_0$ = 0.21. Above the upper dashed line, the convective flow reverses direction and is negative. The region between the two dashed lines is where convection is into the chamber and $w < v$. Each plot shows the effect of varying the ratio of permeability of the non-selective membrane to that of the selective membrane or β. The non-selective membrane with β necessary to span the $(x_{CO_2})_0$ range from at least $(x_{CO_2})_{0,\min}$ to 0.21 (this range meets the optimal concentration ranges of most produce as seen in Figure 6.2) is optimal so that a wide range of concentrations may be attained with fixed selective and non-selective membrane modules. Note that not all design configurations are able to attain the full range of $(x_{CO_2})_0$.

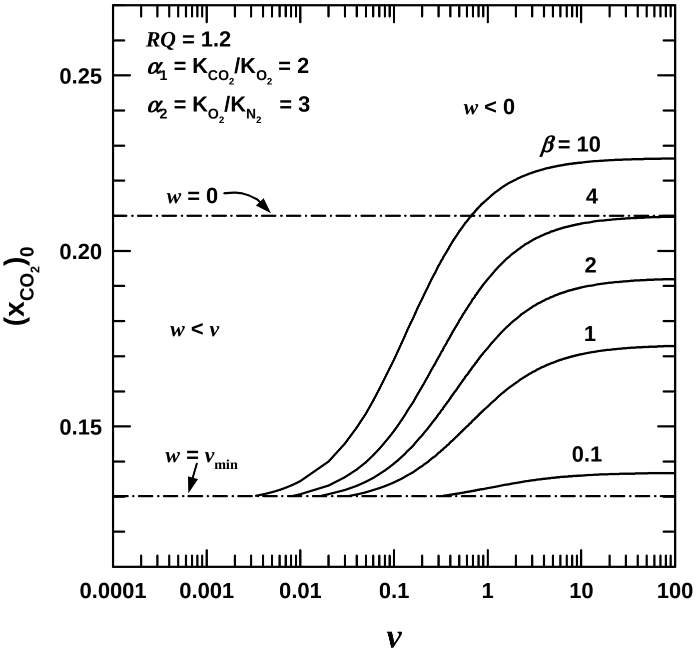

Figure 6.12: Model predictions for $(x_{CO_2})_0$ as a function of v for $\alpha_1 = 2$ and $\alpha_2 = 3$.

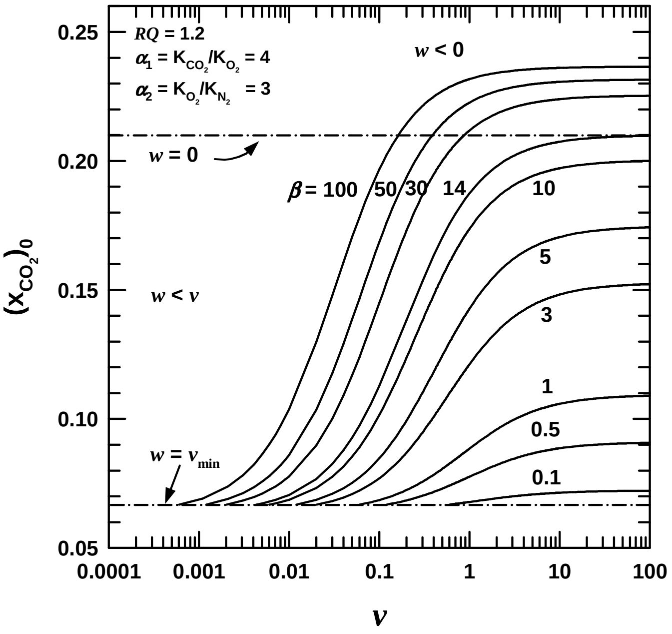

Figure 6.13: Model predictions for $(x_{CO_2})_0$ as a function of v for $\alpha_1 = 4$ and $\alpha_2 = 3$.

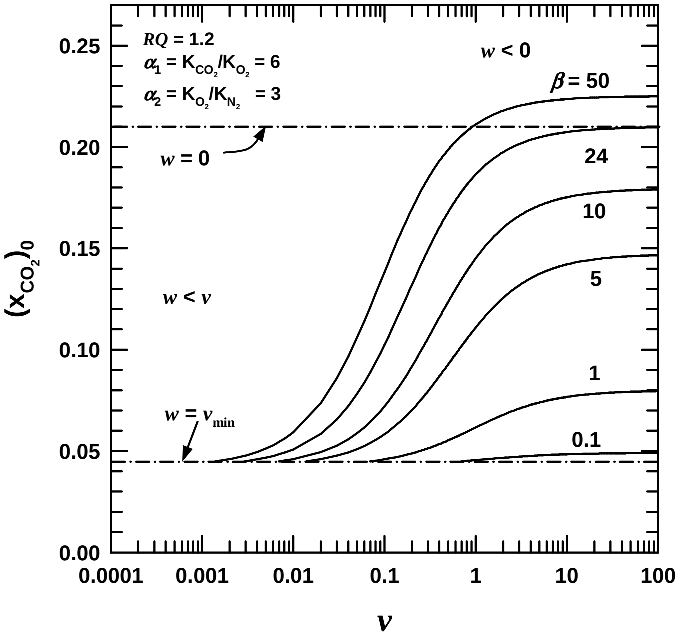

Figure 6.14: Model predictions for $(x_{CO_2})_0$ as a function of v for $\alpha_1 = 6$ and $\alpha_2 = 3$.

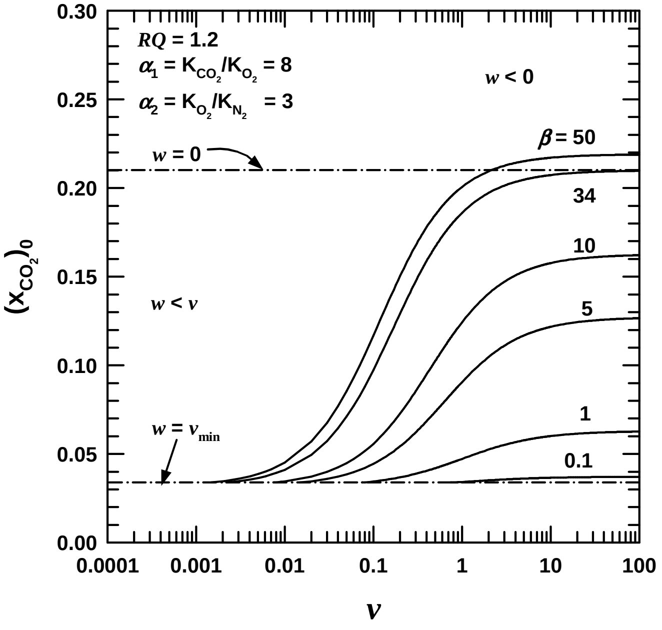

Figure 6.15: Model predictions for $(x_{CO_2})_0$ as a function of v for $\alpha_1 = 8$ and $\alpha_2 = 3$.

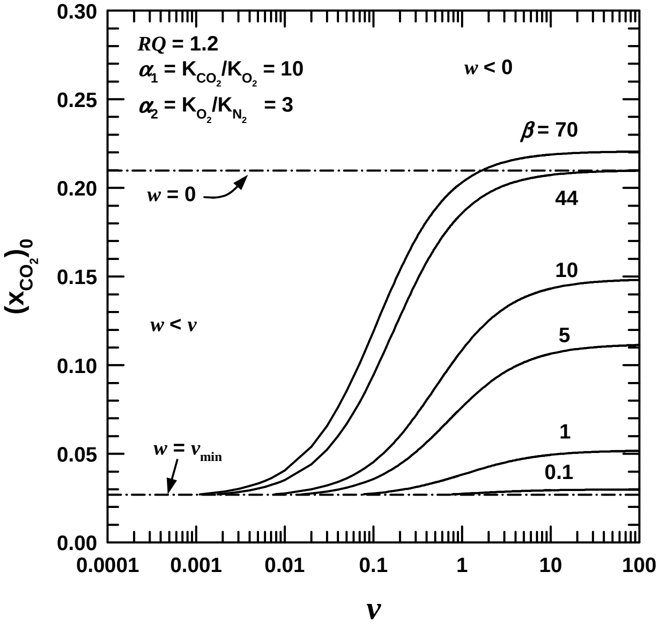

Figure 6.16: Model predictions for $(x_{CO_2})_0$ as a function of v for $\alpha_1 = 10$ and $\alpha_2 = 3$.

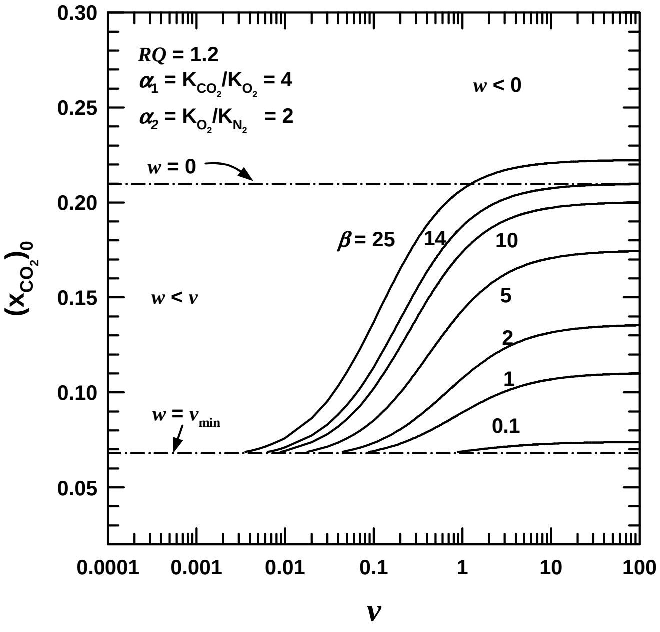

Figure 6.17: Model predictions for $(x_{CO_2})_0$ as a function of v for $\alpha_1 = 4$ and $\alpha_2 = 2$.

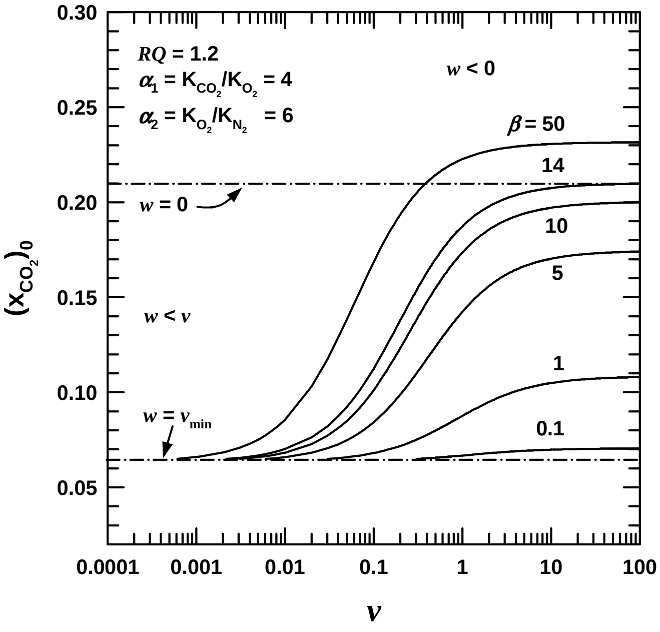

Figure 6.18: Model predictions for $(x_{CO_2})_0$ as a function of v for $\alpha_1 = 4$ and $\alpha_2 = 6$.

Non-selective membranes with less permeation through the pores require higher air feed rates to maintain the same $(x_{CO_2})_0$. Comparing Figures 6.12 – 6.18, it is evident that as the CO_2/ O_2 permselectivity increases, $(x_{CO_2})_{0,\min}$ decreases as the trend illustrates in Figure 5.10.

Although not readily apparent from Figures 6.12 – 6.18, the value of $\beta v_{\min}$ is a constant for a given selective membrane as shown in Figure 6.19. For design purposes, the value of $\beta v_{\min}$ can be useful for determining the range of flow rates necessary to reach a wide range of x_{O_2} and x_{CO_2} for a given selective and non-selective membrane combination.

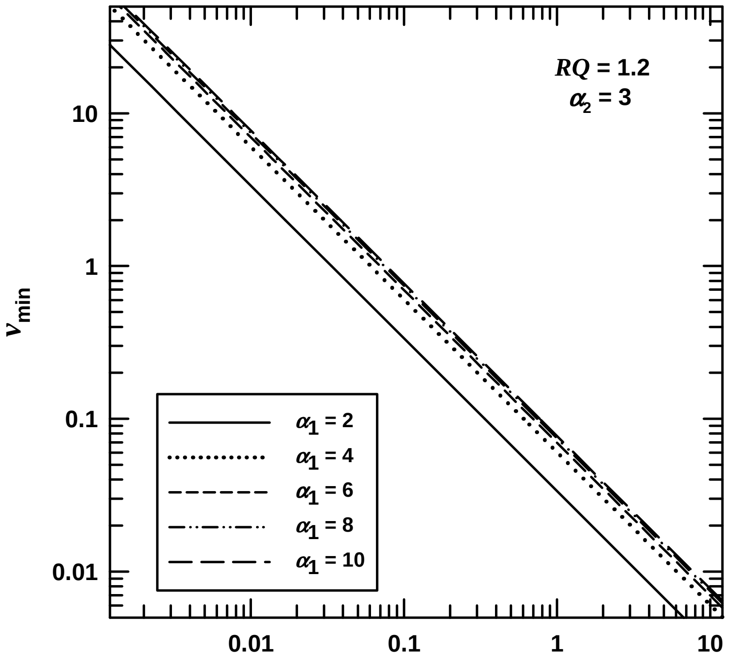

Figure 6.19: The product βv is a constant at $v_{\min}$ for a given selective membrane.

Figure 6.20 shows that the product $\beta v_{\min}$ is a small value that increases with an increase in the CO_2 to O_2 selectivity of the material forming the selective membrane. Although the trends of $\beta v_{\min}$ to CO_2 to O_2 selectivity are the same, O_2 to N_2 selectivity has noticeable effects on the absolute value of $\beta v_{\min}$. Unlike $(x_{CO_2})_0$, this product must be considered when designing the produce chamber.

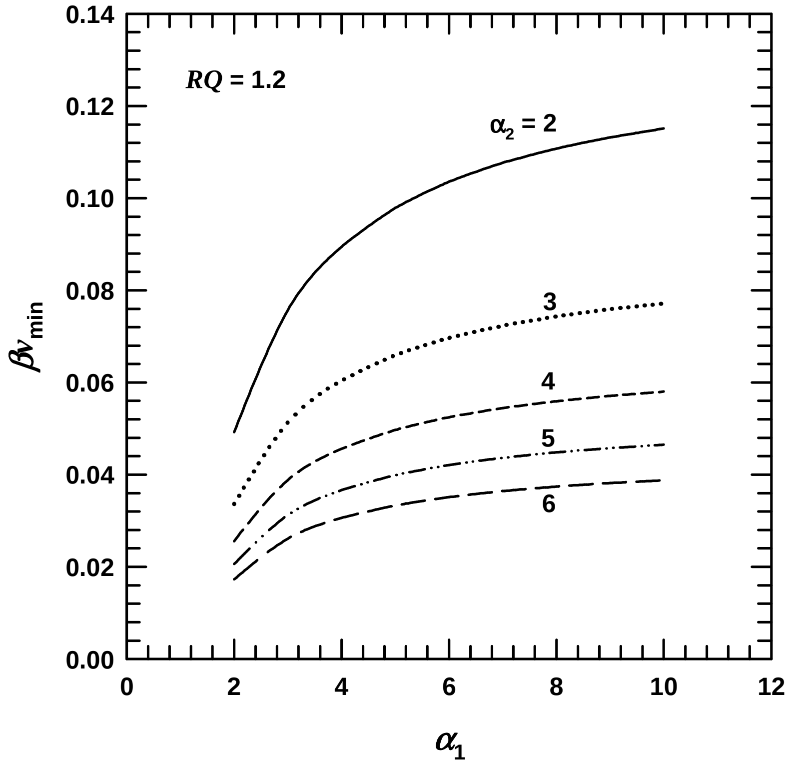

Figure 6.20: The product $\beta v_{\min}$ for various selective membranes.

As mentioned previously, not all non-selective membrane designs are capable of generating a wide range of x_{O_2} and x_{CO_2} concentrations where $(x_{CO_2})_0$ ranges from $(x_{CO_2})_{0,\min}$ to 0.21. However, to increase versatility for design purposes, it is most ideal to know what range of concentrations is attainable so that different produce can be stored with the same equipment. Figure 6.12 shows that for a permselective membrane with $\alpha_1 = 2$ and $\alpha_2 = 3$ setting β = 0.1, 1, or 2 will not allow a value of $(x_{CO_2})_0 = 0.21$ to be reached. However, a β value of 4 can reach the range from $(x_{CO_2})_{0,\min}$ to 0.21 as v increases. Comparing designs with selective membranes of the same CO_2 to O_2 selectivity $\alpha_1 = 4$, but of different O_2/N_2 selectivities show that the O_2/N_2 permselectivity has little effect on $(x_{CO_2})_0$ as shown in Figures 6.13, 6.17, and 6.18. For the cases considered, the ratio of permeation through the non-selective membrane to that of the selective membrane to reach a concentration of $(x_{CO_2})_0 = 0.21$ is unchanged, i.e., β necessary is 14.

In the range where $(x_{CO_2})_0 = 0.21$ and w = 0, this model approaches the Paul-Clarke model, Equation 6.37. This occurs when[6]

$$\frac{K_{CO_2} + H}{K_{O_2} + H} = RQ \tag{6.50}$$

By invoking this condition it is possible to find an explicit expression for β by nondimensionalizing and rearranging of the preceding equation

$$\beta\Big|_{to\ reach\ (x_{CO_2})_0 = 0.21} = \frac{\alpha_1 - RQ}{RQ - 1} \tag{6.51}$$

Figure 6.20 shows the minimum value of β necessary to reach $(x_{CO_2})_0 = 0.21$ for selective membranes with different CO_2 to O_2 permselectivities. This plot shows that a more CO_2 to O_2 selective membrane and produce with a low RQ require more permeation through the non-selective membrane to reduce the CO_2 to O_2 selectivity in order to attain a value of $(x_{CO_2})_0 = 0.21$. If the RQ of the produce is below 1, as seen in Equation 6.51 and Figure 6.22, there will be no value of β capable of reaching $(x_{CO_2})_0 = 0.21$ which is the upper range of CO_2 for optimal produce storage. For typical produce the RQ value is approximately 1.2; therefore, the value of β, such that at least $(x_{CO_2})_0 = 0.21$ can be reached, depends heavily on the selective membrane used for design.

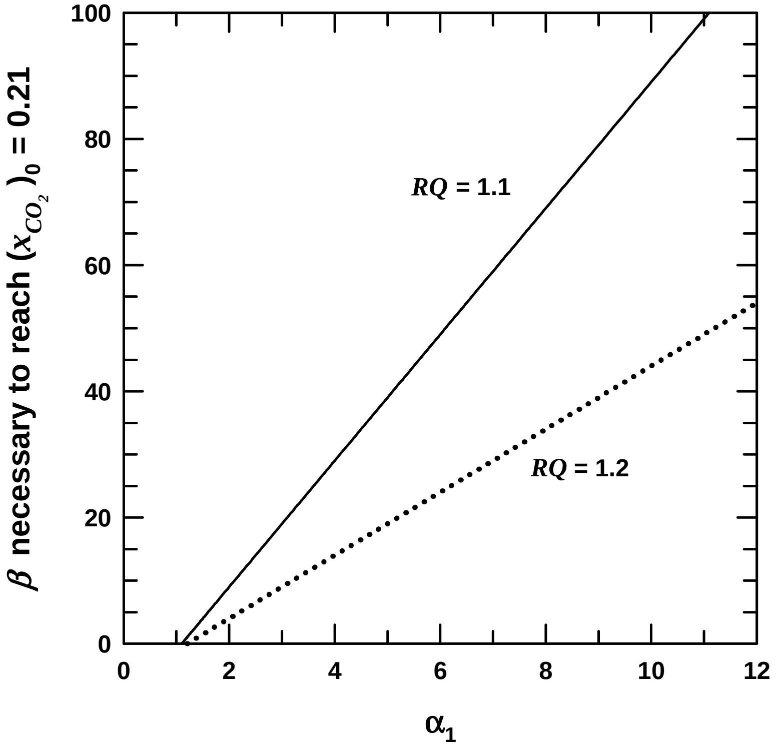

Figure 6.21: Illustrates the permeation through the perforations, β, that are necessary to reach $(x_{CO_2})_{0,\min} = 0.21$ for different polymer materials (α_1).

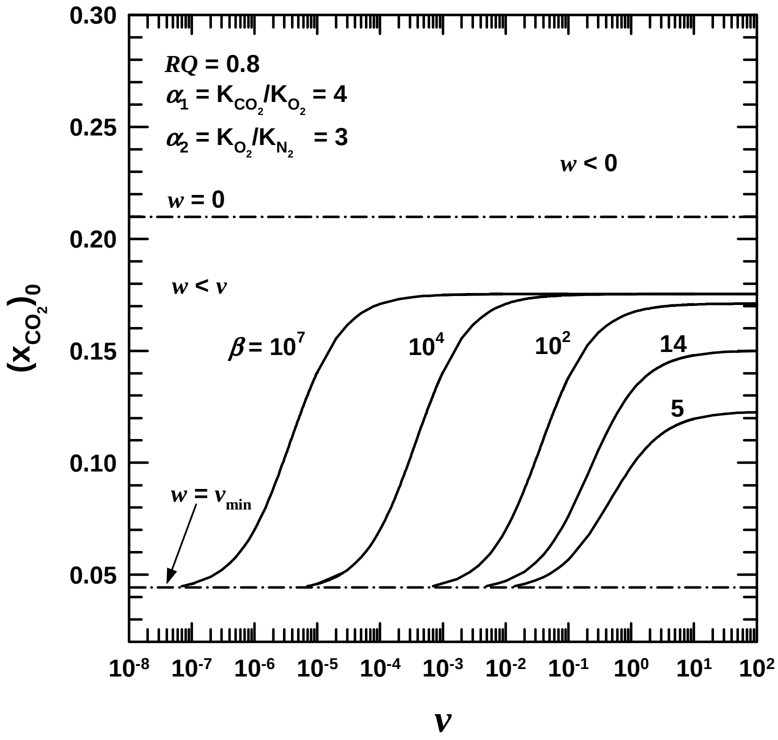

Figure 6.22: Model predictions for $(x_{CO_2})_0$ as a function of v for $\alpha_1 = 4$ and $\alpha_2 = 3$ with an RQ = 0.8.

This passive bulk MA model shows that by varying air flow rate in the upper chamber, it is possible to control the concentration in the main produce compartment within the limits shown in Figure 6.7. The above analysis also illustrates that designing the chamber with the correct equipment, i.e. selective and non-selective membranes, is extremely important to be able to attain the region necessary for optimal storage conditions for various types of produce. The relations shown are extremely useful for cursory examination; however, actual design requires some degree of detail to investigate specific MA storage considerations.

DESIGN PARAMETERS FOR MA OF BULK STORAGE

The mathematical model shows that the selectivity of the gases exchanged by the package (i.e. permselectivity) and the ratio at which the gases are consumed and generated by the produce are inherent to the choice of the membrane material and the fruit or vegetable being transported, respectively. To design a produce storage chamber using the model developed here requires that defined concentrations are met to accommodate the range of produce intended for storage. The model developed here will be examined from a more practical design perspective such as the determination of the mass of produce and the areas of the selective and non-selective membranes.

The parameter that represents permeation for oxygen is

$$K_{O_2} = A_m \left(\frac{P_{mO_2}}{\ell_m} \right) \tag{6.52}$$

As seen in Chapter 5 the respiration rate of the produce changes with the surrounding gas concentration and temperature; the respiration rate is represented by the following expression[6]

$$r_{O_2} = Wf(x_{O_2}, x_{CO_2}, T) \tag{6.53}$$

The storage temperature is assumed constant for this analysis. Solving for x_{CO_2} from Equation 6.12 and substituting the relation from Equation 6.25 results in

$$x_{CO_2} = \frac{r_{O_2} RQ}{K_{CO_2} p_t + \dfrac{Hp_t(q-Q)}{q+Hp_t}} = \frac{Wf(x_{O_2}, x_{CO_2})RQ}{K_{O_2} p_t \left[\dfrac{K_{CO_2}}{K_{O_2}} + \dfrac{\beta(q-Q)}{q+\beta K_{O_2} p_t} \right]} = \frac{Wf(x_{O_2}, x_{CO_2})RQ}{B} \tag{6.54}$$

It is convenient to represent the denominator as B

$$B = K_{O_2} p_t \left[\frac{K_{CO_2}}{K_{O_2}} + \frac{\beta(q-Q)}{q+\beta K_{O_2} p_t} \right] \tag{6.55}$$

Equations 6.32 and 6.40 are used to solve for x_{O_2}

$$x_{O_2} = 0.21\left[1 - \frac{x_{CO_2}}{(x_{CO_2})_0}\right] = 0.21\left[1 - \frac{Wf(x_{O_2}, x_{CO_2})RQ}{(x_{CO_2})_0 B}\right] \tag{6.56}$$

The expressions for x_{CO_2} and x_{O_2} have been arranged into a form similar to those from the Paul-Clarke model. The equations from this bulk model differ from the individual package model by the term representing the ratio of permeation through the porous membrane to that through the selective membrane, β. The term is now a product of the air feed rate to the upper chamber and the convective flow through the non-selective membrane. This clearly illustrates that by changing the air feed rate the composition of the gas in the produce compartment can be altered, thus, offering some control using a more passive MA method. To evaluate x_{CO_2} and x_{O_2}, it is useful to know the required convective gas flow rate Q into the package; however, it is dependent on the gas composition (x_{N_2}) inside the package as seen in Equation 6.23. To eliminate the necessity of knowing the nitrogen composition x_{N_2} directly, this quantity is expressed as a function of the design parameters with the use of Equations 6.26, 6.54 and 6.56

$$x_{N_2} = 0.79 + \left[\frac{0.21}{(x_{CO_2})_0} - 1\right]\frac{Wf(x_{O_2}, x_{CO_2})RQ}{B} \tag{6.57}$$

The preceding equation is substituted into Equation 6.23 to obtain an expression for the convective air flow rate Q.

$$\frac{Q}{Hp_t} = \frac{\left[(v+1)/\alpha_2\beta + v\right]\left(\frac{0.21}{(x_{CO_2})_0} - 1\right)\frac{Wf(x_{O_2}, x_{CO_2})RQ}{B}}{0.79v + 0.79 + \left(\frac{0.21}{(x_{CO_2})_0} - 1\right)\frac{Wf(x_{O_2}, x_{CO_2})RQ}{B}} \tag{6.58}$$

From a design perspective, the selective membrane is chosen to ensure that the lower concentration limit for the produce intended for storage or transport is met and the non-selective membrane choice is based on the necessary CO_2 to O_2 selectivity reduction needed to operate within the desired O_2 and CO_2 range. To design a produce chamber for a range of produce requires an appropriate choice for the selective and non-selective membranes. The following analysis examines a design for produce, cut broccoli (optimal MA with 2 – 3 % O_2 and 6 – 7 % CO_2) and blueberries (optimal MA with 2 – 5 % O_2 and 12 – 20 % CO_2); these choices are near the extremes in the concentration diagram in Figure 6.2. Specifying the produce defines the optimal concentration, RQ, and the respiration rate such that C, δ and $(x_{CO_2})_0$ are computed from Equations 6.32, 6.33 and 6.40 respectively for each produce. The respiration rate for O_2 of cut broccoli and blueberries is 6.09×10^{-3} and 8.84×10^{-4} cc(STP)/kg/sec respectively where both produce are assumed to have a RQ value of 1.2 in accordance with the UC Davis recommended MA database for produce (see Figure 6.2)[23, 24]. The permeability coefficients and selectivities of O_2, N_2, and CO_2 for selected high-flux polymers are shown in Table 6.1.

Table 6.1: Permeability (Barrers) and selectivity of gases O_2, N_2, and CO_2 for selected high-flux polymers.

Polymer	T (°C)	P_{O_2}	P_{N_2}	P_{CO_2}	Selectivity		Ref
					CO_2/O_2	O_2/N_2	
Poly(dimethyl siloxane)	35	830	320	3750	4.6	2.1	[25]
Poly(methyl propyl siloxane)	35	380	170	2300	6.0	2.2	[26]
Poly(dimethylsiloxane-urethane)	35	750	310	2500	3.3	2.4	[27]
Poly(isoprene)	25	23.4	9.2	149	6.3	2.5	[28]
Cis-poly(butadiene)	25	19.0	6.4	138.3	7.3	3.0	[28]
Poly(4-methyl-1-pentene)	35	27.0	6.7	84.6	3.1	4.0	[29]

For this analysis the permeances (P_{O_2}/ℓ_m) of the selective and non-selective membranes are assumed to be 7.6x10^{-8} and 4.57x10^{-8} cc(STP)/cm^2/cmHg/sec, respectively. The area of the selective membrane necessary to satisfy these conditions for the lower concentration limit is determined from either x_{CO_2} or x_{O_2} using design Equations 6.54 or 6.56 such that $q = Q$. At the low air flow rate limit, the variable B simplifies to

$$B\big|_{q=Q} = K_{O_2} p_t \alpha_1 \tag{6.59}$$

Substitution of the preceding expression into the equation for x_{CO_2} enables easy determination of the necessary area for the selective membrane. As mentioned previously, choosing a produce determines C, δ and $(x_{CO_2})_0$, thus, for cut broccoli the necessary CO_2 to O_2 selectivity, α_1, is 3.25 and we will assume a value for the O_2 to N_2 selectivity α_2 of 3 which is similar to the high-flux materials in Table 6.1. A selective membrane with these characteristics must be 56 m^2 to store 100 kg of cut broccoli as determined from the design equation for x_{CO_2}; an area of this size requires use of a compact membrane module design. The minimum air flow rate can be determined from Equation 6.58 by setting $q = Q$, i.e. $v = w$, and solving for Q to obtain

$$q = Q = \left[\frac{0.21}{(x_{CO_2})_0} - 1\right] \frac{Wf\,(x_{O_2}, x_{CO_2})RQ}{0.79\alpha_1\alpha_2} \tag{6.60}$$

For cut broccoli, the minimum air flow rate q is 1015 cc(STP)/hr. Now the requirements for β to meet the demands of the blueberries which have higher CO_2 concentration demands must also be satisfied. The parameters C, δ, α_1, α_2, K_{O_2}, p_t, and RQ are all known. The value of β necessary to achieve $(x_{CO_2})_0$ of 0.21 is determined to be 10.25 from Equation 6.51. Now from Equations 6.36 – 6.39, and the value of β that will satisfy the needs of the produce with the higher CO_2 requirement is computed. Some practical estimate for the air flow rate across the non-selective membrane must be assumed here.

A small air flow rate induces the need for a non-selective membrane with a large area and the opposite is observed for large air flow rates. A moderate air flow rate of 258000 cc(STP)/hr is chosen and the value of β necessary to attain the concentration necessary for blueberries is 9.26. From the previously specified permeance, the area of the non-selective membrane required is 85.7 m^2, requiring a compact membrane module. It is necessary that β is at least equal to or larger than 6.52 to meet the concentration requirements of blueberries, i.e. the value of β at large air flow rates. For this case we can assume that $q \gg Q$, so B simplifies to

$$B = K_{O_2} p_t [\alpha_1 + \beta] \approx K_{O_2} p_t \beta \qquad (6.61)$$

Now from the equations for x_{CO_2} or x_{O_2} and using the preceding expression for B, the mass of the blueberries that can be handled by the system is determined. For this case, the maximum mass is 4200 kg of blueberries. The mass and air flow rate are quite large compared to the requirements for cut broccoli at the lower limit; however, the design system can be flexible so that parameters may be altered to meet the optimal concentration ranges for a smaller mass of blueberries with lower air flow rates. The use of produce with more similar concentration requirements would reduce the flexibility necessary for the design described above. Using this method, one can specify the design, K_{O_2} and β, necessary for a range of produce.

CONCLUSIONS

A bulk MA design is developed here to examine transport of produce with very different concentration requirements using a single produce chamber. This bulk MA unit is equipped with selective and non-selective membranes. The performance of the non-selective membrane can be modified by varying the air flow rate upstream of membrane.

The non-selective membrane is used to reduce the selectivity of CO_2 to O_2 generated by the selective membrane to enable operation at higher CO_2 concentrations. The choice of the selective and non-selective membrane determines the concentration regions attainable by the system. The mathematical model shows that the lower CO_2 concentration limit is largely dependent on the selective membrane, whereas, the higher CO_2 concentration is mostly dependent on the choice of the non-selective membrane. The region between these lower and upper CO_2 concentration limits for the produce chosen can be attained by varying the air flow rate upstream of the non-selective membrane. This model teaches that a passive bulk MA design can be used to transport produce of varying concentration requirements.

REFERENCES

1. Greene C. United States Department of Agriculture: Economic Research Service. AREI Chapter 4.9: U.S. Organic Agriculture: www.ers.usda.gov.
2. Kader AA, Zagory D, and Kerbel EL. Critical reviews in food science and nutrition 1989;28(1):1-30.
3. Kader AA. Bulletin of the International Institute of Refrigeration 2001;LXXXI(1):3-14.
4. Ben-Yehoshua S. Environmentally friendly technologies for agricultural produce quality 2005;61(112):61-112.
5. Exama A, Arul J, Lencki RW, Lee LZ, and Toupin C. Journal of Food Science 1993;58(6):1365-1370.
6. Paul DR and Clarke R. Journal of Membrane Science 2002;208(1-2):269-283.
7. Fishman S, Rodov V, Peretz J, and Ben-Yehoshua S. Journal of Food Science 1995;60(5):1078-1087.
8. Edmond JP, Chau KV, and Brecht JK. Modeling respiration rates of blueberry in a perforation-generated modifeid atmosphere package. Proceedings from the Sixth International Controlled Atmosphere Research Conference. Cornell University, Ithaca, New York, 1993. pp. 134-144.
9. Talasila PC and Cameron AC. Journal of Food Science 1997;62(5):926-930.
10. Fonseca SC, Oliveira FAR, Lino IBM, Brecht JK, and Chau KV. Journal of Food Engineering 2000;43(1):9-15.
11. Makino Y, Iwasaki K-i, and Hirata T. Journal of Agricultural Engineering Research 1997;67:47-59.
12. Silva FM, Chau KV, Brecht JK, and Sargent SA. Applied Engineering in Agriculture 1999;15(4):313-318.
13. Edmond JP, Castaigne F, Toupin CJ, and Desilets D. Transactions of the ASAE 1991;34(1):239-245.

14. Kader AA. Respiration of Gas Exchange of Vegetables. In: Weichmann J, editor. Postharvest physiology of vegetables. New York: Marcel Dekker, Inc., 1987. pp. 25-43.
15. Platenius H. Plant Physiology 1943;18(4):671-684.
16. Cameron AC, Talasila PC, and Joles DW. Hortscience 1995;30(1):25-34.
17. Ooraikul B, M.E. Stiles, and Editors. Modified Atmosphere Packaging of Food. New York: Ellis Horwood, 1991.
18. Brackett RE. Postharvest Biology and Technology 1999;15:305-311.
19. Fidler JC and North CJ. The Journal of Horticultural Science 1967;42:189-206.
20. Kidd F. Proceedings of the Royal Society of London, Series B 1914;87:408-421.
21. Kidd F and West C. Plant Physiology 1945;20(4):467-504.
22. Sanz C, Perez AG, Olias R, and Olias JM. Food Science and Technology International 2000;6(1):33-38.
23. Hagger PE, Lee DS, and Yam KL. Journal of Food Process Engineering 1992;15:143-157.
24. Song Y, Kim HK, and Yam KL. Journal of American Society of Horticultural Science 1992;117(6):925-929.
25. Senthilkumar U and Reddy BSR. Journal of Membrane Science 2007;292(1-2):72-79.
26. Stern SA, Shah VM, and Hardy BJ. Journal of Polymer Science, Part B: Polymer Physics 1987;25(6):1263-1298.
27. Madhavan K and Reddy BSR. Journal of Membrane Science 2006;283(1-2):357-365.
28. Pauly S. Permeability and Diffusion Data. In: Brandrup J, Immergut EH, and Grulke EA, editors. Polymer Handbook. New York: Wiley-Interscience, 1999. pp. 543-569.
29. Mohr JM and Paul DR. Polymer 1991;32(7):1236-1243.

Chapter 7: Conclusions and recommendations

A thorough study of the thermal and gas transport properties of poly(alkyl acrylate) blends of primarily semi-crystalline components has been described to provide a pathway for attaining thermally responsive membranes. A general route to design modified atmosphere packages of retail size has also been explored. In addition, a detailed mathematical model to attain a defined modified atmosphere in a bulk container using selective and non-selective membranes has been developed that may serve as a tool to evaluate the applicability of various produce/membrane combinations or actual container design. This chapter summarizes the conclusions found at the end of each chapter and provides some recommendations for future work.

CONCLUSIONS

Side-chain crystallization in poly(alkyl acrylate)s results in a dynamic change in the permeability as the melting temperature is transgressed. These attributes are retained upon blending the side-chain crystalline polymers. Despite being of similar chemical structure, not all possible blend combinations form homogeneous films. In fact, the range of side-chain length components that form homogenous films is rather narrow.

The permeation response of semi-crystalline poly(alkyl acrylate) blends are significantly influenced by side-chain lengths of the blend components and blend composition. The components of each blends system appear to crystallize independently of one another, but with some hindrance to crystallization that each component imposes on the other. Blends formed using components with side-chain lengths where $|n - m| \leq 4$, show two distinct permeation jumps that occur at the melting temperatures as the crystallites for each of the individual components. As the side-chain length becomes shorter, the crystallite distribution increases causing the crystallites to melt over a broader temperature range. The shorter side-chain length semi-crystalline blends, PA-14 and PA-16, show a more continuous increase in the permeation response, owing to the more progressive melting of the two components with close melting temperatures, than expected by simple Arrhenius considerations for such polymers with fixed morphologies. The broader melting process created by blending poly(alkyl acrylates) of proper side-chain length and composition exceed energetics allowable with other semi-crystalline polymers such as polyethylene. Thermal history appeared to have a significant effect on the morphology of the blends especially in the semi-crystalline state. These effects were lessened in the intermediate state that that gives rise to increased thermal responsiveness, i.e., activation energy of permeation.

A brief look at poly(octadecyl acrylate) and n-aliphatic blends (paraffins, fatty alcohols and an acid) showed that useful polymer films are only possible at low fatty compound content due to the brittle nature of the fatty compounds. The blends that form suitable polymer films all co-crystallize with the poly(*n*-alkyl arylate) and have slight increase in crystallinity. Though permeation measurements were not conducted on the blends, the permeation switch is expected to mimic that of the poly(alkyl acrylate).

Models of the modified atmosphere inside a retail package and bulk chambers were examined. A mathematical model was developed to determine the gas concentration inside a bulk chamber equipped with selective and non-selective membrane modules. The implementation of a non-selective membrane helps to reduce the CO_2 to O_2 selectivity so that higher CO_2 concentration ranges are attainable. The choice of the selective membrane primarily determines the lower CO_2 concentration region attainable. The mathematical model successful shows that a large region of O_2 and CO_2 concentrations are accessible by varying the air flow rate upstream of the non–selective membrane. Clearly, this is advantageous for bulk transport of different produce and offers much possiblity.

RECOMMENDATIONS

Explore the fundamental effect of side-chain length on the permeability jump for the extremes

This systematic investigation of the effect of side-chain length on gas permeability revealed a slight maximum of the permeation switch for the homopolymers at a side-chain length of $n = 16$. Previous studies concerned with the fundamental transport properties showed that the permeability jump increased with side-chain length up to and including poly(octadecyl acrylate) with $n = 18$ and with further increase in n, in particular for poly(behenyl acrylate) with $n = 22$, a slight decrease was observed[1]. Semi-crystalline poly(behenyl acrylate) has a higher diffusion coefficient than poly(octadecyl acrylate) with caused a lower permeability jump. It would be interesting to examine the permeation behavior of poly(hexadecyl acrylate) and an analogue with a significantly lower side –chain length much greater than $n = 22$. It is thought that the longer side-chain poly(*n* alkyl acrylate) will approach the behavior of main-chain crystalline polyethylene with is estimated to have a lower permeation jump than the poly(behenyl acyralte). The monomers to polymerize such materials are available. It becomes increasing difficult as the side-chain length increases to obtain materials of a single side-chain length, but even so such as investigation can help elucidate why this maximum occurs at $n = 16$ and may provide a possible path to altering the side-chain structure to maximize the permeation switch. It was found that the permeability coefficient of poly (*n*-alkyl acrylate)s is primarily diffusion dependent. It is hypothesized that poly(hexadecyl acrylate) has a higher permeability switch due to the a lower diffusion coefficient. The two-phase transport model suggests that the diffusion coefficient is reduced due to the tortuosity and chain immobilization factors. There is currently no clear path to separate these factors, but determination of crystallite size, shape and orientation could provide further insight into the behavior of permeability jump with side-chain length.

Effect of crystallization conditions on the gas permeability of poly(n-alkyl acrylate)s

This analysis showed that the crystallization conditions markedly influenced the absolute permeability in the semi-crystalline state. Homopolymer PA-18 and the equal weight PA16 and PA18 blend cooled at a slow cooling rate (0.1^{o}C/min) had a higher permeability than the corresponding faster cooled samples (1.0^{o}C/min) despite having a higher crystallinity. The two-phase model set for by Michaels and Bixler suggests that the lower permeability is expected for higher crystallinity samples. In agreement with previous studies, it was shown that the crystallization conditions affected the permeability of the larger molecules to a greater extend that the smaller ones. Thus, a clearer understanding of how thermal history relates to the permeability would be useful especially for industrial applications where processing conditions cannot be as tightly controlled during preparation or in application.

Thermal and transport behavior in this study was primarily conducted using samples with similar thermal histories at 1^{o}C/min. However, permeability measurements require samples to remain at a single temperature for periods ranging from 5 hours to a few days depending on the temperature. Thermal characterization of homopolymers and blends under crystallization conditions that more closely parallel permeation experiments, i.e. annealed isothermally, would be of great significance. The varied crystallization conditions can cause different morphologies including crystallite size, shape and orientation. This could have significant effects on membrane performance for many applications. Membranes formed for modified atmosphere packaging with crystallization dependent transport properties can have a detrimental influence on the produce due to changes in gas concentration inside the package.

Gas transport in blends of poly(*n*-alkyl acrylate)s and fatty compounds

The brief examination of thermal behavior of *n*-aliphatics and poly(*n*-alkyl acrylate) blends resulted in useful films at only low concentrations due to the low molecular weight of the fatty compounds. The permeation behavior of these blends was not conducted due to the brittle nature that is a long-known attribute of the homopolymer. Shorter side-chain crystalline analogues such poly(tetradecyl acrylate) with n = 14 and poly (dodecyl acrylate) with n = 12 are not brittle but rather tacky materials. In theory these shorter side-chain homopolymers could better benefit from blending with the fatty compounds that resulted in a slight increase in the crystallinity. Amorphous poly(*n*-alkyl acrylate)s, in particular, could have significant use provided that crystallization is induced. Inomata et al. found that blending low amounts (7 wt%) of *n*-octadecanoic acid with amorphous statistical copolymer poly[(methyl acrylate)-stat-(ocatdecyl acrylate)] with 43 mol% octadecyl ester residue induced crystallization of the side-chains as revealed from structural analysis[2]. The melting temperature occurred at temperature lower than the statistical copolymer with 53 mol% octadecyl ester residue. It is hypothesized that low molecular weight fatty compounds blended with amorphous and short side-chain semi-crystalline poly(*n*-alkyl acyralte)s could provide a route to blends with increased crystallinity at low temperatures.

Examine polymers for modified atmosphere packaging and storage applications

Designing a retail package or a bulk container to attain and subsequently maintain a MA to prolong the freshness of produce requires the balance of the respiration and permeation processes. There is little to help control these processes once a retail package has been implemented. Thus, it is important to careful choose the proper polymer material to construct the package or membrane so that adequate gas flows enter and leave the package to at least maintain the defined concentration. Produce such as apples require very low carbon dioxide concentrations between 1 – 3 %. To reach this low concentration region requires materials with high permeation CO_2/O_2 selectivities. Typical high flux polymers have CO_2/O_2 selectivities between 2 and 6. The development of high-flux polymers with higher CO_2/O_2 selectivities could enable operation in this lower concentration region. The use of non-selective perforations or a porous membrane can be used in parallel to reduce the CO_2/O_2 selectivity of the membrane to work in a larger region; however, high non-selective transport operating regions can result in lower thermal responsiveness owing to the low activation energy of perforations and porous materials.

REFERENCES

1. Mogri Z. Gas transport properties of side-chain crystalline polymers. Chemical Engineering. Austin: University of Texas at Austin, 2001. pp. 289.
2. Inomata K, Sakamaki Y, Nose T, and Sasaki S. Polymer Journal 1996;28(11):986-991.

Appendix A

This appendix includes additional permeation responses of poly(n-alkyl acrylate) and poly (m-alkyl acrylates) blends for O_2, N_2 and CO_2 gases, in some cases H_2, He, and CH_4, that are discussed in Chapter 3. The experimental methods and procedures can be found in Chapter 3.

PA-14/PA-18 BLENDS

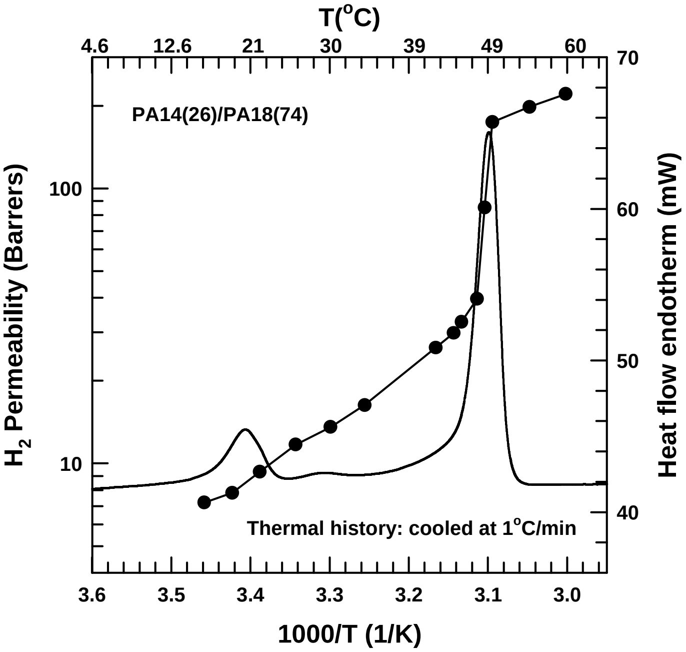

Figure A.1: H_2 permeability and DSC thermogram for PA14(26wt%)/PA18(74wt%) blend.

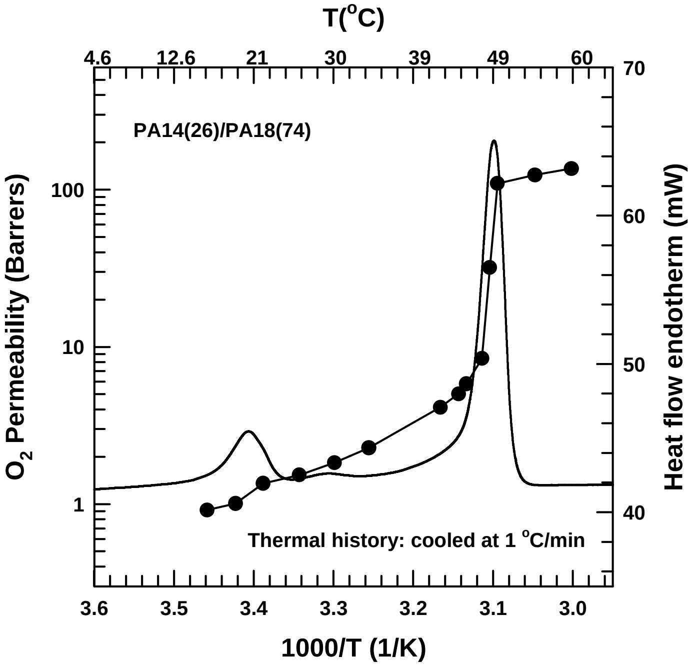

Figure A.2: O_2 permeability and DSC thermogram for PA14(26wt%)/PA18(74wt%) blend.

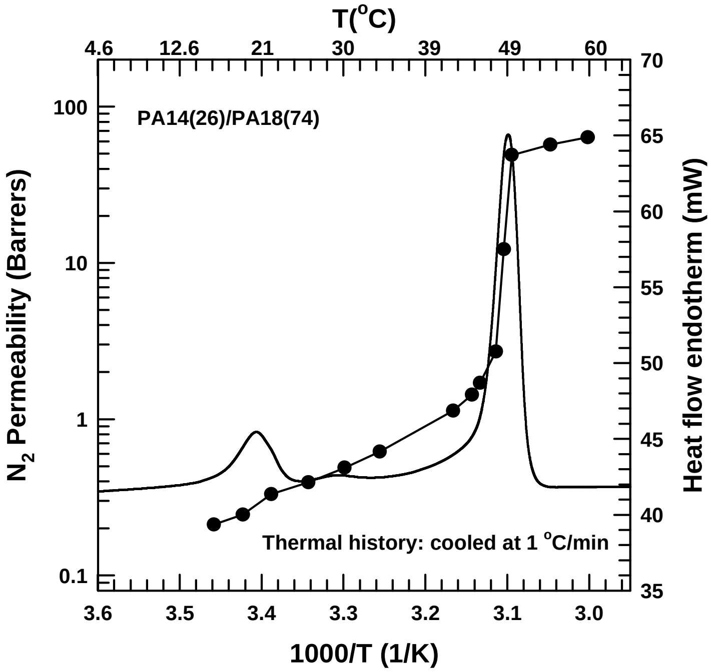

Figure A.3: N_2 permeability and DSC thermogram for PA14(26wt%)/PA18(74wt%) blend.

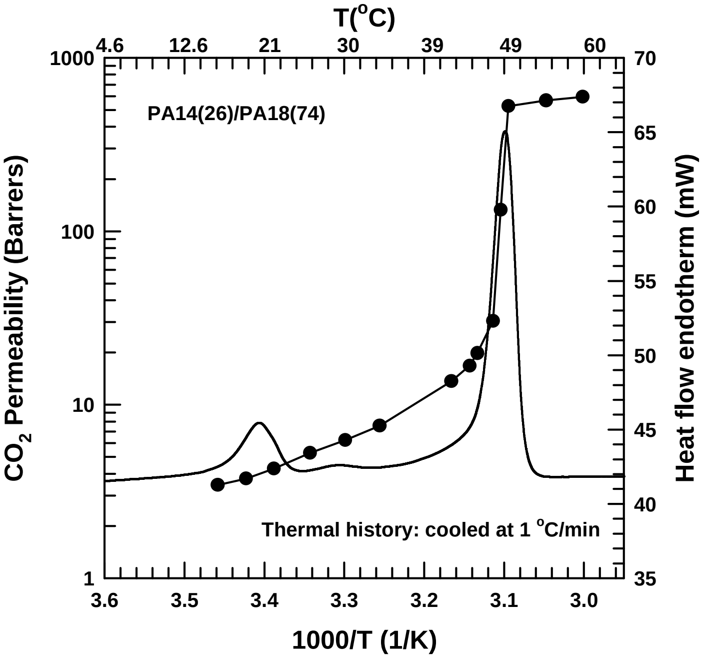

Figure A.4: CO_2 permeability and DSC thermogram for PA14(26wt%)/PA18(74wt%) blend.

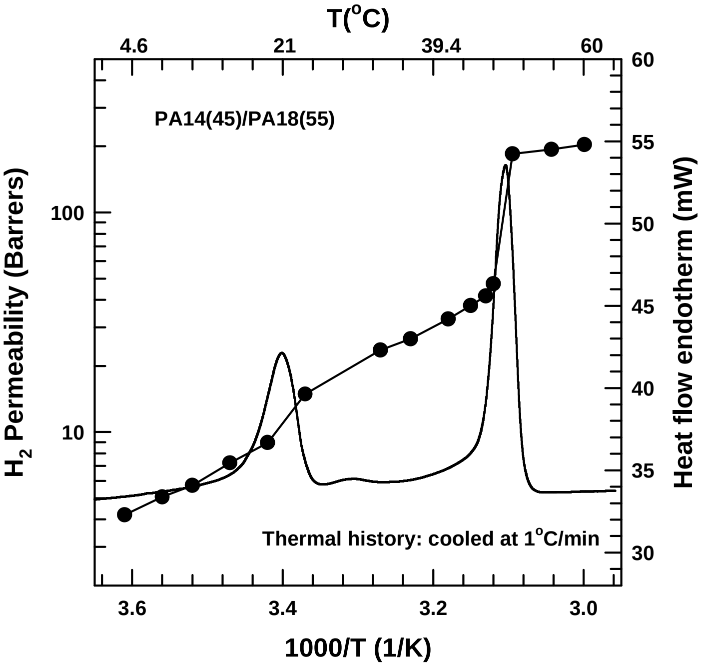

Figure A.5: H_2 permeability and DSC thermogram for PA14(45wt%)/PA18(55wt%) blend.

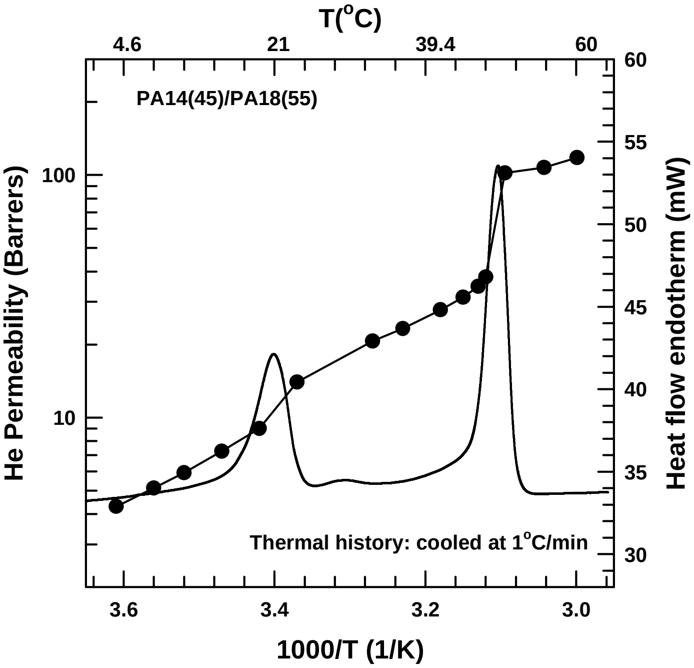

Figure A.6: He permeability and DSC thermogram for PA14(45wt%)/PA18(55wt%) blend.

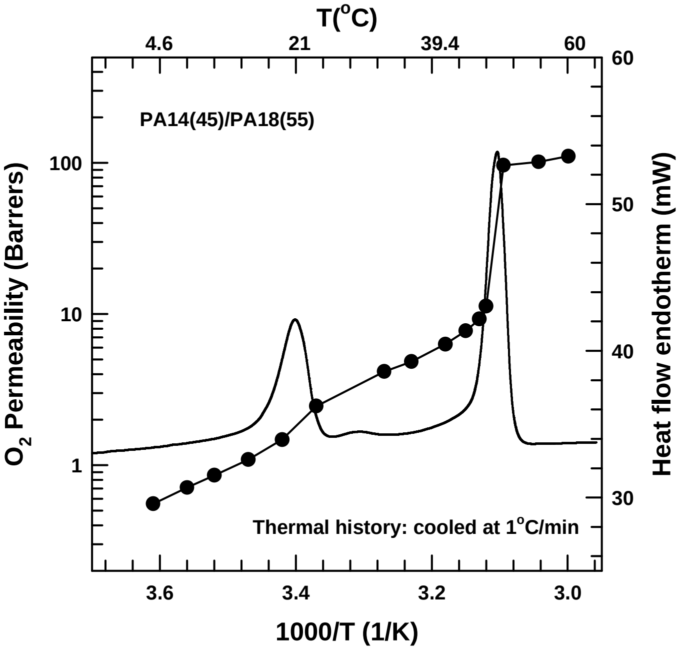

Figure A.7: O_2 permeability and DSC thermogram for PA14(45wt%)/PA18(55wt%) blend.

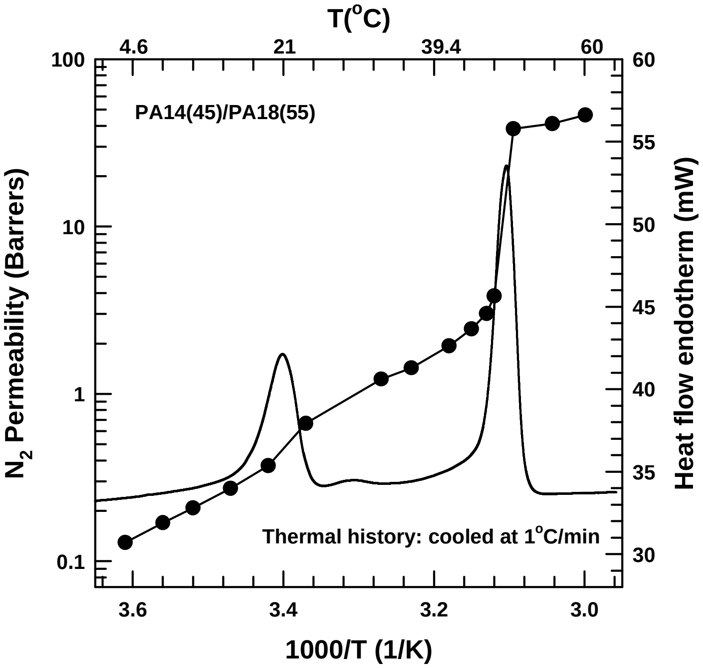

Figure A.8: N_2 permeability and DSC thermogram for PA14(45wt%)/PA18(55wt%) blend.

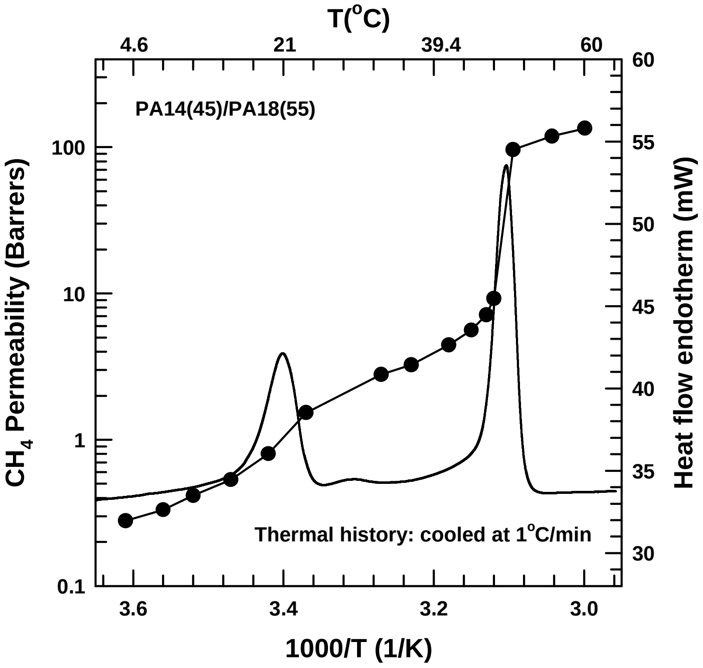

Figure A.9: CH_4 permeability and DSC thermogram for PA14(45wt%)/PA18(55wt%) blend.

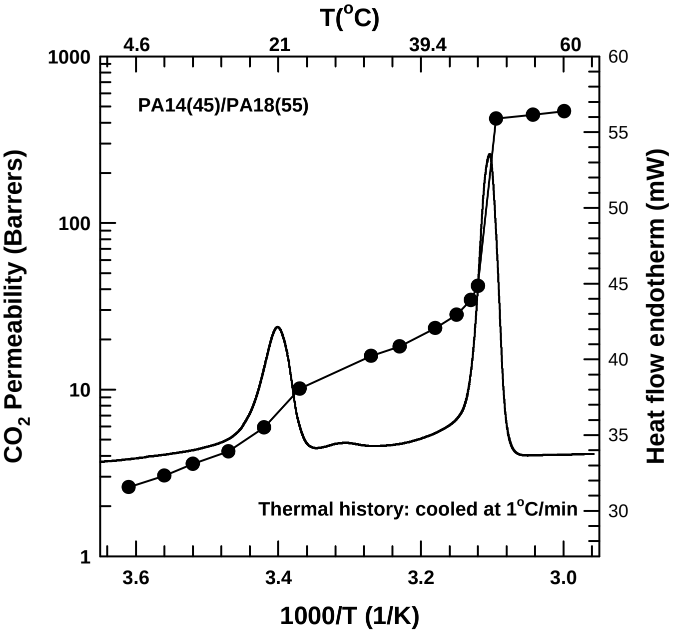

Figure A.10: CO_2 permeability and DSC thermogram for PA14(45wt%)/PA18(55wt%) blend.

PA-16/PA-18 BLENDS

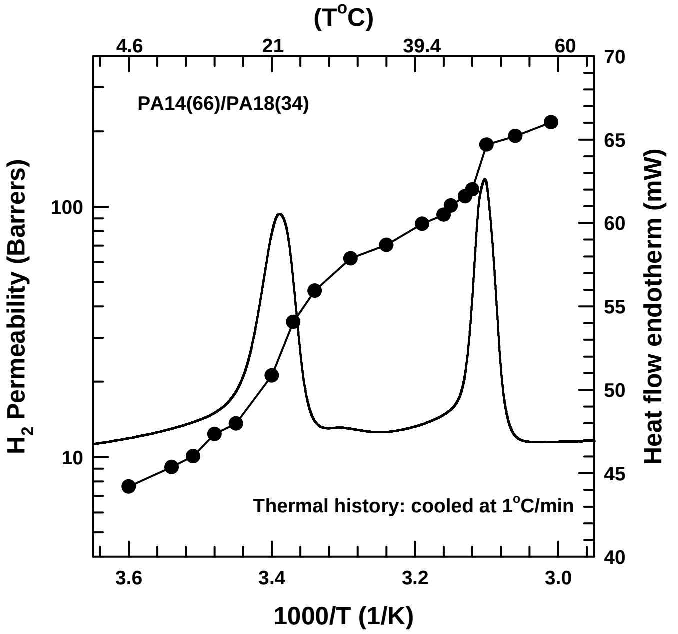

Figure A.11: H_2 permeability and DSC thermogram for PA14(66wt%)/PA18(34wt%) blend.

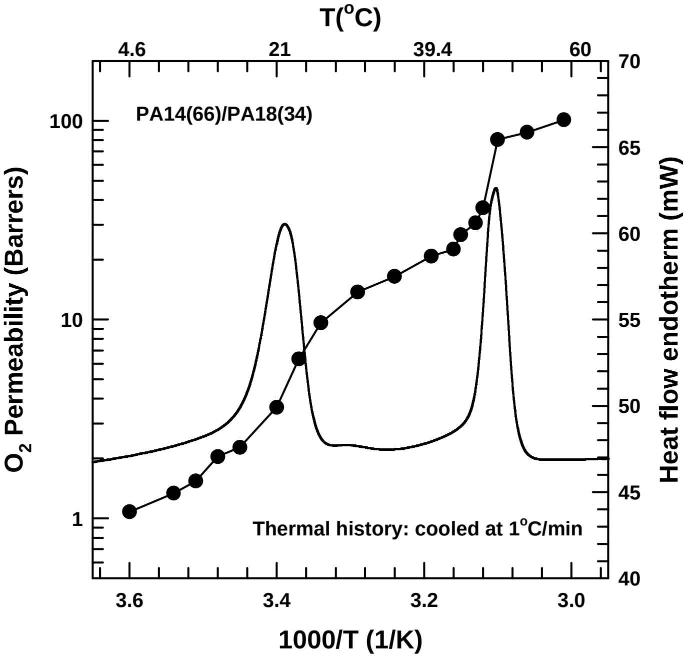

Figure A.12: O_2 permeability and DSC thermogram for PA14(66wt%)/PA18(34wt%) blend.

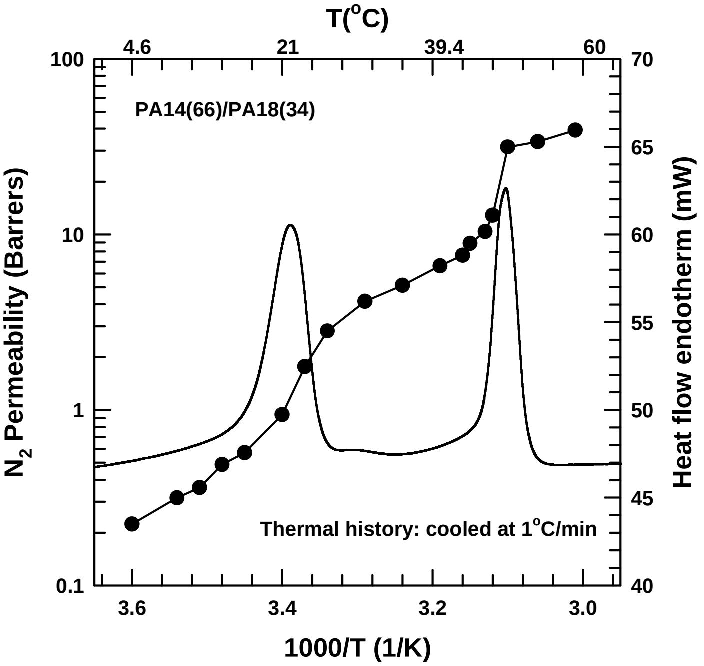

Figure A.13: N_2 permeability and DSC thermogram for PA14(66wt%)/PA18(34wt%) blend.

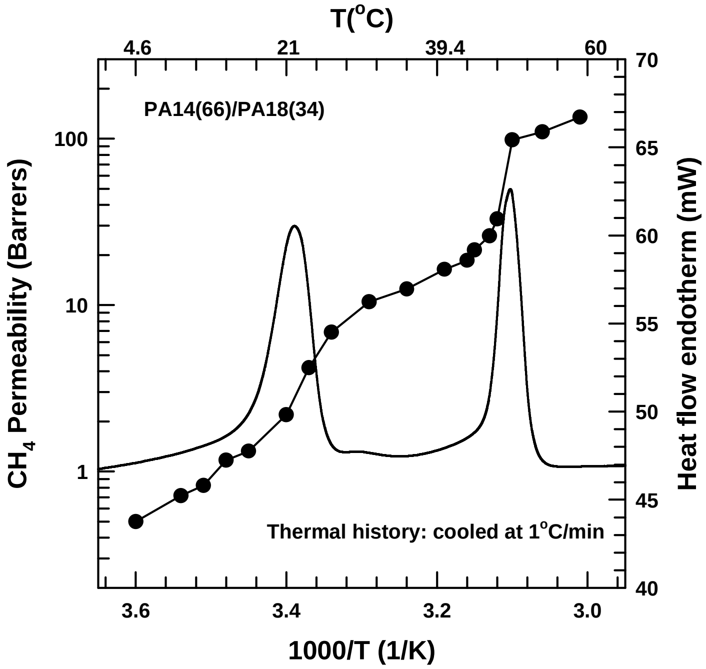

Figure A.14: CH_4 permeability and DSC thermogram for PA14(66wt%)/PA18(34wt%) blend.

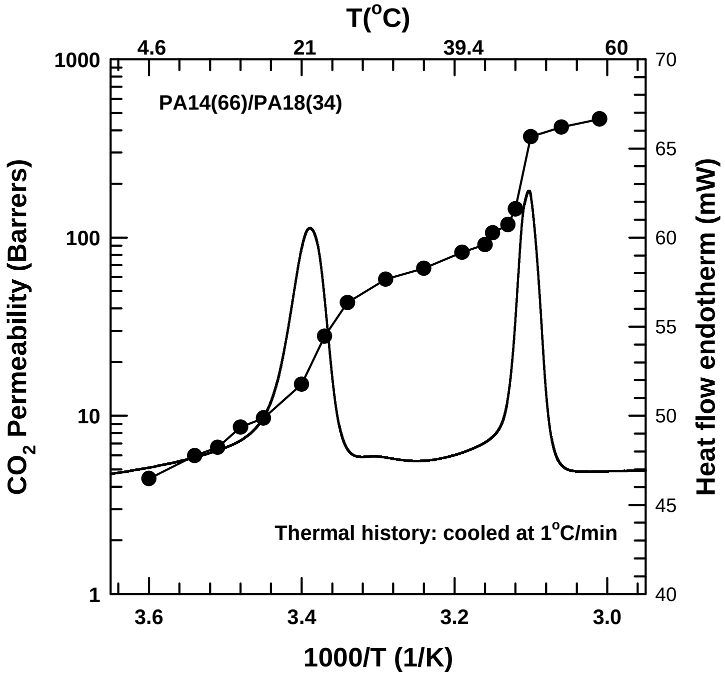

Figure A.15: CO_2 permeability and DSC thermogram for PA14(66wt%)/PA18(34wt%) blend.

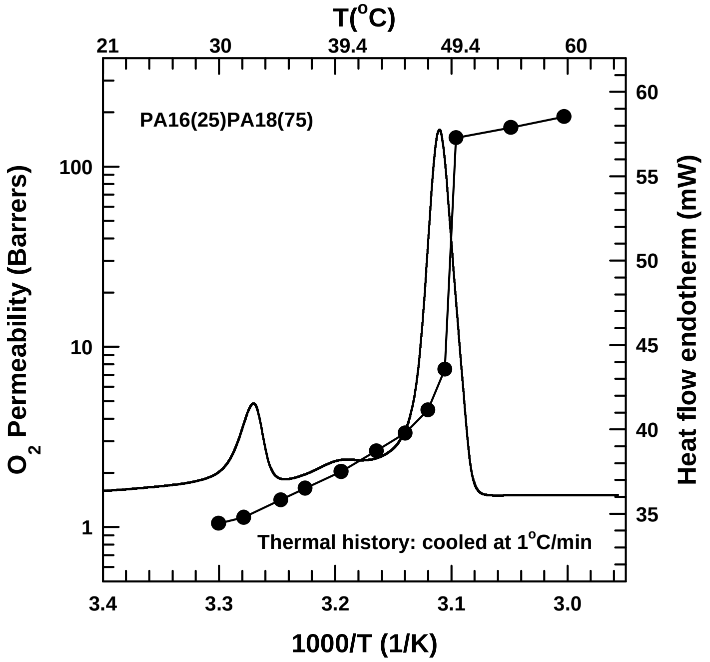

Figure A.16: O_2 permeability and DSC thermogram for PA16(25wt%)/PA18(75wt%) blend.

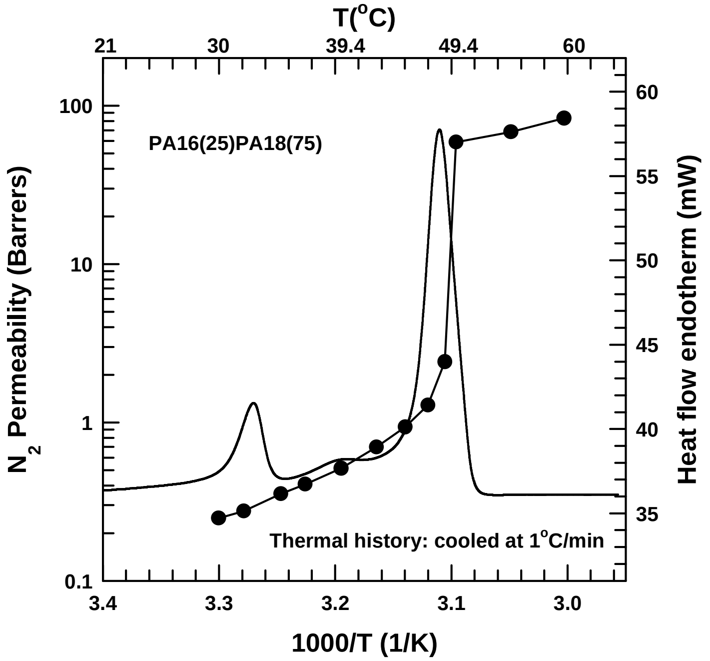

Figure A.17: N_2 permeability and DSC thermogram for PA16(25wt%)/PA18(75wt%) blend.

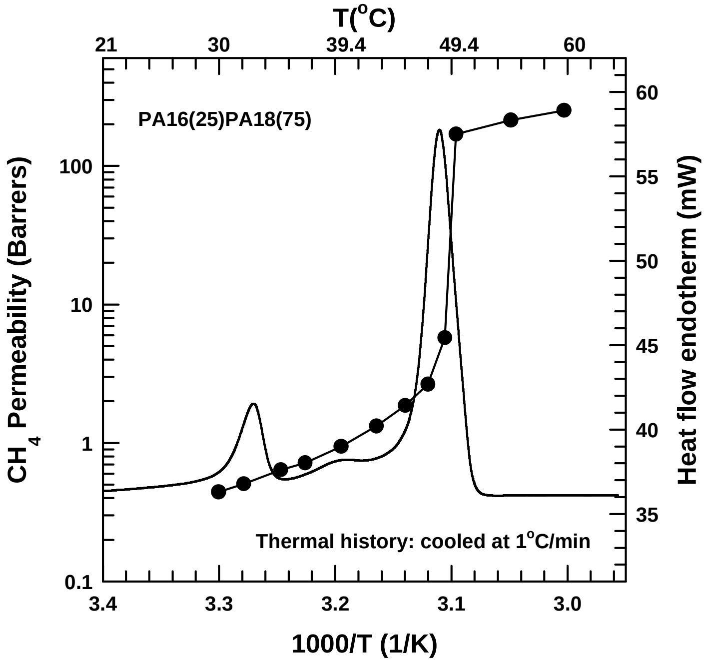

Figure A.18: CH_4 permeability and DSC thermogram for PA16(25wt%)/PA18(75wt%) blend.

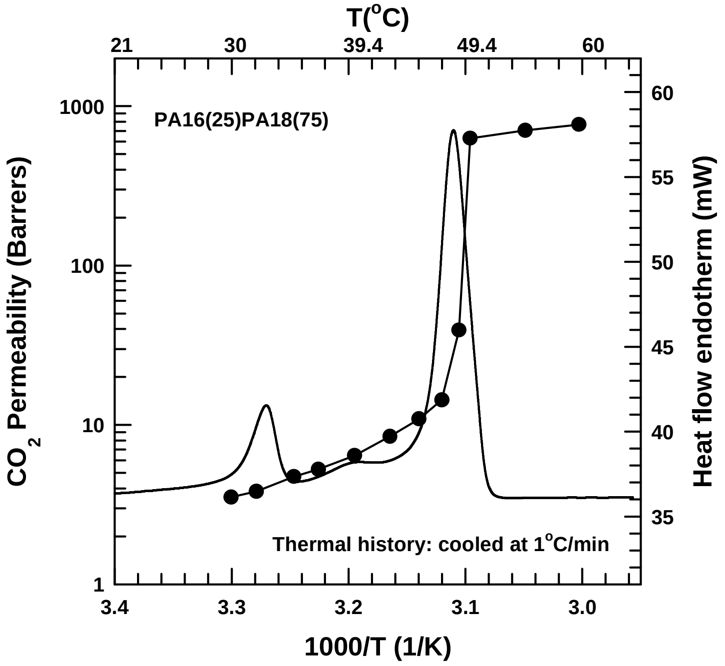

Figure A.19: CO_2 permeability and DSC thermogram for PA16(25wt%)/PA18(75wt%) blend.

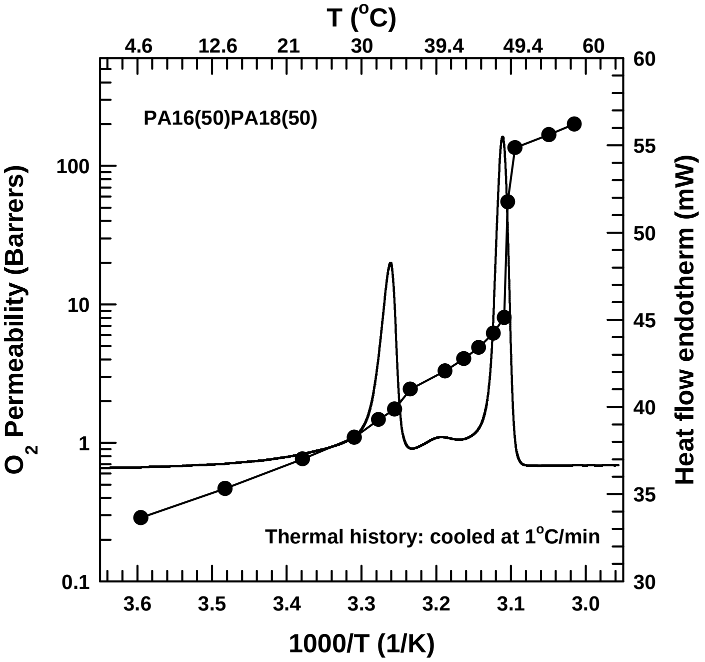

Figure A.20: O_2 permeability and DSC thermogram for PA16(50wt%)/PA18(50wt%) blend.

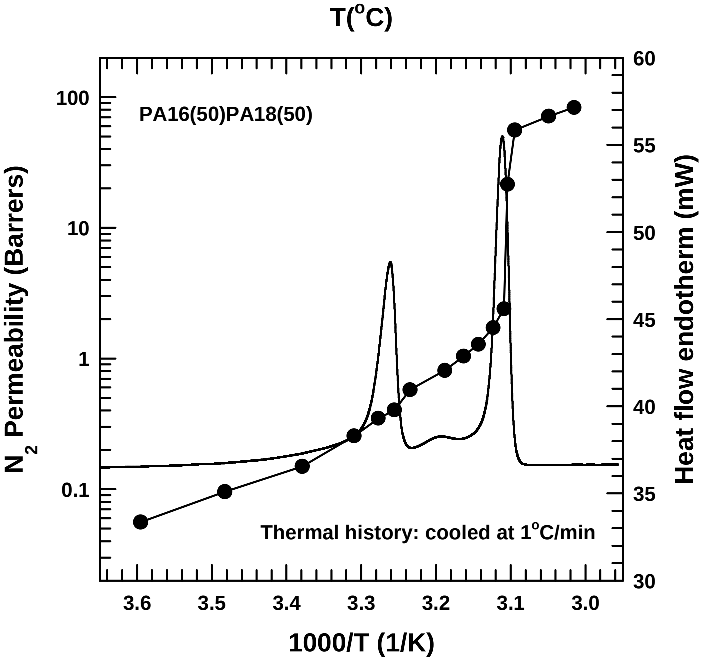

Figure A.21: N_2 permeability and DSC thermogram for PA16(50wt%)/PA18(50wt%) blend.

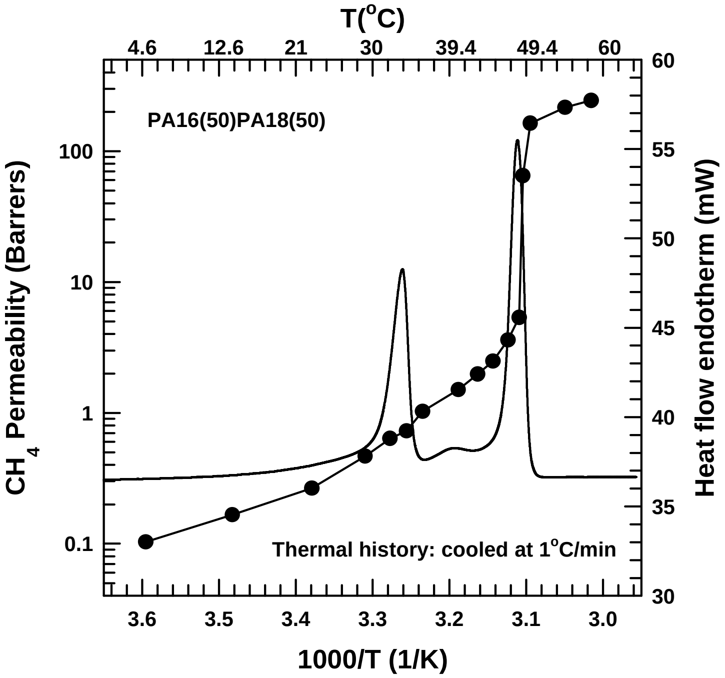

Figure A.22: CH_4 permeability and DSC thermogram for PA16(50wt%)/PA18(50wt%) blend.

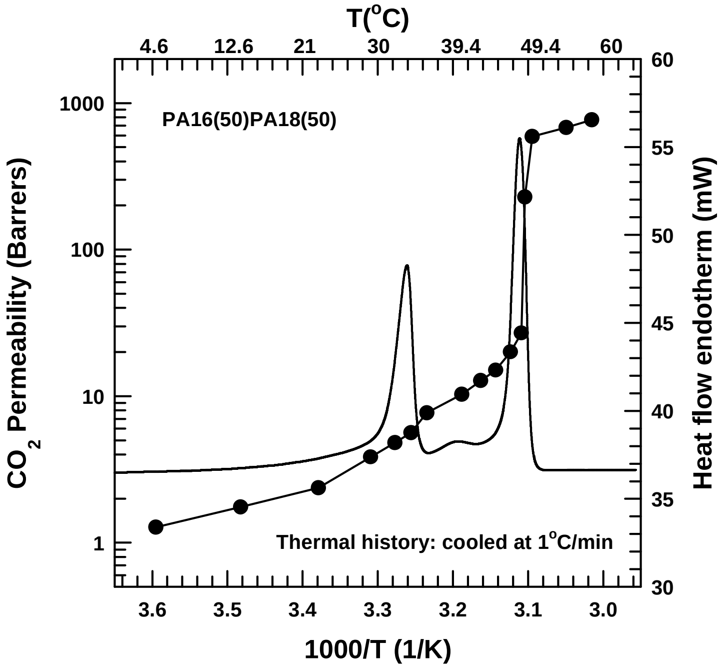

Figure A.23: CO_2 permeability and DSC thermogram for PA16(50wt%)/PA18(50wt%) blend.

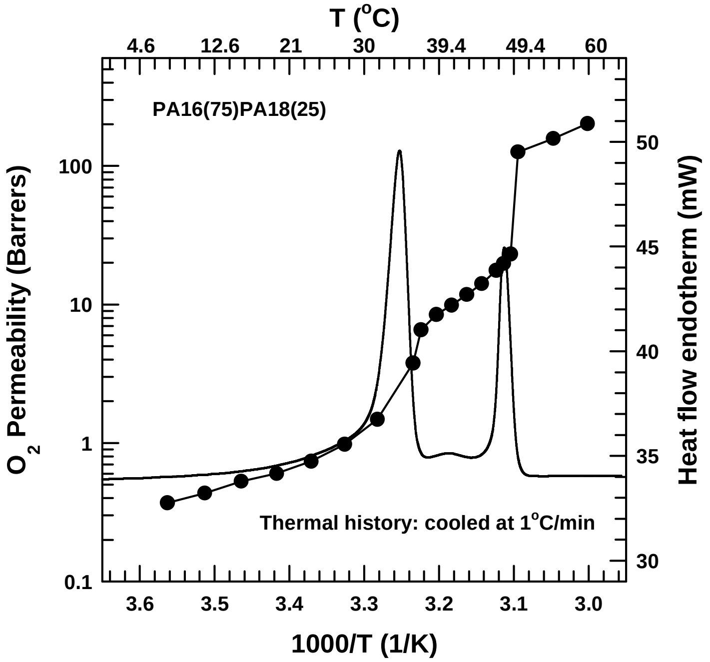

Figure A.24: O_2 permeability and DSC thermogram for PA16(75wt%)/PA18(25wt%) blend.

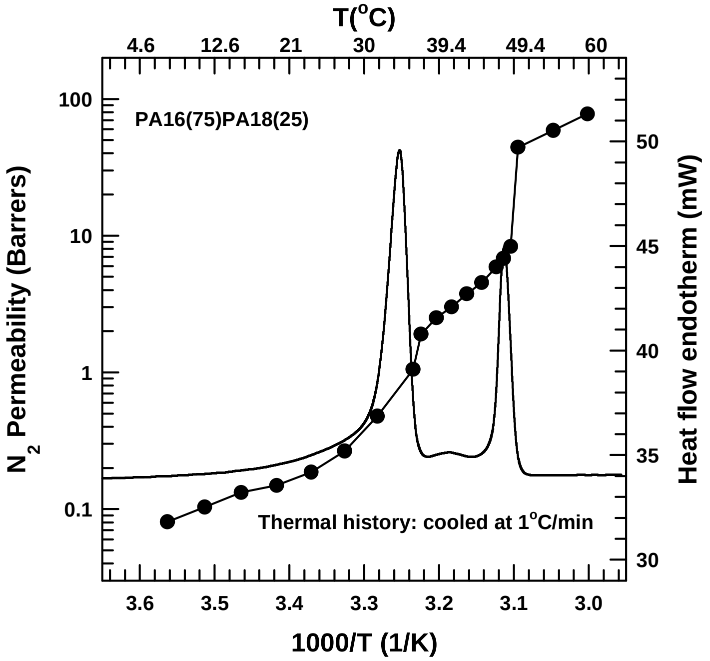

Figure A.25: N_2 permeability and DSC thermogram for PA16(75wt%)/PA18(25wt%) blend.

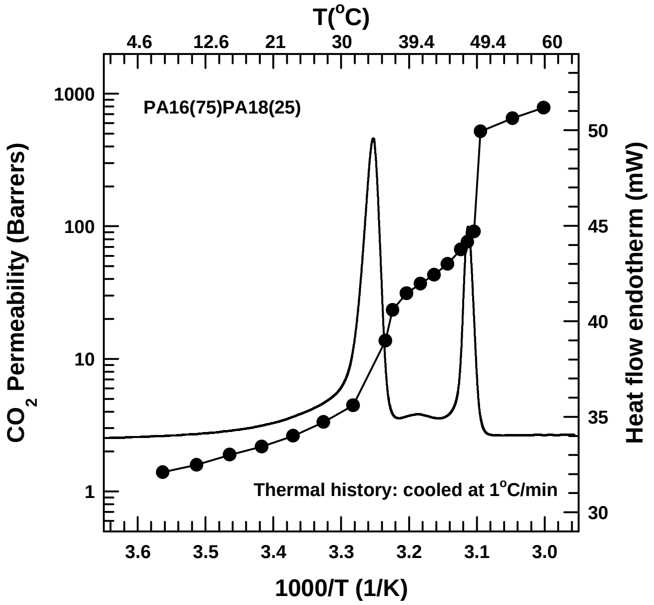

Figure A.26: CO_2 permeability and DSC thermogram for PA16(75wt%)/PA18(25wt%) blend.

PA-14/PA-16 BLENDS

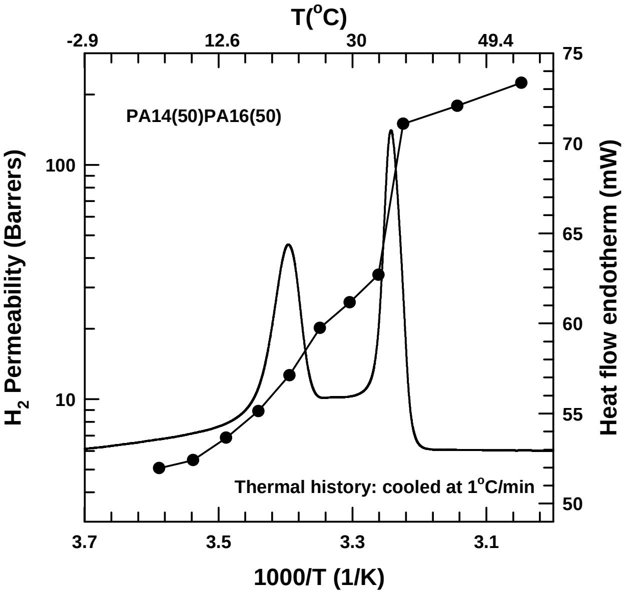

Figure A.27: H_2 permeability and DSC thermogram for PA14(50wt%)/PA16(50wt%) blend.

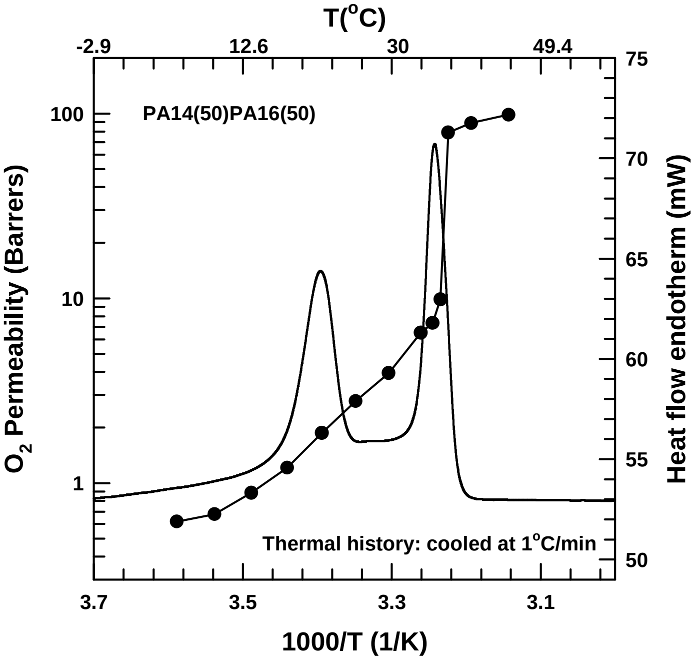

Figure A.28: O_2 permeability and DSC thermogram for PA14(50wt%)/PA16(50wt%) blend.

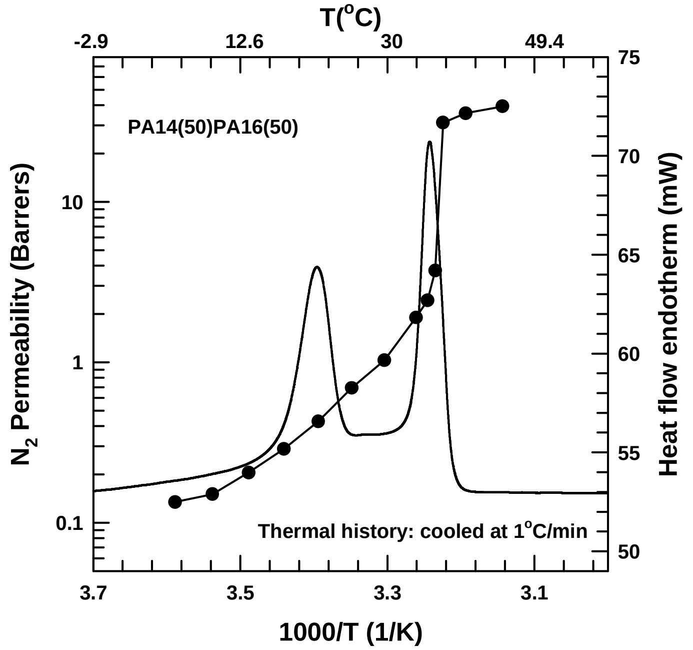

Figure A.29: N_2 permeability and DSC thermogram for PA14(50wt%)/PA16(50wt%) blend.

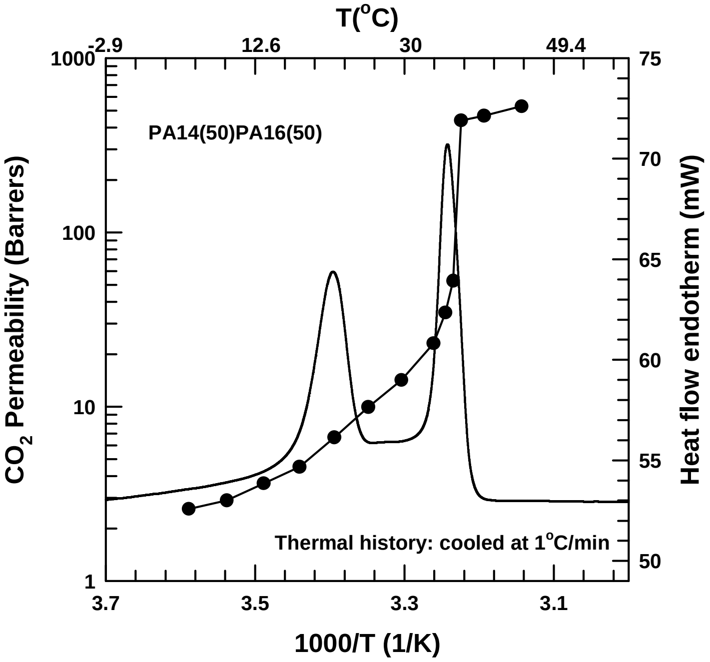

Figure A.30: CO_2 permeability and DSC thermogram for PA14(50wt%)/PA16(50wt%) blend.

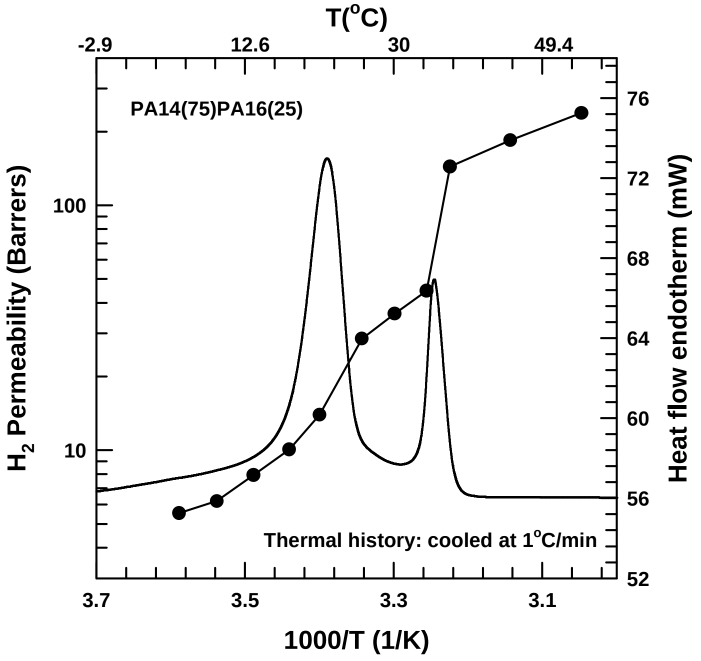

Figure A.31: H_2 permeability and DSC thermogram for PA14(75wt%)/PA16(25wt%) blend.

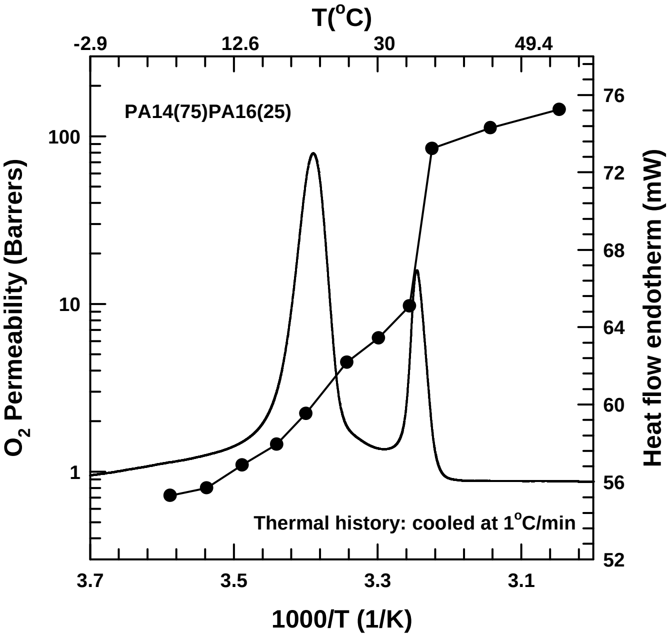

Figure A.32: O_2 permeability and DSC thermogram for PA14(75wt%)/PA16(25wt%) blend.

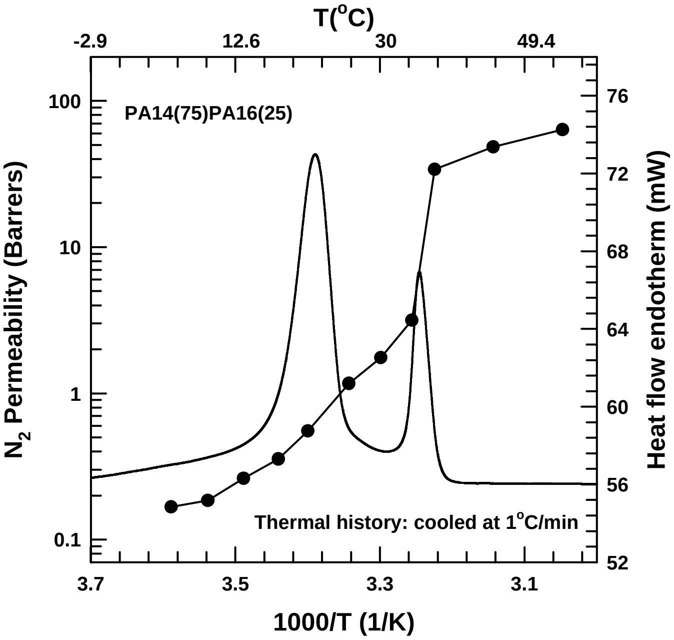

Figure A.33: N_2 permeability and DSC thermogram for PA14(75wt%)/PA16(25wt%) blend.

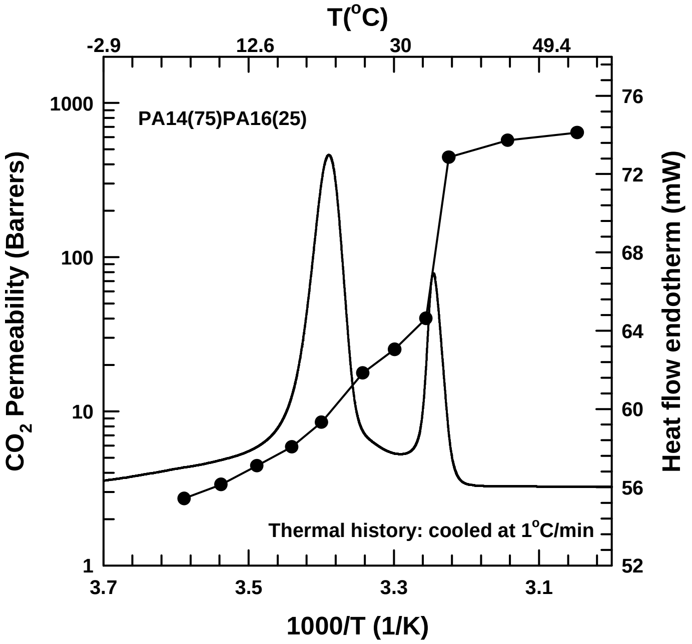

Figure A.34: CO_2 permeability and DSC thermogram for PA14(75wt%)/PA16(25wt%) blend.

PA-8/PA-10 BLENDS

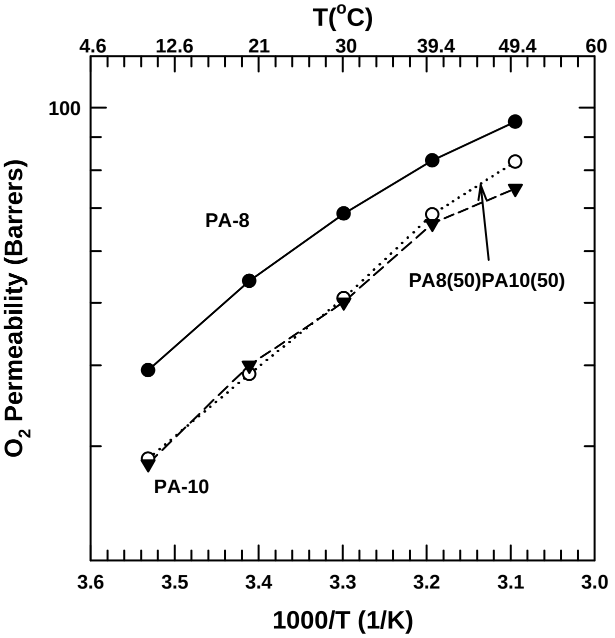

Figure A.35: O_2 permeability for PA8(50wt%)/PA10(50wt%) blend.

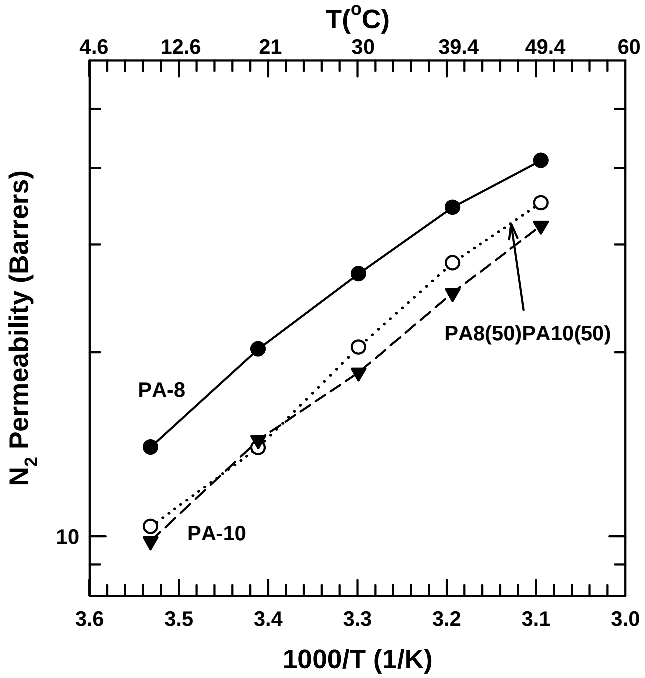

Figure A.36: N_2 permeability for PA8(50wt%)/PA10(50wt%) blend.

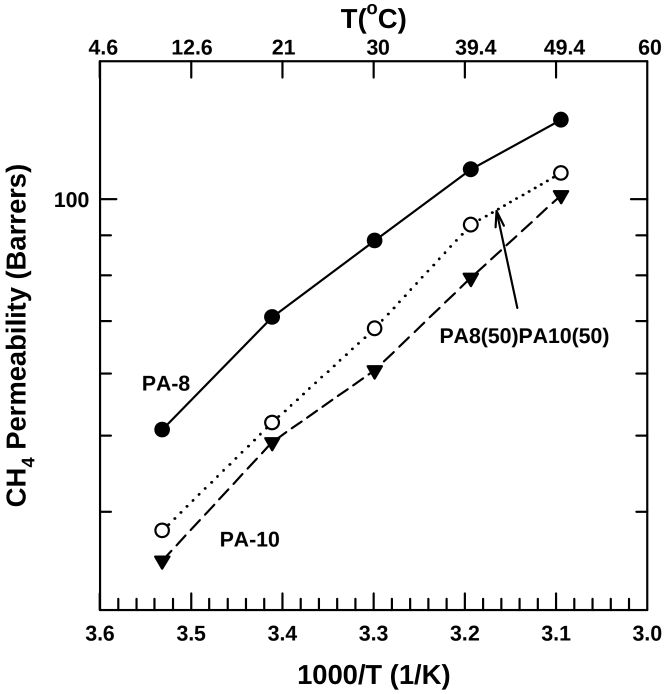

Figure A.37: CH_4 permeability for PA8(50wt%)/PA10(50wt%) blend.

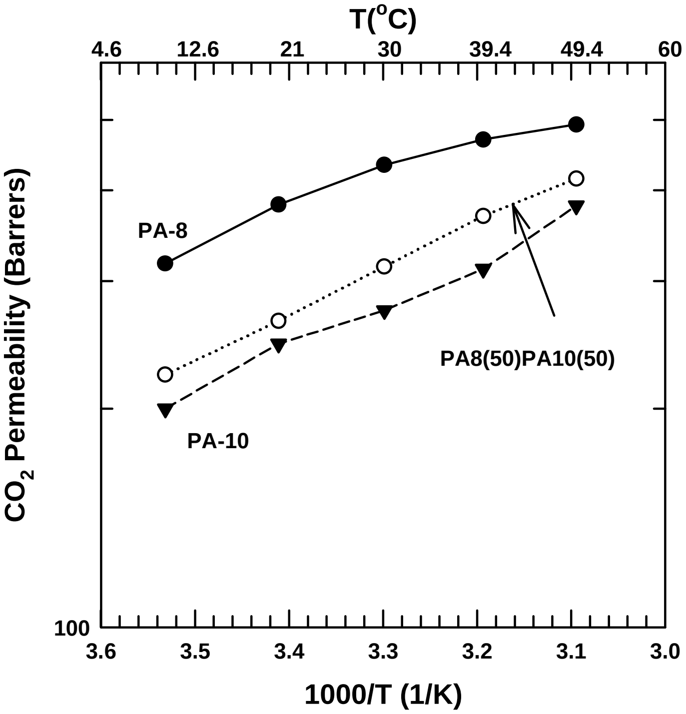

Figure A.38: CO_2 permeability for PA8(50wt%)/PA10(50wt%) blend.

THERMAL EFFECTS ON PERMEABILITY

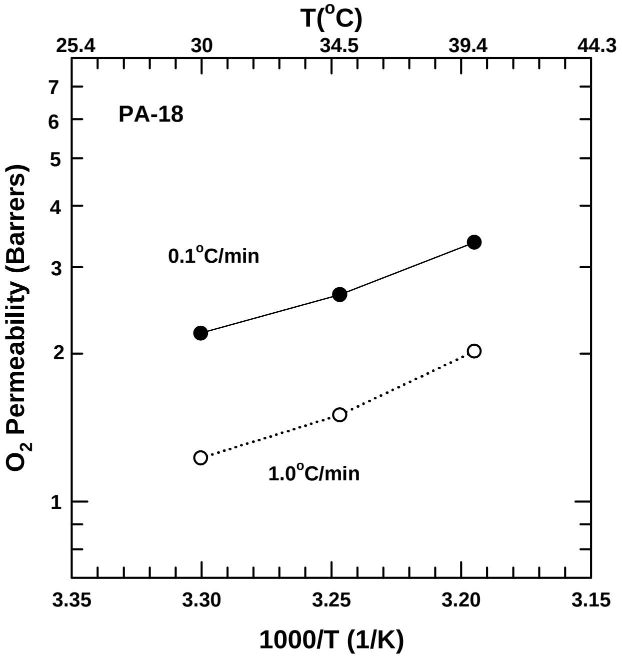

Figure A.39: Effects of thermal history on O_2 permeability of PA-18 as a function of temperature at two cooling rates, 0.1 and 1.0°C/min.

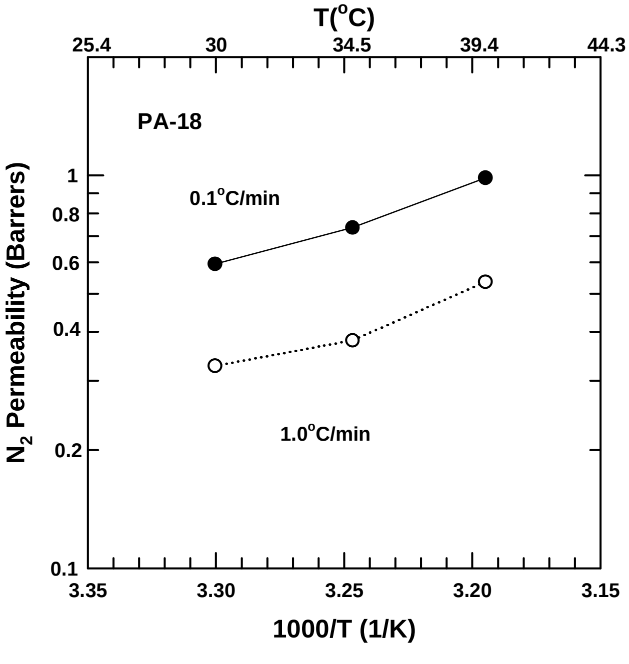

Figure A.40: Effects of thermal history on N_2 permeability of PA-18 as a function of temperature at two cooling rates, 0.1 and 1.0°C/min.

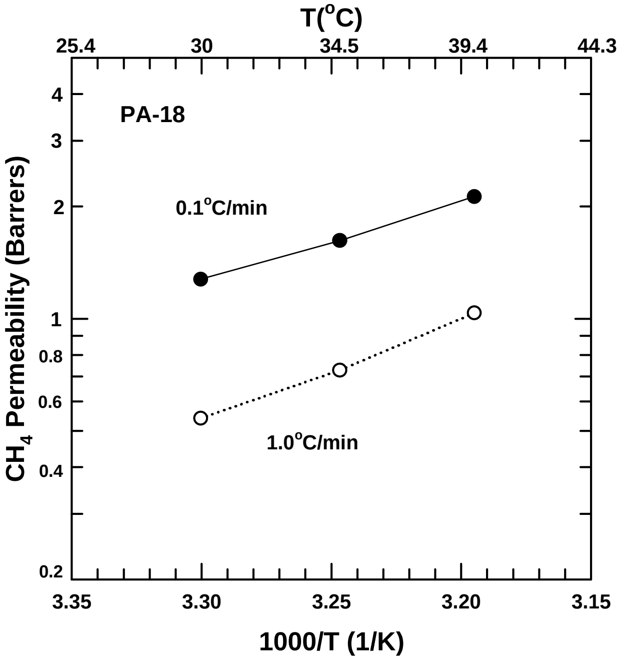

Figure A.41: Effects of thermal history on CH_4 permeability of PA-18 as a function of temperature at two cooling rates, 0.1 and 1.0°C/min.

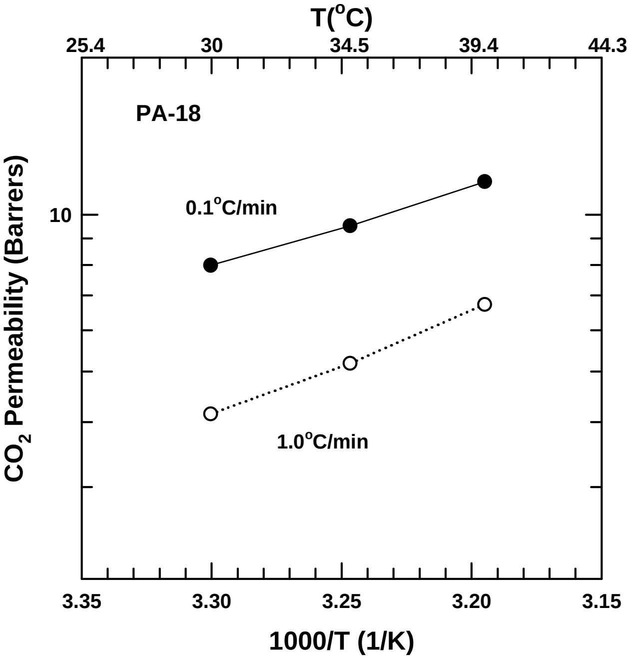

Figure A.42: Effects of thermal history on O_2 permeability of PA-18 blend as a function of temperature at two cooling rates, 0.1 and 1.0°C/min.

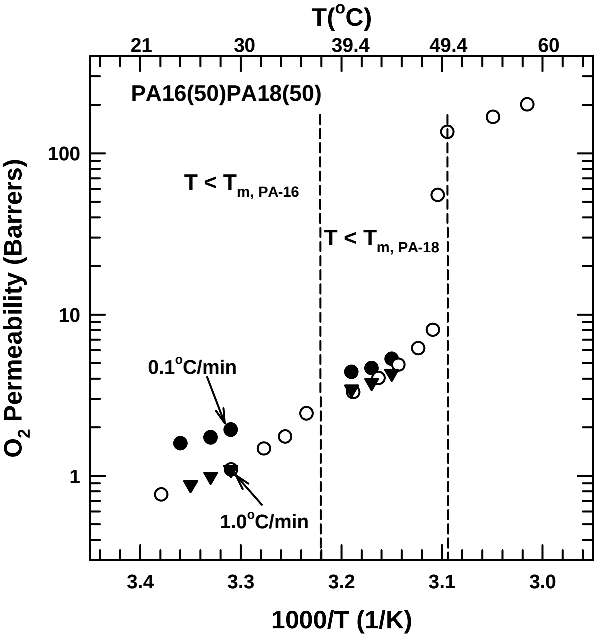

Figure A.43: Effects of thermal history on O_2 permeability of PA16(50wt%)/PA18(50wt%) blend as a function of temperature at two cooling rates, 0.1 and 1.0°C/min.

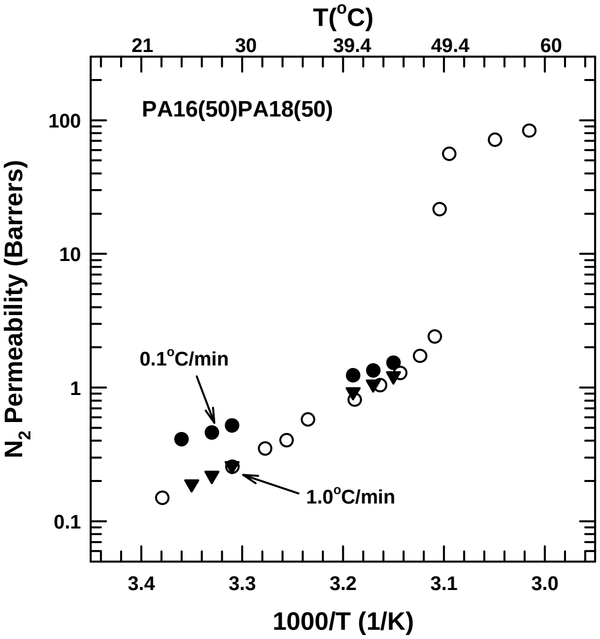

Figure A.44: Effects of thermal history on N_2 permeability of PA16(50wt%)/PA18(50wt%) blend as a function of temperature at two cooling rates, 0.1 and 1.0°C/min.

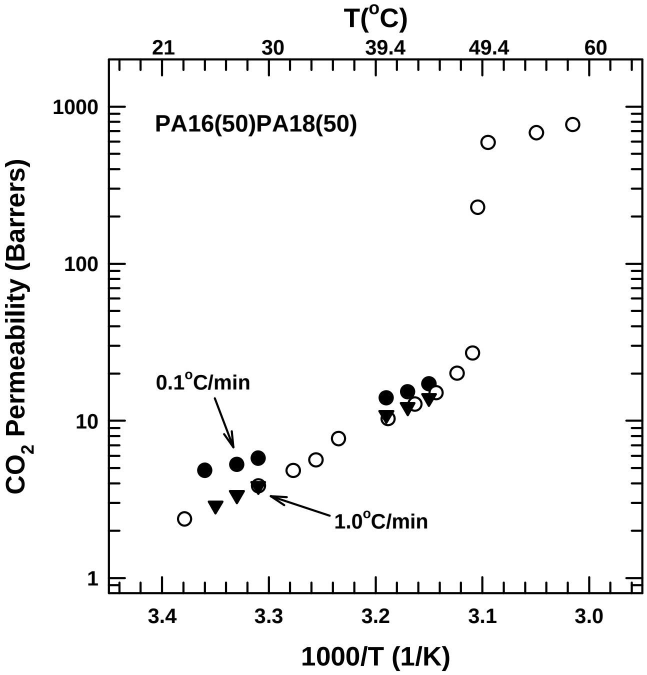

Figure A.45: Effects of thermal history on O2 permeability of PA16(50wt%)/PA18(50wt%) blend as a function of temperature at two cooling rates, 0.1 and 1.0oC/min.

Bibliography

Temperature compensating films for produce. Prepared Foods, vol. v161: Business News Publishing Co., 1992. pp. 95(91).

Alig I, Jarek M, and Hellmann GP. Macromolecules 1998;31(7):2245-2251.

Andrich G, Fiorentini A, Tuci A, Zinnai A, and Sommovigo G. Journal of the American Society for Horticultural Science 1991;116(3):478-481.

Armarego WLF and Chai CLL. Purification of Laboratory Chemicals, 5th ed. Amsterdam: Butterworth-Heinemann, 2003.

Artyukhov AI, Borisova TI, Birshtein LL, Dmitrochenko DA, and Shevelev VA. Vysokomolekulyarnye Soedineniya, Seriya A 1975;17(11):2552-2557.

Barrer RM and Chio HT. Journal of Polymer Science: Part C 1965(10):111-138.

Beaudry RM, Cameron AC, Shirazi A, and Dostallange DL. Journal of the American Society for Horticultural Science 1992;117(3):436-441.

Ben-Yehoshua S. Environmentally friendly technologies for agricultural produce quality 2005;61(112):61-112.

Bird RB, Stewart WE, and Lightfood EN. Transport Phenomena: Wiley, 2002.

Brackett RE. Postharvest Biology and Technology 1999;15:305-311.

Cameron AC, Beaudry RM, Banks NH, and Yelanich MV. Journal of the American Society for Horticultural Science 1994;119(3):534-539.

Cameron AC, Boylan-Pett W, and Lee J. Journal of Food Science 1989;54(6):1413-1416.

Cameron AC, Talasila PC, and Joles DW. Hortscience 1995;30(1):25-34.

Chapman D. Journal of the Chemical Society 1957:4489-4491.

Chen DS, Hsiue GH, and Hsu CS. Makromolekulare Chemie-Macromolecular Chemistry and Physics 1992;193(6):1469-1479.

Clarke R. Temperature switchable pressure sensitive adhesives. Adhesives Age, vol. 36, 1993. pp. 39.

Clarke R and De Moor CP. The future in film technology: A tunable packaging system for fresh produce. In: Gorny JR, editor. Proceedings of the 7th International

Controlled Atmosphere Research Conference, vol. 5. University of California, Davis, 1997. pp. 68-75.

Compan V, Zanuy D, Andrio A, Morillo M, Aleman C, and Munoz-Guerra S. Macromolecules 2002;35(11):4521-4530.

Edmond JP, Castaigne F, Toupin CJ, and Desilets D. Transactions of the ASAE 1991;34(1):239-245.

Edmond JP, Chau KV, and Brecht JK. Modeling respiration rates of blueberry in a perforation-generated modifeid atmosphere package. Proceedings from the Sixth International Controlled Atmosphere Research Conference. Cornell University, Ithaca, New York, 1993. pp. 134-144.

Exama A, Arul J, Lencki RW, Lee LZ, and Toupin C. Journal of Food Science 1993;58(6):1365-1370.

Fidler JC and North CJ. The Journal of Horticultural Science 1967;42:189-206.

Fishman S, Rodov V, Peretz J, and Ben-Yehoshua S. Journal of Food Science 1995;60(5):1078-1087.

Flory PJ. Journal of Chemical Physics 1949;17:223-240.

Fonseca SC, Oliveira FAR, and Brecht JK. Journal of Food Engineering 2002;52(2):99-119.

Fonseca SC, Oliveira FAR, Frias JM, Brecht JK, and Chau KV. Journal of Food Engineering 2002;54(4):299-307.

Fonseca SC, Oliveira FAR, Lino IBM, Brecht JK, and Chau KV. Journal of Food Engineering 2000;43(1):9-15.

Gong S and Corey K. Journal of the American Society for Horticultural Science 1994;119(3):546-550.

Greenberg SA and Alfrey T. Journal of the American Chemical Society 1954;76:6280-6285.

Greene C. United States Department of Agriculture: Economic Research Service. AREI Chapter 4.9: U.S. Organic Agriculture: www.ers.usda.gov.

Hagger PE, Lee DS, and Yam KL. Journal of Food Process Engineering 1992;15:143-157.

Hemminger WF and Sarge SM. Journal of Thermal Analysis 1991;37(7):1455-1477.

Hirabayashi T and Yokota K. Polymer Journal (Tokyo, Japan) 1987;19(9):1115-1119.

Hsieh HWS, Post B, and Morawetz H. Journal of Polymer Science, Polymer Physics Edition 1976;14(7):1241-1255.

Inomata K, Sakamaki Y, Nose T, and Sasaki S. Polymer Journal 1996;28(11):986-991.

Joles DW, Collier Cameron A, Shirazi A, Petracek PD, and Beaudry RM. Journal of the American Society for Horticultural Science 1994;119(3):540-545.

Jordan EF, Jr., Feldeisen DW, and Wrigley AN. Journal of Polymer Science, Polymer Chemistry Edition 1971;9(7):1835-1852.

Jordan EF, Jr., Smith S, Jr., Parker WE, Artymyshyn B, and Wrigley AN. Journal of Applied Polymer Science 1978;22(6):1509-1528.

Jurin V and Karel M. Food Technology 1963;17(6):104-108.

Kader AA. Increasing food availability by reducing postharvest losses of fresh produce. In: Mencarelli R and Tonutti O, editors. Proceedings of the Fifth International Postharvest Symposium, 2005. pp. 2169-2175.

Kader AA. HortScience 2003;38(5):1004-1008.

Kader AA. Respiration of Gas Exchange of Vegetables. In: Weichmann J, editor. Postharvest physiology of vegetables. New York: Marcel Dekker, Inc., 1987. pp. 25-43.

Kano Y, Akiyama S, Kasemura T, and Kobayashi S. Polymer Journal 1995;27(4):339-346.

Karel M and Go J. Modern Packaging 1964;37:123-127.

Kaufman HS, Sacher A, Alfrey T, and Fankuchen I. Journal of the American Chemical Society 1948;70:3147.

Kidd F and West C. Plant Physiology 1945;20(4):467-504.

Kirkland BS and Paul DR. Gas transport in poly (n-alkyl acrylate)/ poly (m-alkyl acrylate) blends. The University of Texas at Austin.

Koros WJ. Sorption and transport of gases in glassy polymers. Chemical Engineering. Austin, Texas: University of Texas at Austin, 1977. pp. 253.

Lakakul R, Beaudry RM, and Hernandez RJ. Journal of Food Science 1999;64(1):105-110.

Lee DS, Haggar PE, Lee J, and Yam KL. Journal of Food Science 1991;56(6):1580-1585.

Lee DS, Song YS, and Yam KL. Journal of Food Engineering 1996;27(3):297-310.

Lobering H-G and Polzere H. Gel, especially for ophthalmology. United States: Medproject Pharma Entwicklungs and Vertriebs Gesellschaft, 1993.

Lucier G, Pollock S, Ali M, and Perez A. Fruit and Vegetable Backgrounder. Electronic Outlook Report from the Economic Research Service, United States Department of Agriculture, www.ers.usda.gov, 2006.

Madhavan K and Reddy BSR. Journal of Membrane Science 2006;283(1-2):357-365.

Makino Y, Iwasaki K, and Hirata T. Journal of Agricultural Engineering Research 1997;67(1):47-59.

Makino Y, Iwasaki K, and Hirata T. Transactions of the ASAE 1996;39(3):1067-1073.

Maneerat C. A transient model to predict O_2 and CO_2 concentrations in modified atmosphere packaging of bananas at various temperatures. CA '97 proceedings : Seventh International Controlled Atmosphere Research Conference : July 13-18, 1997, University of California, Davis., vol. 5. University of California, Davis, 1997. pp. 191-197.

Mazee WM. The phase behavior of n-alkanes and some of their binary mixtures. Symposium on Recent Advances in the Chemical Thermodynamics of Hydrocarbons and Related Substances, vol. 3. Chicago, IL, 1958. pp. 35-47.

McLaughlin CP and O'Beirne D. Journal of Food Science 1999;64(1):116-119.

Michaels AS and Bixler HJ. Journal of Polymer Science 1961;50:413-439.

Michaels AS and Parker RB, Jr. Journal of Polymer Science 1959;41:53-71.

Mogri Z. Gas transport properties of side-chain crystalline polymers. Chemical Engineering. Austin: University of Texas at Austin, 2001. pp. 289.

Mogri Z and Paul DR. Polymer 2001;42(18):7765-7780.

Mogri Z and Paul DR. Polymer 2000;42(6):2531-2542.

Mogri Z and Paul DR. Journal of Membrane Science 2000;175(2):253-265.

Mogri Z and Paul DR. Journal of Polymer Science, Part B: Polymer Physics 2001;39(10):979-984.

Mohr JM and Paul DR. Polymer 1991;32(7):1236-1243.

O'Leary KA and Paul DR. Polymer 2006;47(4):1226-1244.

O'Leary KA and Paul DR. Polymer 2006;47(4):1245-1258.

Ooraikul B, M.E. Stiles, and Editors. Modified Atmosphere Packaging of Food. New York: Ellis Horwood, 1991.

Overberger CG, Frazier C, Mandelman J, and Smith HF. Journal of the American Chemical Society 1953;75:3326-3330.

Paul DR and Clarke R. Journal of Membrane Science 2002;208(1-2):269-283.

Pauly S. Permeability and Diffusion Data. In: Brandrup J, Immergut EH, and Grulke EA, editors. Polymer Handbook. New York: Wiley-Interscience, 1999. pp. 543-569.

Peppelenbos HW and Leven JV. Postharvest Biology and Technology 1996;7:27-40.

Pittman AG and Ludwig BA. Journal of Polymer Science, Polymer Chemistry Edition 1969;7(11):3053-3066.

Plate NA and Shibaev VP. Comb-shaped polymers and liquid crystals. New York: Plenum Press, 1987.

Plate NA, Shibaev VP, Petrukhin BS, and Kargin VA. Journal of Polymer Science, Polymer Symposia 1968;No. 23(Pt. 1):37-44.

Platenius H. Plant Physiology 1943;18(4):671-684.

R.T. Parry and Editor. Principles and Applications of Modified Atmosphere Packaging of Food, 1st ed. London: Blackie Academic and Professional (Am Imprint of Chapman & Hall), 1993.

Ranby BG. Journal of Polymer Science, Polymer Symposia 1975;51(Int. Symp. Macromol. Honor Professor Herman F. Mark):89-104.

Refojo MR. Polymers and devices in ophthalmology. Biomedical Engineering Conference, 1995., Proceedings of the 1995 Fourteenth Southern, 1995. pp. 143-147.

Rehberg CE and Fisher CH. Journal of the American Chemical Society 1944;66:1203-1207.

Rubin ID and Pugliese RD. Angewandte Makromolekulare Chemie 1989;171:165-173.

Saikia PJ and Baruah SD. Journal of Applied Polymer Science 2007;104:1226-1231.

Sanz C, Perez AG, Olias R, and Olias JM. Food Science and Technology International 2000;6(1):33-38.

Senthilkumar U and Reddy BSR. Journal of Membrane Science 2007;292(1-2):72-79.

Shibaev VP, Petrukhin BS, Zubov YA, Plate NA, and Kargin VA. Vysokomolekulyarnye Soedineniya, Seriya A 1968;10(1):216-226.

Shur YJ and Ranby B. Journal of Applied Polymer Science 1975;19(5):1337-1346.

Shur YJ and Ranby B. Journal of Applied Polymer Science 1976;20(11):3105-3119.

Shur YJ and Ranby B. Journal of Applied Polymer Science 1976;20(11):3121-3131.

Shur YJ and Ranby B. Journal of Macromolecular Science, Physics 1977;B14(4):565-572.

Silva FM, Chau KV, Brecht JK, and Sargent SA. Applied Engineering in Agriculture 1999;15(4):313-318.

Smyth AB, Song J, and Cameron AC. Journal of Agricultural and Food Chemistry 1998;46(11):4556-4562.

Song Y, Kim HK, and Yam KL. Journal of the American Society for Horticultural Science 1992;117(6):925-929.

Stern SA, Shah VM, and Hardy BJ. Journal of Polymer Science, Part B: Polymer Physics 1987;25(6):1263-1298.

Talasila PC and Cameron AC. Journal of Food Science 1997;62(5):926-930.

Talasila PC, Chau KV, and Brecht JK. Transactions of the ASAE 1992;35(1):221-224.

Wiley RH and Brauer GM. Journal of Polymer Science 1948;3:455-461.

Yang CC and Chinnan MS. Transactions of the ASAE 1988;31(3):920-925.

Ying L. Journal of Southeast University 2005;21(3):314-318.

Yokota K and Hirabayashi T. Polymer Journal (Tokyo, Japan) 1986;18(2):177-180.

Yokota K, Kougo T, and Hirabayashi T. Polymer Journal (Tokyo, Japan) 1983;15(12):891-898.

Vita

Bertha S. Kirkland, daughter of Thelma and James, was born in Augusta, Georgia on September 24, 1976. She graduated from Screven County High School in Sylvania, Georgia and received a Bachelor of Science degree in Chemical Engineering from the Georgia Institute of Technology in 2000. In August of 2000, she entered work in the chemical industry for one year. She then returned to school at The University of Texas at Austin and earned a Masters of Science degree in Engineering in the Chemical Engineering program.

Permanent address: 626 Rifle Road
Sylvania, Georgia 30467

This dissertation was typed by the author.